Monte Carlo Isotopic Inventory Analysis for Complex Nuclear Systems

Phiphat Phruksarojanakun

January 2007

UWFDM-1323

Ph.D. thesis.

FUSION TECHNOLOGY INSTITUTE

UNIVERSITY OF WISCONSIN

MADISON WISCONSIN

Monte Carlo Isotopic Inventory Analysis for Complex Nuclear Systems

Phiphat Phruksarojanakun

Fusion Technology Institute
University of Wisconsin
1500 Engineering Drive
Madison, WI 53706

http://fti.neep.wisc.edu

January 2007

UWFDM-1323

Ph.D. thesis.

MONTE CARLO ISOTOPIC INVENTORY ANALYSIS FOR COMPLEX NUCLEAR SYSTEMS

by

Phiphat Phruksarojanakun

A dissertation submitted in partial fulfillment of
the requirements for the degree of

Doctor of Philosophy

(Nuclear Engineering and Engineering Physics)

at the

UNIVERSITY OF WISCONSIN – MADISON

2007

ABSTRACT

Monte Carlo Inventory Simulation Engine or MCise is a newly developed method for calculating isotopic inventory of materials. The method offers the promise of modeling materials with complex processes and irradiation histories, which pose challenges for current deterministic tools. Monte Carlo techniques based on following the history of individual atoms allows those atoms to follow randomly determined flow paths, enter or leave the system at arbitrary locations, and be subjected to radiation or chemical processes at different points in the flow path.

The method has strong analogies to Monte Carlo neutral particle transport. The fundamental of analog method is fully developed, including considerations for simple, complex and loop flows. The validity of the analog method is demonstrated with test problems under various flow conditions. The method reproduces the results of a deterministic inventory code for comparable problems. While a successful and efficient parallel implementation has permitted an inexpensive way to improve statistical precision by increasing the number of sampled atoms, this approach does not always provide the most efficient avenue for improvement. Therefore, six variance reduction tools are implemented as alternatives to improve precision of Monte Carlo simulations. *Forced Reaction* is designed to force an atom to undergo a predefined number of reactions in a given irradiation environment. *Biased Reaction Branching* is primarily focused on improving statistical results of the isotopes that are produced from rare reaction pathways. *Biased Source Sampling* is aimed at increasing frequencies of sampling rare initial isotopes as the starting particles. *Reaction Path Splitting* increases the population by splitting the atom at each reaction point, creating one new atom for each decay or transmutation product. *Delta Tracking* is recommended for a high-frequency pulsing to greatly reduce the computing time. Lastly, *Weight Window* is introduced as a strategy to decrease large deviations of weight due to the uses of variance reduction techniques.

A figure of merit is necessary to evaluate the efficiency of a variance reduction technique. A number of possibilities for the figure of merit are explored, two of which offer robust figures of merit. One figure of merit is based on the relative error of a known target isotope ($1/R^2T$) and another on the overall detection limit corrected by the relative error ($1/D_kR^2T$). An automated Adaptive Variance-reduction Adjustment (AVA) tool is developed to iteratively define necessary parameters for some variance reduction techniques in a problem with a target isotope. Initial sample problems demonstrate that AVA improves both precision and accuracy of a target result in an efficient manner.

Potential applications of MCise include molten salt fueled reactors and liquid breeders in fusion blankets. As an example, the inventory analysis of an actinide fluoride eutectic liquid fuel in the In-Zinerator, a sub-critical power reactor driven by a fusion source, is examined using MCise. The result reassures MCise as a reliable tool for inventory analysis of complex nuclear systems.

Dedicated to my late grandfather,
Silapachai Phruksarojanakun.
1920–2006

ACKNOWLEDGEMENTS

I would like to extend my greatest gratitude and regard to my advisor, Professor Paul Wilson, for years of invaluable advice and guidance on this work. I have learned a great deal from his methodical analysis and engineering judgment which I can never learn in the classroom.

Sincere thanks are given to individuals in the Department of Engineering Physics, especially those in Fusion Technology Institute (FTI), who have helped me during the course of my study. Tony Hammond has done a good job keeping a cluster active. Milad Fatenejad has been a reliable person to talk to when I struggle with a programming problem. I would also like to thank Professor Douglass Henderson, Dr. Timothy Tautges, Research Professor Laila El-Guebaly and Research Professor Mohamed Sawan for all their help.

I would like to thank my friends who have made my stay in Madison a memorable experience. Thanks to the wonderful people from the Badminton Club, I am fortunate enough to know and hang out with them. I feel privileged to be a part of this university from which I have learned so much. Though the Badgers sports let me down at times, they are always fun to watch. I will forever be a Badgers fan. On Wisconsin!

Finally, I would like to express my deepest thank to the Suns family, my grandmother, mother, father, brothers Phichat and Phinat and a very special person, Tulaya Limpiti, for the endless love and support they have given me. Without their encouragement, I would not have reached my goal. I am deeply grateful to have the family that I have.

TABLE OF CONTENTS

LIST OF TABLES

LIST OF FIGURES

Chapter 1

Introduction

Many current nuclear power systems rely on the fuel cycles in which material is exposed to a small number of irradiation environments over long periods of time, with little to none on-line chemical processing. However, the fuel cycles for future systems are gradually changing as ongoing developments for the fuel cycles tend to involve *dynamic* material. The material is anticipated to mix and circulate throughout the system and, therefore, be exposed to a wide range of neutron spectra over much shorter time scales. This dynamic nature of fuel cycle also allows the possibility of integrating an on-line chemical process as a component of the system. Aside from improving overall performance of the system, such changes are typically introduced with the purpose of reducing the burden of the disposal facility. It is hoped that the amount of high-level waste repository can eventually be decreased. Furthermore, such changes often raise concerns about an increase in the proliferation risk of the system, regardless of possible intrinsic proliferation barriers, because the fuel cycle is no longer confined in a highly radioactive reactor. Both radioactive waste disposal and proliferation risk are sensitive issues that need to be addressed before future nuclear power systems become more viable options of global energy resource. Although the realization of novel nuclear systems and fuel cycles may not be practical in a number of years, early investigations of these issues would certainly promote efforts in developing technology in this area.

A precise study of how these changes affect the waste streams and proliferation risk requires tools that allow the transient analysis of the isotopic inventory throughout the lifetime of the system or fuel cycle. For example, the accurate determination of isotopic inventory, particularly the actinides inventory, of the nuclear power systems is one of the inputs most used to quantitatively assess their waste disposal and to evaluate their resistance to proliferation. The current tools and methodologies for performing this type of analysis are designed for the slowly varying systems of today. They are not suitable for the dynamic systems of the future. The work in this thesis employs a Monte Carlo (MC) technique to provide a new approach for performing isotopic inventory analyses of dynamic material in a complicated fuel cycle.

1.1 Overview on Traditional Methods

Accurate determination of isotopic inventory, particularly the actinide inventory, of the nuclear power systems is one of the most important inputs used to quantitatively assess their waste disposal and to evaluate their resistance to proliferation. Such calculation requires tools and methodologies that permit a transient analysis of the isotopic inventories throughout the lifetime of the system or fuel cycle. Traditional methodologies for inventory analysis focus on the conversion of a macroscopic mixture of isotopes via transmutation, fission, and decay reactions. The first order ordinary differential equations (ODE) that describe the reactions for each isotope are collected into a system of equations that can be written as

$$\dot{\vec{N}}(t) = \mathbf{A}\vec{N}(t), \tag{1.1}$$

where $\vec{N}(t)$ is the inventory of isotopes at time t and $\mathbf{A}$ is a transfer matrix that represents decay, production and destruction rates of all isotopes. The general solution to Equation (1.1) is given in terms of matrix exponential [1]:

$$\vec{N}(t) = e^{\mathbf{A}t}\vec{N}(0), \tag{1.2}$$

where $\vec{N}(0)$ is the initial inventory vector. Equation (1.1) can be solved using a variety of methods. Several activation codes, such as FISPIN [2], FISPACT [3] and RACC [4], use simple time-step methods by applying a difference operator to approximate the time derivative on the left hand side of Equation (1.1) and converting a system of first order differential equations into a system of algebraic equations. An alternative method treats the system of equations as a matrix and employs one of existing computational techniques to solve the exponential as in Equation (1.2). ORIGEN [5] employs Taylor's series expansion to calculate the term $e^{\mathbf{A}t}$. In addition to above methods which attempt to solve the problem as one large system of ODE's, a linear chain method which is implemented by DKR [6] and CINDER [7] breaks down the reaction tree into a number of chains such that each isotopic node has only one product. Each linear chain has its associated transfer matrix **A** which is bi-diagonal. Its analytical solution is popularly known as the Bateman equations [8]. Lastly, ALARA [1], the most recent activation code, considers a combination of mathematical methods and selects the optimal technique for a particular problem. Even though ALARA makes a tremendous improvement over its preceding activation codes, the drawback is that it is not appropriate for accurate modeling of dynamic problems.

All of the mentioned techniques have their own limitations and advantages, depending on the physical problems they model. When the numerical methods are used to simulate complicated systems, dynamic systems in particular, their effectiveness and accuracy are the issues of concern. The highly stiff nature of a transfer matrix **A** is a major difficulty that affects the performance of the numerical methods. Several other issues that need to be accounted for in using these methods are briefly discussed here. First, most methodologies assume *a priori* that a finite set of isotopes is produced during the simulation time. Approaches taken to construct the set ranges from including all isotopes for which data exists, to arbitrarily applying the maximum number of isotopes in each reaction chain, to specifying the size of reaction tree based on desired accuracy and truncation of the simulation. Secondly, these traditional techniques are suitable for analyzing a fixed volume of static material exposed to a steady-state, pulsed or slowly varying irradiation environment. As mentioned earlier, future nuclear systems and fuel cycles are likely to have constant or regular addition or removal of material, which causes flowing streams of fuel or other materials to experience a variety of neutron flux throughout the operating lifetime of the system.

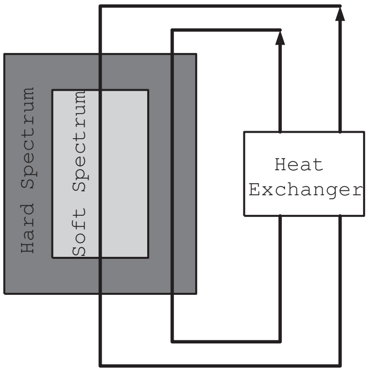

Figure 1.1 A simple example of mixing flow paths. Two flows of coolant coming from a hard and soft spectrum region mix in the heat exchanger and re-enter the reactor.

While current methodologies are capable of modeling some of these characteristics of future system to some degree of accuracy, they are clearly short of the ability to perform the computation efficiently. Finally, the implementation of flowing streams of fuel or other materials into a nuclear system suggests two supplementary features to the model: on-line chemical processes and mixing of flow paths. The on-line chemical processes would create a unique set of equations that must be solved concurrently with those representing transmutation and decay processes. The definition of chemical processes may be extended to include a sink in the system. Flow paths can have an unpredictable effect because the materials in the flow paths previously experience different neutron fluxes. The performances of traditional techniques are susceptible to error in modeling the mixing of flow paths.

A simple reactor design as shown in Figure 1.1 is used to illustrate a problem from using traditional techniques to approximate the mixing of flow paths. Inside the reactor, the coolant passes through two different regions (hard spectrum and soft spectrum). Two coolant outflows mix in the heat exchanger. The following reaction chain that involves two consecutive transmutation reactions, both with energy threshold in the 1 MeV range is considered.

$$A \xrightarrow{(n,\alpha)} B \xrightarrow{(n,2n)} C$$

To approximate this situation, one traditional approach is to have samples of coolant alternately flowing through the hard spectrum region and the soft spectrum region. In this case, the approximation would overestimate the amount of C in the hard region while underestimating the amount of C in the soft region, with respect to its average value in the real calculation because in reality, the coolant would randomly pass through the two regions after leaving the heat exchanger.

Aiming to overcome the drawbacks of traditional techniques, MC techniques for modeling isotopic inventories offer the promise of modeling materials with complex flowing paths and irradiation histories. They are particularly suitable in the situations where the arbitrary flow paths lead to non-predetermined irradiation histories. Overview and benefits of MC techniques are discussed in the following section.

1.2 Overview of a Monte Carlo Method

A MC method is a stochastic technique that provides approximate solutions to a variety of physical and mathematical problems of which the quantities of interest can be described in terms of their probability density functions (PDFs) [9]. The MC methods have been widely used in many fields, for example, computer science, economics, finance, molecular dynamics, statistics, and radiation transport. The last application of the MC method appears to be useful to the isotopic inventory problem because of the similarities of the underlying PDFs, which will be discussed in the later chapters of this thesis. The close analogy between radiation transport and isotopic inventory, along with a lack of literature on MC isotopic inventory prompt us to rely on existing literature in the field of transport. Some of this literature are reviewed in this section.

The MC method utilizes random numbers, or more precisely, pseudo-random numbers, to perform statistical sampling experiments and the desired result is obtained by taking an average over the number of observations. This result is always associated with a statistical error, which is governed by the central limit theorem [10] and is given by

$$error \sim \frac{constant}{\sqrt{N}}. \tag{1.3}$$

where N is the number of experiments and is sufficiently large. In order to reduce the statistical error by a factor of two, N must be quadrupled. The development of variance reduction techniques is the result of an effort to reduce the statistical error by reducing the constant in the error expression instead of increasing N, and therefore improve efficiency of the simulations. To quantitatively evaluate the efficiency of a given MC simulation, Hammersley and Handscomb [11] proposed that the efficiency is given by $\frac{1}{\epsilon T}$, where ϵ is a sampling variance and T is a computational time. This quantity has been used as an efficiency estimator in many subsequent Monte Carlo codes.

In the field of MC radiation transport, variance reduction techniques such as forced collision [12], source biasing [13], and weight window [14] have been thoroughly studied and thus can be used as references for the development of variance reduction techniques in MC isotopic inventory. For a forced collision technique, a particle is forced to undergo a specific number of collision in a given phase space. A source biasing technique increases the sampling frequencies of initial source particles with high importances. A weight window technique is designed to keep a weight variation among simulated particles within designated bounds by fairly splitting over-weighted particles or killing under-weighted particles.

Use of variance reduction techniques requires adjusting various parameters to achieve the highest level of efficiency attainable. It is not a simple task for a user to define an optimum set of parameters required by different techniques in a given simulation. In responding to this difficulty, researchers have developed a variety of automated algorithms to help define variance reduction parameters. In general, there are two categories of the automated algorithms: Monte Carlo and deterministic. Booth and Hendricks [14] developed a Monte Carlo-based importance estimation technique to generate parameters for weight window. This technique is called the forward-adjoint generator, which becomes widely known as the weight window generator as implemented in the Monte Carlo N-Particle transport code or MCNP. Alternatively, the AVATAR method [15] relies on adjoint deterministic solutions to generate a weight window for source-detector problems.

1.3 Advantages of a Monte Carlo Method in Isotopic Inventory

In isotopic inventory, MC techniques are based on tracing the history of individual atoms, allowing atoms to randomly follow determined flow paths, to enter or leave the circulating system at arbitrary locations, and to be exposed to radiation or chemical processes at different portions of the flow paths. Under MC methodology, a simulation of a flowing network is realized by defining control volumes into which a set of flow paths merge and other control volumes from which a set of flow paths diverge. As the tracked atom reaches the end of a control volume, it must continue on to one of the defined flow paths leading to the next control volume. The simplest approach is for the probability that the atom will flow into each of the flow paths to be governed by the relative macroscopic flow rates in each path. It is also possible to use other factors to determine such probability such as atomic identities as a model for chemical separation.

Some early potential applications of these MC methods include liquid breeder in fusion blankets, molten salt fueled reactor, and possibly advanced fuel cycles based on symbiotic combinations of reactors. The liquid breeder probably is the most immediate application of MC techniques. A Pb-Li coolant is used in many designs to ensure adequate tritium (^{3}H) production. Lead and its impurities are subject to activation under different neutron flux environments as the coolant arbitrarily enters various regions of the reactor, e.g., first wall, shield, blanket. After exiting the reactor, the coolant is diverted to the heat exchanger, a chemical treatment system installed to extract the tritium, and back to the reactor. In summary, MC methods appear to have distinct advantages over traditional methodologies when a dynamic nuclear system is of concerns.

1.4 Goals

The goal of this work is to develop a MC inventory simulation engine(MCise) to perform isotopic inventory analysis of dynamic materials exposed to a variety of nuclear and chemical environments in complex nuclear systems. This development proceeds in a number of phases.

The goal of the first phase is to develop the fundamental methodology for an analog system and test it for situations with flowing and mixing materials. This is described in Chapter 2. This chapter presents the basic concepts of Monte Carlo isotopic inventory. The development begins with the solution for a mixture of isotopes under a fixed steady-state irradiation environment. The complexity is increased by allowing the mixture to flow through a network of irradiation environments. Atom source and different types of tally are defined. The validity of the Monte Carlo isotopic inventory methodology is tested with a variety of test problems. Finally, high-efficiency parallel computing is developed to increase the number of simulations for a given computational time.

The goal of the second phase is to develop variance reduction techniques to improve computational efficiency. Chapter 3 discusses six variance-reduction tools implemented to increase the simulation efficiency for different types of analog problems. The validity of each developed technique is demonstrated using an analytical proof or a numerical benchmark with a deterministic calculation. Chapter 4 explores potential formulae for the figure of merit and discusses their usefulness. A figure of merit is a quantitative metric that measures the efficiency of a given simulation. It is necessary for a fair comparison among problems with different sets of variance reduction parameters. Chapter 5 applies two figure of merit formulae developed in Chapter 4 in two test problems and observes the characteristics of both figures of merit in response to the variations of variance reduction parameters.

The goal of the third phase is to automate the determination of variance reduction parameters. Chapter 6 develops Adaptive Variance-reduction Adjustment (AVA), which is an iterative scheme that automatically generates variance reduction parameters for forced reaction, biased reaction branching and biased source sampling techniques. A goal of AVA is to improve statistics of the target result. Sample problems are used to illustrate the efficacy of AVA.

Chapter 7 uses MCise to model three real-world applications, namely a water-cooled reactor, the In-Zinerator and the ARIES-CS. The responses such as decay heat, isotopic inventory and activity, can be effectively calculated with the algorithm.

Chapter 8 discusses some potential ideas for future direction of this research. The thesis is concluded with an overall research summary.

Chapter 2

Analog Monte Carlo Isotopic Inventory

2.1 Introduction

This section introduces the methodology with specifics for implementing single point steady-state activation calculations, the first step in this development. The basic extensions to allow flowing systems are described and demonstrated. Finally, some additional enabling concepts and fundamental capabilities are shown. A variety of well-crafted problems, some with analytic solutions and others with solutions from deterministic methods, are used to demonstrate the validity of the method.

2.2 Methodology

The development of this methodology follows a logical progression of complexity. First, it is necessary to develop and implement the solution for a mixture of isotopes exposed to a single steady-state flux. This is extended by adding the possibility of a simple flow path– one in which all material flows through the same sequence of control volumes– and then by allowing for complex flow paths with splitting/combining of flows. Finally, loop flow allows an atom to return to a previous control volume. Many combinations of these different flow/complexity regimes are possible. Throughout this development, a number of enabling concepts must be implemented, most importantly sources of atoms and tallies of results. This section discusses the development of both the primary methodology and its enabling concepts.

2.2.1 Problem Formulation

The Monte Carlo simulation of isotopic inventory is based upon following the histories of individual *atoms* as they pass between *control volumes.* An atom always has a specific isotopic identity characterized by its atomic number, mass number and isomeric state, but this identity is subject to change due to transmutation reactions and radioactive decay processes. Each control volume is characterized by a (neutron) *flux*[1] and a *residence time*, t_{res}. The flux for each control volume, typically expressed as a multi-group spectrum, is assumed to be constant throughout the control volume. The residence time represents the average amount of time that any atom spends in the control volume. By placing an atom in a control volume, a number of new important quantities can be determined. The *total effective reaction rate coefficient* for an isotope i in control volume v, $\lambda^v_{i,eff}$, can be determined by collapsing the total transmutation cross-section for that isotope, $\sigma_{i,tot}(E)$, with the neutron flux for that control volume, $\phi^v(E)$, and adding the decay constant for that isotope, $\lambda_{i,decay}$:

$$\lambda^v_{i,eff} \quad = \quad \lambda_{i,decay} + \int \phi^v\left(E\right)\sigma_{i,tot}(E)\,dE \tag{2.1}$$

(For simplicity, the index for the isotope, i, and control volume, v, will henceforth be suppressed unless necessary for clarity.) The *mean reaction time* is defined as the inverse of this total effective reaction rate coefficient, $t_m \equiv \lambda_{eff}^{-1}$. The probability of the atom undergoing a reaction of any kind between time, t, and time, $t + dt$, is

$$p(t)\,dt = \lambda_{eff} e^{-\lambda_{eff} t}\,dt. \tag{2.2}$$

The corresponding cumulative density function is given by integrating Equation (2.2),

$$\begin{aligned} P(t) &= \int_0^t \lambda_{eff} e^{-\lambda_{eff} t'}\,dt' \\ P(t) &= 1 - e^{-\lambda_{eff} t} \qquad (2.3) \end{aligned}$$

---

[1] In principle, if nuclear data is available, this methodology could treat transmutation by fluxes of any type of particle and even fluxes of more than one type of particle.

At any point in time, an atom has a known amount of time before it leaves the current control volume, the remaining residence time, $0 < t_{rem} (\leq t_{res})$, and thus a *remaining number of mean reaction times*,

$$n_{rem} = \lambda_{eff}\, t_{rem} = \frac{t_{rem}}{t_m}. \tag{2.4}$$

2.2.2 Basic Elements

Steady-State Simulation

Consider an atom that has just entered a control volume [2]; its remaining residence time is equal to the control volume's residence time, $t_{rem} = t_{res}$, and its remaining number of mean reaction times is defined by equation (2.4). The *number of mean reaction times until the next reaction*, n_{rxn}, can be randomly sampled, using the inverse transformation of Equation (2.3) with a uniform random variable between 0 and 1, ξ:

$$n_{rxn} = -\ln(\xi). \tag{2.5}$$

If $n_{rxn} < n_{rem}$, the atom reacts before leaving the control volume. The remaining residence time is updated,

$$t_{rem} \leftarrow t_{rem} - n_{rxn} t_m. \tag{2.6}$$

A new isotopic identity is determined by randomly sampling the list of possible reaction pathways, and a new value is calculated based on the new isotopic identity. Finally, n_{rem} is updated using equation (2.4), and n_{rxn} for the next reaction is sampled using equation (2.5). The history continues by repeating the comparison of n_{rxn} and n_{rem}.

If $n_{rxn} > n_{rem}$, the atom leaves the control volume before reacting (and in a 0-D simulation the history is ended).

It is perhaps clear at this point that standard steady state inventory analysis can be performed with this simple 0-D treatment. Since the physics/mathematics of inventory analysis does not introduce coupling between spatial regions, "multi-dimensional" steady-state problems are solved by simply performing a 0-D solution at each spatial point of interest

---

[2] Note that for a 0-D analog simulation, entering and leaving the control volume represent the beginning (birth) and end (death) of the history for that atom, respectively.

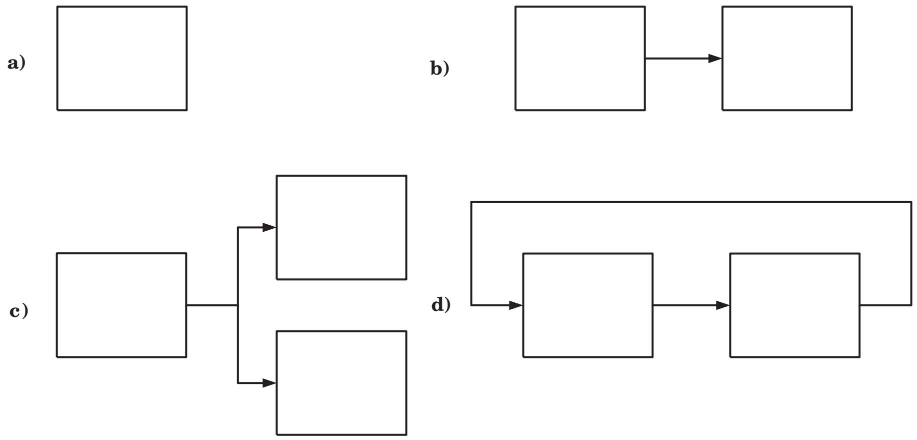

Figure 2.1 Four different flow and complexity regimes: a) 0-D b) simple flow c) complex flow, d) loop flow.

in the problem.

Simple Flow

In a simple flow system, as an atom leaves one control volume, it enters another (Figure 2.1(b)). In this case, n_{rxn} is updated

$$n_{rxn} \leftarrow n_{rxn} - n_{rem}, \tag{2.7}$$

a new value for λ_{eff} is calculated based on the new flux in this control volume, and t_{rem} is reset to the residence time for the new control volume, t_{res}. Finally, n_{rem} is updated using equation (2.4). Again, the history continues by repeating the comparison of n_{rxn} and n_{rem}. Note that for simple flows, entering a new control volume requires no random sampling.

So far, time is only measured relative to the time at which a control volume is entered. It is useful to introduce a more universal definition of time, the *absolute simulation time*, t_{sim}, measured relative to some arbitrary starting time, most logically the beginning of the first control volume. This would be a property of each atom and be incremented each time a reaction takes place or a control volume boundary is reached. Furthermore, since the atoms now flow from one control volume to another, it is more important that the current control volume of an atom be maintained as a property of that atom. In systems with simple flows and simple sources, all atoms would originate in the first control volume at $t_{sim} = 0$.

Complex Flow

In complex flow systems, atoms leaving one control volume may flow into one of any number of other control volumes — flows split and combine so that not all atoms follow the same flow path (Figure 2.1(c)). Implementing this is straightforward under the assumption that the relative volumetric flow rate to each control volume is known and properly characterizes the probability that a given atom will take each path. As such, random sampling of the discrete probability density function [PDF] derived from these relative flow rates fully determines which flow path a given atom takes. The absolute simulation time becomes more important here since different atoms may experience different flow paths and irradiation histories but still need to be tallied on an absolute time scale to report results.

Loop Flow

The distinguishing feature of loop flow is the ability for a given atom to return to a control volume in which it has already been resident (Figure 2.1(d)). Loop constructs can be combined with both simple and complex flow. If the total simulation time is being tracked properly, the implementation of loop flow does not introduce complexity to the methodology.

2.2.3 Enabling Concepts

Atom Sources

To this point, this discussion has quietly implied that all atoms come from the same simple source, their histories beginning in the same control volume at the same time ($t_{sim} = 0$). As such, implementation of the source would be trivial — random sampling of a discrete PDF representing the isotopic mix of the initial material. The method is rendered far more versatile; however, by accommodating different source locations, compositions and time-dependencies. In fact, the implementation is not significantly complicated by such improvements.

In its most general form, each source would be associated with a single control volume, have a single specific isotopic composition, and would have a well-defined time-dependence, $r(t)$. In a problem with many sources, the *total strength* of each source, R_s, would be defined by integrating the time-dependent form over the total simulation time:

$$R_s = \int_{0}^{t_{sim}^{max}} r(t)\, dt. \tag{2.8}$$

The set of total source strengths defines a discrete PDF which can be sampled to determine from which source a new atom comes. Once a particular source is chosen, its initial control volume is explicitly defined and its isotopic identity and birth time can be randomly sampled from the discrete PDF representing the isotopic mix and from the time-dependent source strength, $r(t)$,respectively. Note that the 0-D steady state source is still supported by this generalized scheme by defining a source with a delta function time-dependence, $r(t) = R_s\delta(t_{sim})$.

Further accommodations are needed to allow atoms to begin their histories at arbitrary places in a control volume, allowing a simulation to start with control volumes already containing material, some of which just entered and some of which is almost leaving. This is implemented by permitting different PDFs for the remaining residence time, t_{rem}, when an atom is created from a source.

Tallies

The primary result to be estimated by tallies is the time-dependent population of atoms, possibly separated into bins based on the isotopic identity. From this result, most other quantities of interest (activity, decay heat, radiation dose) can be derived by simple scalar transformations based on nuclear data or using this result as the input to another simulation. Two types of tallies have been developed: *atom current* tallies that take a snapshot of the isotopic spectrum and *atom population* tallies that average the isotopic spectrum over a time interval.

An *atom current* tally simply counts the atoms as they reach user-defined points in time, but scoring in bins based upon the isotopic identity of the atom. In the simplest case, these points in time correspond to the simulation times at which atoms leave specific control volumes. In an analog simulation, every history contributes the same total score (unity) to each tally. As a result, this type of tally provides an accurate estimate of the isotopic inventory at that particular point in time but is susceptible to missing the existence of very short-lived isotopes that are both produced and consumed between two points in time. This consequence of atom current tallies is related to the analog detection limit discussed in the results of the next section.

An atom population tally is designed to counter this limitation. In such tallies, histories contribute scores to time bins, rather than points in time. Again each history contributes the same total score (unity) to each time bin in each tally. However, the total score is divided among bins that correspond to the isotopic identity of the atom during that time bin. Each isotope bin receives a score that is equal to the fraction of the time bin that the atom existed as that isotope. While this is guaranteed to detect all isotopes regardless of when they are produced or consumed, since the results are time-averaged over the width of the bins, they only estimate the results at a specific time within a discretization error of first order in time. As the number of bins becomes very large within a fixed time interval, a population tally and a current tally approach the same result.

Figure 2.2 shows a representative reaction sequence occurring between two points in time and Table 2.1 indicates how each tally type would respond to this reaction sequence. None of the time bins in the current tally would include a contribution for isotope B but will be exact at the times indicated. Conversely, the population tally will not be exact at any time, but will include a contribution for isotope B.

2.2.4 Compound Capabilities

Taken in various combinations, the above elements and concepts can be used to derive additional capabilities. This section outlines some of these compound capabilities.

Arbitrary Flow

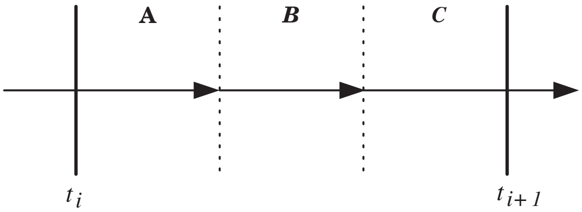

Figure 2.2 Representative reaction sequence between points of time to illustrate difference between current and population tallies.

Tally type	**Time bin**	**Contribution to isotopic tally bin**			**Exact time**
		Isotope A	Isotope B	Isotope C	
Current	i	1	0	0	t_i
	$i+1$	0	0	1	t_{i+1}
Population	i	1/3	1/3	1/3	none

Table 2.1 Contributions to different tally types from sample reaction sequence shown in Figure 2.2.

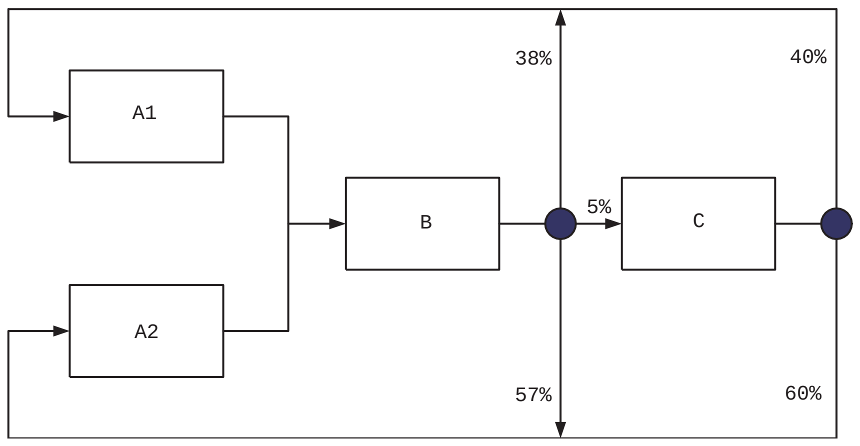

Figure 2.3 An arbitrary flow system (with complex and loop flows) representing a simplified two region coolant (A1 and A2) with chemical cleaning step (C) following the heat exchanger (B). In addition to the 40/60 flow split between regions A1 and A2, 5% of the flow leaving the heat exchanger is diverted to the cleanup system.

Once the basic constructs of simple, complex and loop flow have been implemented and validated, they can be combined in simulations with arbitrary complexity without adding complexity to the implementation of the methodology. A simplified schematic of a two region coolant with chemical cleanup system is shown in Figure 2.3. In this system, as the coolant loops through the system repeatedly, the flow through the two cooling regions is split unevenly and only 5% of the flow passes through the chemical cleanup system in each pass through the system.

Atom Reservoirs: After Shutdown Decay Calculations and Atom Sinks

In many activation calculations, the isotopic composition at various times following the shutdown of the facility is of primary importance because of its role in performing analysis of decay heat removal of waste disposal alternatives. The basic constructs of this methodology make this possible by having all material flow into a control volume with no neutron flux and a residence time that is longer than the longest cooling time of interest, an atom reservoir. A tally in this control volume at all the cooling times of interest will represent the shutdown decay inventory of the system.

Element	**Transport**	**Inventory Analysis**
Source quanta	Neutral particles	Individual atoms
Characteristic dimension	Length of geometric cell	Residence time in control volume
Basic sampling quanta	Mean free paths between reactions (macroscopic cross-section)	Mean times between reactions (effective transmutation & decay rate)
Primary particle characteristic	Energy	Isotopic identity
Fundamental tallies	Surface & volume flux (energy dependent)	Atom current & population (Isotope dependent)

Table 2.2 Analogies between elements of Monte Carlo neutral particle transport and Monte Carlo inventory analysis.

Some systems might include the removal of material either at regular intervals or continuously throughout the operation period. Moreover, it may be important to simulate the instantaneous or cumulative isotopic composition of such *atom sinks* over the operation period. In fact, most systems with complex atom sources will require atom sinks to ensure that atom quantities of the system are conserved appropriately. This is implemented as an atom reservoir, placed anywhere in the system, representing the effluent of a chemical processing step, possible diversionary pathway or some other extraction process.

2.2.5 Relationship to Monte Carlo neutral particle transport

Many of the elements of Monte Carlo inventory analysis have natural analogs in the field of Monte Carlo neutral particle transport [16].

Table 2.2 highlights the most important of these.

2.3 Testing

This section describes a variety of cases that have been designed to test and demonstrate the operation of the methodology described in the previous section. Following a fundamental test with a simple decay problem, a numerical benchmark for 0-D steady state problem was used as the foundation for testing each of the basic elements and enabling concepts. The results of the ALARA activation code were used as the reference solution for this benchmarking exercise. ALARA adaptively employs a variety of exact and approximate methods to solve the matrix exponential that arises as the solution of the system of first order ordinary differential equations. Finally, some sample calculations were then performed to demonstrate the compound capabilities using the 0-D steady state problem as a reference.

2.3.1 Single Control Volume: 0-D Analytic and Numerical

In order to demonstrate that the underlying methodology is valid, the simplest possible analytic test case was used: pure decay from a single isotope. Figure 2.4 shows the results of this comparison for 10^{10} Monte Carlo particles simulated for 4 half-lives where the statistical error of the results is 0.001%. This simple result serves to demonstrate the fundamental validity of this technique for modeling the first order ordinary differential equations that govern isotopic inventory problems and a verification of its correct implementation.

With the basic Monte Carlo sampling technique validated, the next test case was a full transmutation and decay problem: a single isotope, ^{56}Fe, irradiated for 10 years with a steady-state 175-group (vitamin-j) neutron flux where the first seven groups fluxes are zero and the remaining group fluxes are 5×10^{12} n/cm^2·s. The FENDL-2/A activation library and FENDL-2/D decay library were used in the calculation. The Monte Carlo results using 10^{10} atoms were compared to ALARA using a truncation tolerance of 10^{-9}.

The ALARA results included 39 isotopes whereas the Monte Carlo results only included 20. Figure 2.5 shows the relative difference between the Monte Carlo result and the deterministic result for 19 of these isotopes (^{56}Fe is not included) as a function of the deterministic result itself. The line indicates the statistical error (2σ) associated with a result of that

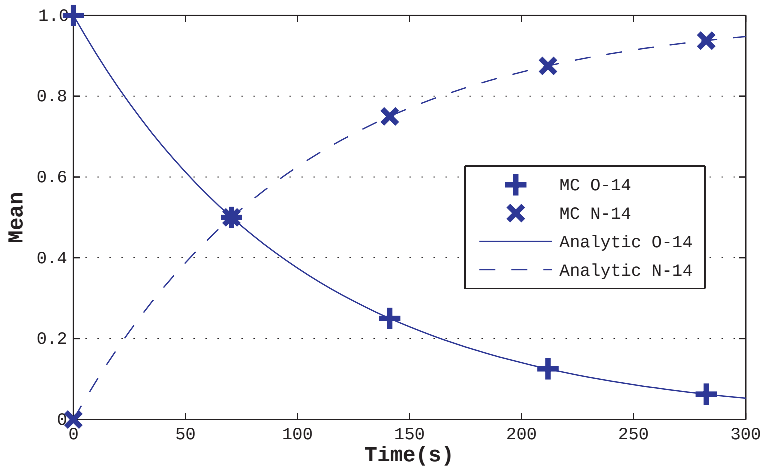

Figure 2.4 Comparison of Monte Carlo results to analytic benchmark results showing good agreement. Since the half life of ^{14}O was 70.60 seconds long, an initial unit amount of ^{14}O was reduced to a half and a quarter after 70.60 seconds and 141.20 seconds, respectively.

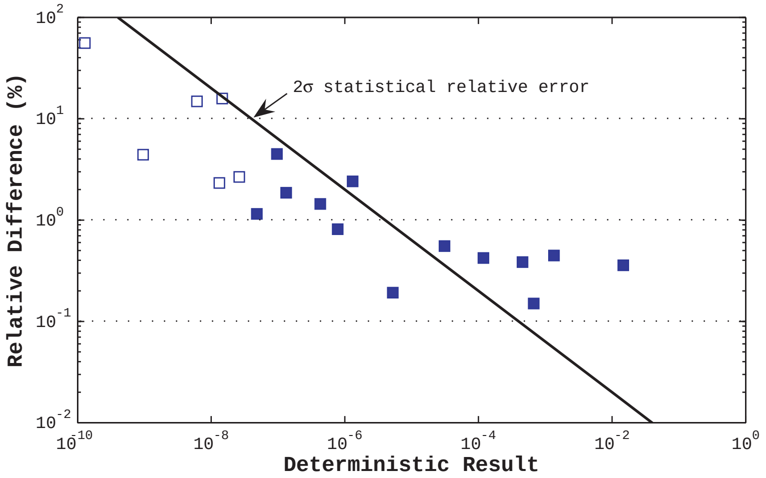

Figure 2.5 Variation of relative difference between Monte Carlo (MC) and deterministic results as a function of the deterministic result. The expected statistical error (2σ) as a function of the result is also shown for a MC problem with 10^{10} initial atoms. Results with a 1σ statistical error greater than 5% are shown with open symbols ($\diamond$).

magnitude in an analog Monte Carlo calculation. For each isotope, the relative difference is a consequence both of the statistical variations in the Monte Carlo results and of the approximations in the deterministic calculation. The deterministic solution will include truncation errors due to the physical modeling techniques as well as an accumulation of numerical errors introduced by the mathematical methods. This representation permits some qualitative assessment of the relative contribution of these two sources of discrepancy. For seven of the isotopes, the relative difference is larger than the 2σ statistical error, with relative differences ranging from 0.15% to 2.41%. In this case, the relative difference is most likely dominated by modeling discrepancies. The remaining 12 isotopes have results with relative differences that are less than the statistical error. Of these, six have statistical errors that indicate they are statistically credible results ($2\sigma < 10\%$). For these isotopes, the difference is most likely dominated by the statistical variations in the results, suggesting that smaller relative differences could result from improved statistics, i.e. more initial atoms.

This hypothesis was tested by performing the same calculation with 32 times as many initial atoms. In particular, there are five isotopes that represent the intersection between those isotopes that have statistically credible results ($2\sigma < 10\%$) and those that have a relative difference greater than 1%. If the relative difference for these isotopes does not decrease, it would indicate a potentially unreasonable difference between the techniques. Table 2.3 shows how both the relative difference and the statistical error change with an increased number of initial atoms. Two isotopes, ^{54}Fe and ^{56}Mn, converge to relative differences less than 1%. Two more isotopes, with relative differences initially between 1% and 2%, ^{59}Co and ^{50}Ti, converge to relative differences that remain above 1% and are larger than the 2σ statistical error. The last isotope, ^{60}Co, converges to a relative difference greater than 1% but still less than its statistical error. This suggests that the modeling discrepancy could be as large as 1.28% for some isotopes.

Figure 2.6 shows how the ratio between the Monte Carlo and the deterministic results, averaged over all 20 isotopes, varies with increasing Monte Carlo sample size. For each sample size, the average ratio for all isotopes is shown. The statistical error of this average

Isotope	10^{10} **MC Atoms**		32×10^{10} **MC Atoms**	
	Relative Difference	2σ **Statistical Error**	**Relative Difference**	2σ **Statistical Error**
^{50}Ti	1.86%	5.6%	1.18%	0.97%
^{56}Mn	4.49%	6.3%	0.65%	1.1%
^{54}Fe	2.41%	1.7%	0.46%	0.31%
^{59}Co	1.49%	3.0%	1.20%	0.54%
^{60}Co	1.15%	9.1%	1.28%	1.6%

Table 2.3 Comparing improvements in results (relative to deterministic calculation) and statistical error with increasing number of initial atoms.

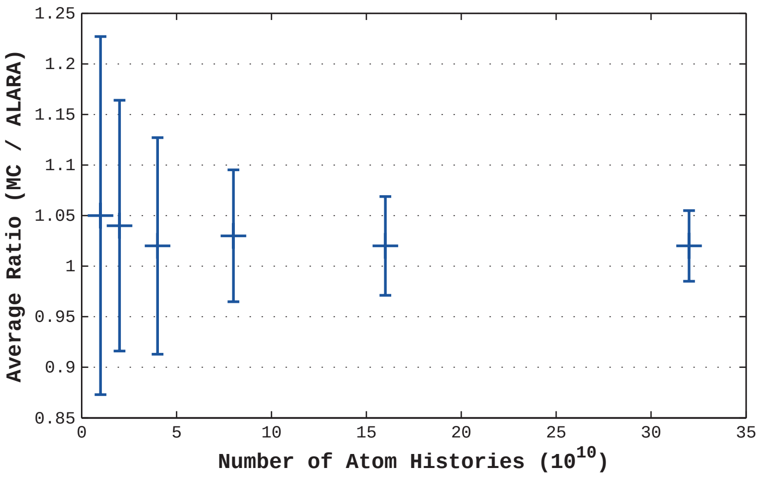

Figure 2.6 The average ratio (averaged over all isotopes) improves with more atom histories. The statistical error of the average is the root-mean-squared average of the individual statistical errors and is shown here as a 1σ statistical error.

is calculated by propagating the individual statistical errors using the standard root-mean-squared summation, and is shown with error bars representing 1σ statistical error (68% confidence). Such a plot demonstrates the (expected) steadily improving precision of the Monte Carlo results even if the mean value does not change monotonically.

Returning to the isotopes missing from the Monte Carlo results, it is important to note that their production rate according to ALARA is less than 10^{-10} in all cases. This draws attention to a fundamental limitation of atom current tallies for the analog Monte Carlo methodology — a raw detection limit that is the inverse of the number of MC atoms, N, and a statistically significant detection limit (assuming a goal of a relative statistical error, $R < 5\%$) of $400/N$. The relative statistical error for the tally of a given isotope, j, can be derived as

$$R_j = \sqrt{\frac{\sum_{i=1}^{N} x_{ij}^2}{\left(\sum_{i=1}^{N} x_{ij}\right)^2} - \frac{1}{N}}, \tag{2.9}$$

and by the definition of analog Monte Carlo, the score contribution to isotope j, x_{ij}, from a given sample atom, i, is 1 if that atom is the isotope in question and 0 otherwise. By defining the yield, Y_j, as the probability of producing isotope j from a source atom, this can be reduced to

$$\begin{aligned} R_j &= \sqrt{\frac{Y_j \cdot N}{(Y_j \cdot N)^2} - \frac{1}{N}} \\ &= \sqrt{\frac{1}{N}\left(\frac{1}{Y_j} - 1\right)}. \end{aligned} \tag{2.10}$$

Since the goal is to determine the detection limit for rare product isotopes, $Y_j \ll 1$, and

$$R_j \approx \sqrt{\frac{1}{Y_j \cdot N}} \Rightarrow Y_j \approx \frac{1}{N \cdot R_j^2} \Rightarrow N \approx \frac{1}{Y_j \cdot R_j^2} \tag{2.11}$$

statistical error of less than 5% for results with yields of 10^{-9} requires $N = 4\times10^{11}$ for an analog implementation. Moreover, if an important product isotope derives only from a single isotope, k, that has a small relative initial concentration, C_k, the statistically significant detection limit for this resultant isotope is reduced to $C_k \cdot \left(N \cdot R_j^2\right)^{-1}$. Fortunately, variance reduction techniques are available to improve this situation and this methodology is well-suited to parallelization; both will later be explored.

2.3.2 Simple, Complex and Loop Flow

A steady-state problem with a single control volume (CV) can be duplicated by a steady-state problem with two CVs in series (Figure 2.7(S1)), provided they each have identical neutron fluxes and the two residence times add to the same residence time of the single CV problem (Figure 2.7(B)). The same is true for 10 CVs in series each with 10% of the single CV residence time (Figure 2.7(S2)). This is the strategy for testing the simple flow capability.

If the second CV is replaced by two CVs in parallel (Figure 2.7(C1,C2)), each with the same neutron flux and the same residence time, valid results at the end of the two parallel CVs will have two predictable features: a) they will sum to the same as the 1 CV results, b) their ratio to each other will be equal to the flow distribution between them. Two cases are analyzed, one with a 50/50 flow split (C1) and another with a 90/10 flow split (C2). Another test of the complex flow is achieved by having the flow split and rejoin, with a total of 4 CVs and the total residence time through either path being identical to the residence time in the single (Figure 2.7(C3,C4)). The same two flow distributions, 50/50 in C3 and 90/10 in C4, are used to test this model. In this case, the final results should be the same as the single CV results and independent of the flow split.

Finally, both simple and complex loop flow can be tested by looping through short residence time CVs enough times to be equivalent (or comparable) to the single 0-D base case (Figure 2.7(L1, L2, L3)). These three cases include a simple loop (L1), a 50/50 flow split loop (L2) and a 90/10 flow split loop (L3).

Figure 2.8 summarizes the results for all 10 cases, including the steady-state base case, compared to the deterministic results from ALARA and normalized for the correct solution

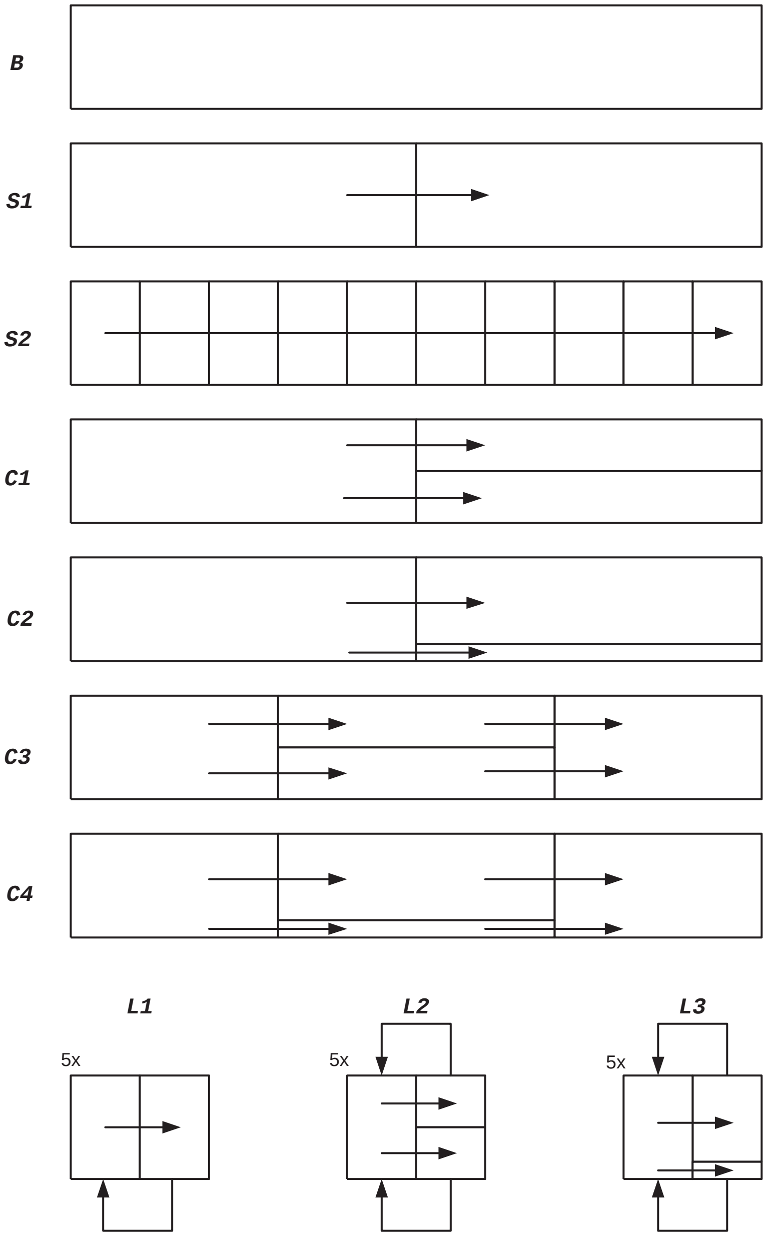

Figure 2.7 Physically equivalent/comparable test cases for testing flow capabilities.

(e.g. the case C1 [50/50 complex flow] should have a result of 0.5). In all cases, the total number of Monte Carlo atoms is 10^{10} and the error bars represent the 1σ statistical error of the mean. All results are within the statistical error of the correct result. The importance of variance reduction is further demonstrated here, especially in cases C2 and L3 where the number of atoms reaching some tally points is 10% of the total due to the 90/10 flow splitting. In general, however, this set of results serves to demonstrate the functionality of this method for this varied set of flow conditions.

2.3.3 Sources, Tallies, Decay and Sinks

With the basic elements implemented and tested, some of the enabling concepts and compound capabilities can be demonstrated. The first case demonstrates sources and sinks using a variation, shown in Figure 2.9, of the L1 loop case. A single control volume has a residence time of two years and a steady-state flux of 5×10^{12} n/cm^{2}s. A fraction, f, of the flow leaving the control volume is diverted to a sink while the rest simply returns to the control volume. The same flow rate of source material is used to make-up the flow entering the first control volume. Note that to conserve the atom volume of the control volume, the atoms that begin in the control volume must have the same simulation time ($t_{sim} = 0s$) but must have their remaining residence time, t_{rem}, distributed uniformly throughout the two-year residence time of the control volume, allowing some to leave immediately to make room for those that are entering.

Figure 2.10 shows the declining isotopic inventories of transmutation products as the loss rate, f, increases. Qualitatively, this is consistent with expectations since the average amount of time each atom spends in the control volume decreases with increasing loss rate.

In order to quantitatively benchmark these results, a mathematically equivalent problem can be constructed as the superposition of six more simple problems. The first simple problem tracks only the atoms that begin in the control volume, those with their remaining residence time, t_{rem}, uniformly distributed in the two-year time span of the control volume. Each of the atoms that are still in the control volume at the end of ten years has faced

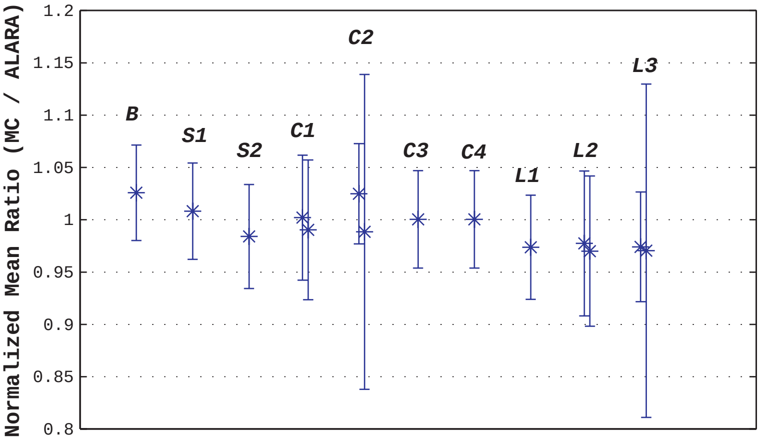

Figure 2.8 Summary of results for 10 cases shown in Figure 2.7 show that mean ratio between the Monte Carlo results and the deterministic results is within statistical error of the correct answer. The ratios have been normalized by the expected results (e.g. case C1 has an expected result of 0.5) and the error bars represent the 1σ statistical error of that mean.

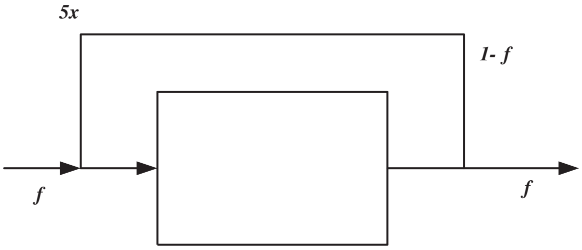

Figure 2.9 Test case for sources and sinks shows a fraction, f, of the flow being diverted to a sink and a corresponding make-up flow.

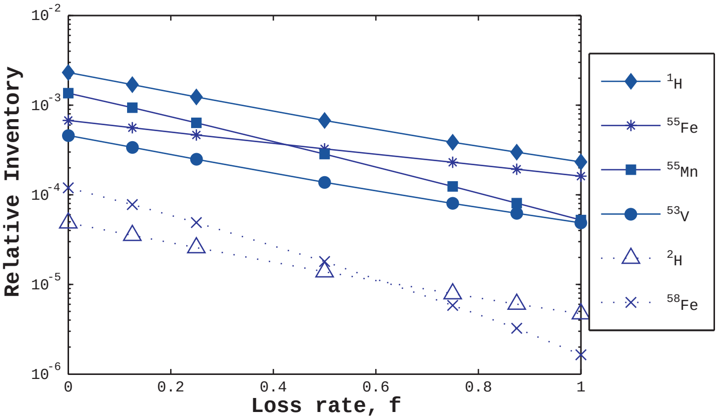

Figure 2.10 Relative isotopic inventories for a select sample of isotopes. Declining transmutation rates accompany a higher loss rate in source/sink problems because the average atom spends less time in the neutron flux.

five decisions about whether or not to leave the system, and chosen, with probability $1 - f$, to remain each time. More importantly, those that have remained have been exposed to a constant flux for 10 years, regardless of the initial value of t_{rem}, so that the contribution from these atoms is simply

$$[g_i^B(10y)](1-f)^5, \tag{2.12}$$

where $g_i^B(10y)$ is the solution to the base single CV case for isotope, i. The other five simple problems track the atoms that are introduced during each of the five 2-year periods, facing successively fewer decision points about whether or not to stay in the system. More specifically, during each of the 2-year periods, the atoms enter with the same remaining residence time, $t_{rem} = 2y$, but with a simulation time, t_{sim}, uniformly distributed between $2(j-1)$ and $2j$ years, where $j = [1, 5]$, and are tallied at $t_{sim} = 10y$. By simple variable transformation, this can instead be considered as five problems in which all the initial atoms have $t_{rem} = 2y$, t_{sim} uniformly distributed between 0 and 2 years, and tallied at $2j$ years. Thus, the results of a single such problem with a tally at 2, 4, 6, 8, and 10 years, $g_i^{(2)}(t)$, will provide the necessary information to include these contributions. Each of the contributions is thus

$$f \cdot [g_i^{(2)}(j \cdot 2y)](1-f)^{(j-1)}, \tag{2.13}$$

where j=[1,5]. The benchmark solution for the fully modeled loop extraction case shown in Figure 2.9 will therefore be the results of this six source superposition

$$g_i^{bench} = [g_i^B(10y)](1-f)^5 + f\sum_{j=1}^{5}[g_i^{(2)}(j \cdot 2y)](1-f)^{(j-1)}. \tag{2.14}$$

Figure 2.11 shows the relative difference between the test case and the benchmark case for three different loss rates, 0, 0.5 and 1. While numerical results $g_i^B(t)$ have been described above, a simple Monte Carlo problem was performed to generate results for the $g_i^{(2)}(t)$ problem. The 2σ statistical error in this case is found by combining the 2σ errors for the test case and the benchmark case in quadrature since both are Monte Carlo calculations. These results show the expected level of agreement, with most isotopes falling within the 2σ error for all values of f.

The functionality of the two tally types was compared by performing the base case, B, with both a current tally every 0.5 years and a population tally with 0.5 year bins. Over the 10 year simulation time, the current tally detected 20 isotopes while the population tally detected 26. For the 20 common isotopes, the two tallies produce nominally the same results but differ in their precision depending on the half-life of the isotope in question. For relatively short-lived isotopes (those with half-lives less than 0.5 y in this case) the population tally is more precise than the current tally, sometimes significantly. The population tally is nearly 25 times more precise than the current tally for ^{56}Mn with a 3.6 h half-life. For longer-lived or stable isotopes, the current tally is slightly more precise, typically by a multiple of 1.25 or less, and decreasing at later times. The six isotopes missed by the current tally are all present in the population tally at levels below 10^{-11} (below the detection limit) and all had half-lives below 11 minutes.

This half-life dependent behavior is a natural consequence of the tallying methods. The population tally detects all isotopes that occur within its time bin no matter when they occur and for how long they occur while the current tally only detects isotopes that occur when the atom crosses a certain point in time. Thus current tallies are less likely to detect the presence of a short-lived isotope. Conversely, long-lived isotopes that build up slowly throughout the simulation are rare at early times and only contribute over a fraction of a time bin to population tallies while they contribute a uniform (unit) amount to current tallies. Even if the same number of atoms is detected by the two tallies, at early times the population tally will have a more statistically diverse set of contributions than the current tally.

Finally, the ability to model post-irradiation decay time, where the isotopes are not subjected to a flux was demonstrated by adding a 100-year cooling time to the base case, B. This is implemented simply as a control volume with uniformly zero flux and a 100-year residence time. Figure 2.12 shows the relative difference between the MC results and the deterministic (ALARA) results, as a function of the deterministic result, for three times: shutdown, 10 years post-shutdown and 100 years post-shutdown.

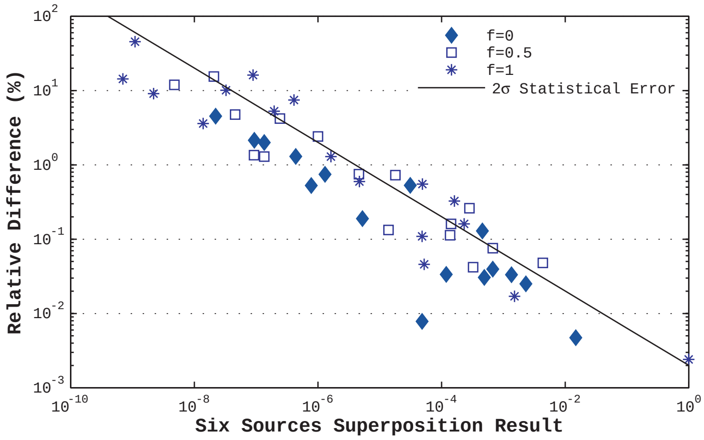

Figure 2.11 A comparison of relative difference as a function of the benchmark result compared to the statistical error shows agreement for values of f=0, 0.5, and 1.

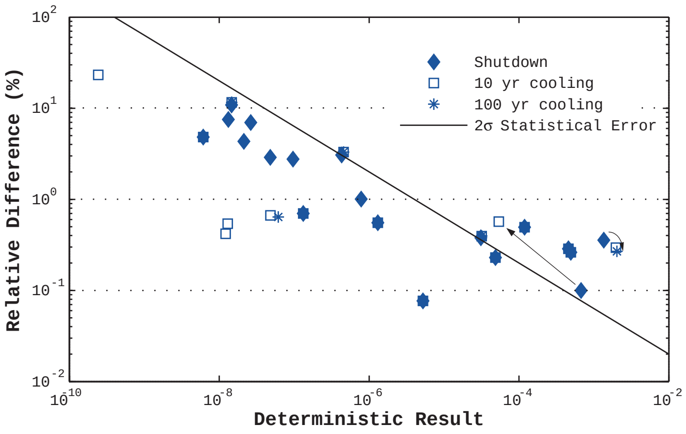

Figure 2.12 Relative difference as a function of deterministic result for shutdown and two difference cooling times for a 10-year steady-state irradiation of ^{56}Fe. Two arrows demonstrate the decay of ^{55}Fe resulting in the accumulation of ^{55}Mn.

The results are consistent with the previous analyses. All results are either within 1% of the deterministic result or within 2σ statistical error of the deterministic result. Additionally, however, the impact of the statistical error in closely matching results can be seen in the simple decay paths. Figure 2.12 includes an indication of the decay of ^{55}Fe to ^{55}Mn in this representation. One arrow shows the decay of ^{55}Fe ($t_{\frac{1}{2}} = 2.73$ years) over the first 10 years (the Monte Carlo results do not include any ^{55}Fe after 100 years) while the other arrow shows the accumulation of additional ^{55}Mn as a result of this decay. In both cases, the relative difference between the MC results and the deterministic result changes as the inventories change, most clearly in the ^{55}Fe case. Pure (deterministic) exponential decay based on the same decay constant, would result in a relative difference that is independent of time. The changing relative difference here reflects the role of the statistical uncertainty as a contribution to the total relative difference. As the decay occurs, the contribution from statistical uncertainty changes while the contribution from the modeling differences is likely unchanged.

2.3.4 Parallel Performance

As indicated above, the analog Monte Carlo methodology has clear limits on its detection precision that can only be overcome by sampling more atoms. Fortunately, this type of problem is straightforward to parallelize with good performance. Two different approaches can be used to demonstrate this: problems of fixed total work (i.e. work per processor decreases) and problems of fixed work per processor (i.e. total work increases). Table 2.4 and Table 2.5 show the performance for each of these approaches, respectively, on a typical Linux cluster (1.4 GHz AMD Athlon, 512 MB RAM, 100 Mbps LAN).

In both tables, *wall time* refers to the time that a user would wait for the code to produce results where *cpu time* refers to the amount of computational resources used to produce those results. Such high parallel performance allows for improved statistical results by simply adding more computers to a computing cluster; however, given the scaling of

Number of Processors	**Wall Time (seconds)**	**CPU Time (seconds)**	**Speedup**	**Efficiency (percent)**
1	941.496	941.496		
2	475.556	951.070	1.980	98.989
4	241.665	966.370	3.896	97.397
8	122.296	977.347	7.699	96.231
10	98.553	984.341	9.553	95.532

Table 2.4 Summary of computing efficiency as different numbers of processors were used on the same problem. Nearly 100% parallel efficiency can be achieved for problems of fixed total work.

Number of Processors	**Number of Atoms (10^6 particles)**	**Wall Time (seconds)**	**CPU Time (seconds)**
1	30	279.808	279.808
2	60	283.064	566.075
4	120	282.777	1130.767
8	240	284.041	2271.366
10	300	282.929	2828.671

Table 2.5 Constant run-time can be achieved for problems with fixed work per processor.

statistical error with the number of particles in analog Monte Carlo simulation, only modest gains can be realized in this fashion.

2.4 Summary

A new methodology has been developed and implemented for the simulation of changing isotopic inventories in nuclear systems, particularly those with material flowing in arbitrary paths through the system. The current tool focuses primarily on "activation type" problems where the change in isotopics is assumed to have negligible impact on the neutron flux. The current implementation includes the ability to simulate simple, complex and loop flows, and any combination of those. These advanced abilities can then be used to implement features of real systems including sources, sinks, post-irradiation decay and extraction processes.

Pure analog calculations are limited in the relative inventories they are able to detect, either absolutely or statistically. Without implementing variance reduction techniques, large numbers of source atoms must be modeled requiring either long runtimes or large parallel clusters to achieve necessary precision. In the following chapter, many variance reduction techniques are being explored and expected to improve the ability of this method to provide useful results in a broader range of problems.

Chapter 3

Variance Reduction Techniques

3.1 Introduction

The early benchmarks of analog results with results from a well-validated activation code in various flowing schemes were found to be successful. At the early stage, using a large number of sampled atoms, which requires long runtimes or large parallel clusters, was the only means to improve precision. It was intuitively simple as it eliminated the need to modify an existing code or exploit the physics of the problem. However, this approach was not always favorable as the computing time was linearly proportional to number of sampled atoms and the detection limit might not be improved quickly enough. An effort to develop variance reduction techniques as alternatives to improve precision has been investigated. Variance reduction techniques are applied to improve statistical precision of the analog Monte Carlo method by modifying the underlying probability distributions that govern Monte Carlo processes so that the desired effects are produced more frequently. The importance or weight of each particle must be adjusted to obtained unbiased results.

Several variance reduction techniques have been explored and are expected to provide useful results in a broad range of problems. Each has its own unique implementation and capability for different types of problems. Accuracy and precision improvement will be thoroughly evaluated by specifically designed test problems for each variance reduction technique. The test problems here are traditionally simple so that results from a traditional code, ALARA in this case, can be used to benchmark results from Monte Carlo simulations. The efficiency enhancement will not be discussed until after the appropriate efficiency measurement tool is developed.

3.2 Forced Reaction

In the activation analysis, isotopes with low inventories are sometimes the most concerning. The results of these isotopes are not reliable due to their production nature. They often occur in the reaction tree which has an isotope with a very low total effective reaction rate coefficient in front of them. Based on a current analog calculation, the Monte Carlo simulation spends an inordinate amount of time to follow a history of this almost stable isotope without advancing further into the reaction tree. Even though some Monte Carlo particles manage to transmute through this isotope, a small overall contribution yields poor statistical results for all consequent isotopes. A variance reduction technique, forced reaction (FR), improves the precision of low-production isotopes by requiring an atom to undergo a specified number of reactions in a control volume. The weight is adjusted accordingly by considering how likely each of the forced reactions would be. This technique increases the contributions not only from the isotopes produced after an almost stable isotope but also from the isotopes produced after many reactions.

3.2.1 Methodology

The forced reactions technique is directly analogous to the forced collision technique common in Monte Carlo radiation transport methods [12]. The forced reaction technique is based on sampling the mean time needed by an atom to undergo a reaction from the conditional probability that the reaction is to occur within the remaining residence time, t_{rem}, of a control volume. The underlying probability distribution can be described by an exponential distribution with a parameter λ_{eff} where λ_{eff} is a total effective reaction rate coefficient of a current atom entering a control volume. If t is a random variable that represents the amount of time the atom resides before having a reaction, the probability density function is then given by

$$f(t) = \lambda_{eff} e^{-\lambda_{eff} t} \qquad , t \geq 0 \tag{3.1}$$

A reaction time, t_{rxn}, can then be randomly sampled from the conditional probability density. Given that the reaction occurs within the remaining residence time of the control volume, t_{rem}, the probability that the atom will spend t_{rxn} before undergoing a reaction is given by:

$$\begin{aligned} P(t \leq t_{rxn} | t \leq t_{rem}) &= \frac{P((t \leq t_{rxn}) \cap (t \leq t_{rem}))}{P(t \leq t_{rem})} \\ &= \frac{P(t \leq t_{rxn})}{P(t \leq t_{rem})} \qquad \because t_{rxn} \leq t_{rem} \\ &= \frac{1 - e^{-\lambda_{eff} t_{rxn}}}{1 - e^{-\lambda_{eff} t_{rem}}} \end{aligned} \tag{3.2}$$

If ξ is a uniform random variable in [0,1), t_{rxn} can be calculated by inverting the above conditional cumulative density function.

$$t_{rxn} = -\frac{1}{\lambda_{eff}} \ln[1 - \xi(1 - e^{-\lambda_{eff} t_{rem}})] \tag{3.3}$$

Consequently, a number of mean reaction times until the next reaction, n_{rxn}, can be obtained.

$$n_{rxn} = \lambda_{eff} \cdot t_{rxn} = -\ln[1 - \xi(1 - e^{-\lambda_{eff} t_{rem}})] \tag{3.4}$$

To ensure an unbiased simulation, a Monte Carlo particle with an initial weight, w_0, must be split into two particles: a reacted particle and a non-reacted particle with weights, $w_{reacted}$ and w_{non}, respectively. Both particles have the same identity as the initial particle. The weights of both particles depend on how likely the atom will undergo a reaction and both weights are added up to be w_0.

$$\begin{aligned} w_{reacted} &= w_0 \cdot P(t \leq t_{rem}) \\ &= w_0 \cdot \int\limits_0^{t_{rem}} f(t)\, dt \\ &= w_0 \cdot \int\limits_0^{t_{rem}} \lambda_{eff} e^{-\lambda_{eff} t}\, dt \\ &= w_0(1 - e^{-\lambda_{eff} t_{rem}}) \end{aligned} \tag{3.5}$$

$$\begin{aligned} w_{non} &= w_0 \cdot P(t > t_{rem}) \\ &= w_0 \cdot \int\limits_{t_{rem}}^{\infty} f(t)\, dt \\ &= w_0 \cdot \int\limits_{t_{rem}}^{\infty} \lambda_{eff} e^{-\lambda_{eff} t_{rem}}\, dt \\ &= w_0 e^{-\lambda_{eff} t} \end{aligned} \tag{3.6}$$

The non-reacted particle will leave the control volume without having a reaction while the reacted particle will be forced to transmute within the control volume at the sampled t_{rxn}.

The forced reaction is controlled by the *forced reaction parameter*, which defines how many times a reaction is forced in a given control volume. While the forced reaction parameter is still greater than zero, another forced reaction will occur and the *forced reaction parameter* will be decremented by one.

3.2.2 Test Problems

The precision(statistical error) and accuracy(difference from reference) of FR were tested by calculating the inventory at shutdown following a 10-year steady-state irradiation of ^{56}Fe with a uniform multi-group neutron flux of 5×10^{12} n/cm^{2}s. The results from five non-analog test cases were compared to the analytical results by ALARA using a truncation tolerance of 10^{-9}. The test cases with 10^{10} atoms had different forced reaction parameters: 1, 2, 3, 5 and 8. In all cases the FENDL-2/A activation library and FENDL-2/D decay library were used.

3.2.3 Simulation Results

The analytical result yields 39 isotopes but only 26 isotopes are produced at levels above the absolute analog MC detection limit (10^{-10}) and only 21 are above the 10% detection limit[1] (10^{-8}) whereas the Monte Carlo analog case produces 26 isotopes. As the forced reaction parameter increases from 1 to 8 in non-analog cases, very rare/deep reaction pathways are followed, producing isotopes at levels far below the relative production tolerance used to truncate the ALARA calculation, and increasing the number of isotopes from 34 to 94, respectively. For non-analog cases, the number of isotopes that have a relative statistical error less than 10% increases from 25 to 46. Some characteristics of the results are summarized in Table 3.1. Figure 3.1 shows the average relative differences for 26 isotopes common to all cases, with error bars representing the 2σ statistical error of their respective means. It is important to note that based on this metric alone, the effectiveness of forced reaction technique reaches a saturation limit, in this case, when a forced reaction parameter is three. This suggests two possible scenarios. First, these 26 isotopes occur within three reactions of the ^{56}Fe root in the activation tree. Once the forced reaction parameter is greater than three, the additional forced reactions do not contribute significantly to their tallies. Second, there might be a number of isotopes with relatively low total effective reaction rate coefficients, occurring within three reactions from the initial isotope, ^{56}Fe; therefore, the effects of additional forced reactions greater than three are not relevant. Since there is no significant improvement after increasing force parameter beyond three, it is likely that a number of inert isotopes occur at the third ranks of the reaction tree. These species limit the depth of the reaction tree of the problem.

---

[1] The k-percent detection limit is later defined and discussed in 4.3.3

Category	**ALARA**	**Monte Carlo**					
		Analog	**1**	**2**	**3**	**5**	**8**
A number of products (n)	39	26	34	42	57	71	94
n > 10% detection limit	21	26	27	26	26	26	26
n < 10% statistical error	-	21	25	29	35	44	46
Mean statistical error	-	4.90%	1.97%	1.97%	0.47%	0.46%	0.52%
Mean relative difference	-	5.53%	1.71%	1.87%	1.16%	1.21%	1.26%

Table 3.1 Comparisons of different characteristic numbers of products between the analytical result and Monte Carlo results governed by six forced reaction parameters. The mean reative differences and mean statistical errors are derived from twenty-six isotopes common in all cases.

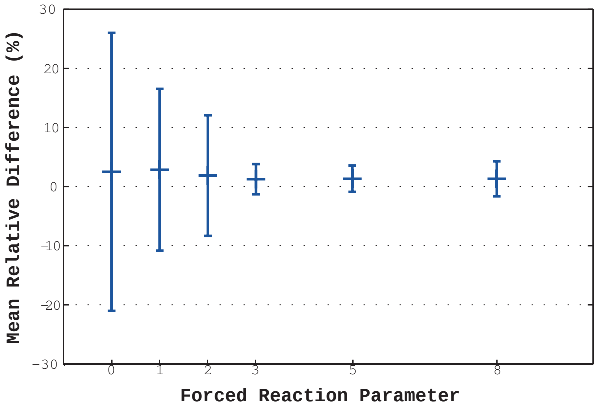

Figure 3.1 Average relative differences (%) from an analog case and five non-analog cases are compared. The error bars represent 2σ statistical errors.

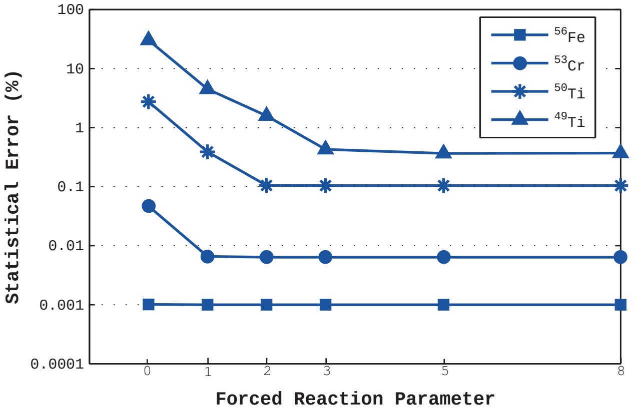

Figure 3.2 The statistical errors of products in one reaction chain of ^{56}Fe as a function of force parameter.

To further illustrate the effectiveness/limitations of forced reaction technique in reducing the statistical errors of specific isotopic products, the sample reaction chain of ^{56}Fe–^{53}Cr–^{50}Ti–^{49}Ti was investigated. Figure 3.2 shows the statistical errors of four isotopes as a function of the number of forced reactions. As the number of forced reactions increases, the statistical errors of the products deeper in the chain are improved while the statistical errors of the earlier isotopes reach their minima. Forcing an additional reaction will only reduce the variance of deeper products in the reaction chain. Hence, each daughter's statistical error reaches its minimum at different numbers of forced reactions depending on its position in the reaction chain. The forced reaction technique is effective at increasing the number of isotopes with statistically significant results, but its effectiveness for any given isotope is limited. This suggests that other variance reduction techniques are needed.

3.3 Biased Reaction Branching

As a simulated atom undergoes a reaction, it will be assigned a new isotopic identity by sampling a discrete random variable representing a list of possible products whose probability density is characterized by the effective reaction rates for each reaction pathway. The product isotopes with small effective reaction rates will rarely be selected. Consequently, those isotopes and their respective daughters usually have results with high statistical variance. *Biased reaction branching* is introduced to increase the occurrences of the products with low branching probabilities. The technique is based on sampling products from a modified probability density and adjusting the weight by considering the natural likelihood of the selected product. Without a significant increase in the number of simulated particles, the reaction tree will become broadened and thus contain a higher number of isotopic products. The modified probability density can be biased in many ways, including one special case that biases towards a specific isotopic product and another that creates a uniform probability for each product.

3.3.1 Methodology

In a control volume v, the branching ratio for a reaction from a parent isotope, x_i, to a daughter isotope, x_j, is defined as

$$P_{ij} = \frac{\lambda^v_{ij,eff}}{\lambda^v_{i,eff}} \tag{3.7}$$

where $\lambda^v_{ij,eff}$ is the effective reaction rate coefficient for the specific reaction path and $\lambda^v_{i,eff}$ is the total effective reaction rate coefficient for the parent isotope. The subscript, *eff*, and superscript, v, will be suppressed for simplicity. Given that the isotope x_i undergoes a reaction in an analog problem, the branching ratio, P_{ij}, is the relative probability that the isotope x_i will transmute to the isotope x_j.

The biased reaction branching technique alters the probability of transmuting x_i to x_j by multiplying by a *biasing score*, s_{ij}. The weight is adjusted accordingly to ensure a fair game. Let X be a random variable representing the choice of the product isotope, N be a total number of possible isotopic products from the parent, x_i, and w_0 be the initial weight of the atom. The biased probability of sampling the product x_j with a weight, w_j, as a resulting product is given by

$$B_{ij} = P(X = x_j) = \frac{s_{ij} P_{ij}}{\sum_{k=1}^{N} s_{ik} P_{ik}} \tag{3.8}$$

$$w_j = w_0 \frac{P_{ij}}{B_{ij}} \tag{3.9}$$

It can easily be shown that the above formulations conserve the overall weight of Monte Carlo particles by showing that the expected value of W is the same for the analog and non-analog case.

$$\begin{aligned} E(W) &= \sum_{k=1}^{N} w_k \cdot P(W = w_k) = \sum_{k=1}^{N} w_k \cdot B_{ik} \\ &= w_0 \sum_{k=1}^{N} \frac{P_{ik}}{B_{ik}} \cdot B_{ik} = w_0 \sum_{k=1}^{N} P_{ik} = w_0 \end{aligned}$$

Additionally, a fair game can be demonstrated by calculating the expected value of W_j. The expectation of W_j corresponds to the branching ratio of the product, x_j, multiplied by the initial weight.

$$E(W_j) = w_j \cdot P(W = w_j) = w_j \cdot B_{ij} = w_0 \frac{P_{ij}}{B_{ij}} \cdot B_{ij} = w_0 P_{ij}$$

Uniform reaction branching is a special case for biased reaction branching when s_{ij} is equal to $1/P_{ij}$. Each product is sampled with equal biased probability, $B_{ij} = 1/N$, and the weight is multiplied by that product's branching ratio multiplied by the total number of isotopic products, $N \cdot P_{ij}$.

3.3.2 Test Problems

The inventories at shutdown following a 10-year steady state irradiation of ^{56}Fe with a uniform multi-group neutron flux of 5×10^{12} n/cm^{2}s were calculated from three test problems with different reaction sampling schemes. The first problem was a pure analog test problem while the second problem had a uniform reaction branching technique applied and the third problem was designed to improve the results of ^{53}Mn. If ^{53}Mn was present as a product, the

Category	**Analog**	**Uniform Reaction Branching**
A number of products (n)	26	63
n < 5% statistical error	17	19
Mean statistical error	1.58%	1.84%
Mean relative difference	0.91%	2.13%

Table 3.2 Comparisons of different characteristic numbers of products between the analog result and the results from a uniform reaction branching. The mean relative differences and mean statistical errors are derived from those with statistical error less than 5% in each case.

biased reaction rates were calculated by increasing the ^{53}Mn reaction rate by a factor of ten and renormalizing the set of reaction rates. The test cases were simulated with 10^{10} Monte Carlo particles and FENDL-2/A activation library and FENDL-2/D decay library were used throughout. In addition, the results were compared with deterministic results from ALARA using the truncation tolerance of 10^{-9}.

3.3.3 Simulation Results

Table 3.2 compares the results between the analog problem and the non-analog test problems. The analog problem produced 26 isotopes, including ^{56}Fe. Of these, 17 have statistical errors less than 5%. When compared to deterministic results, the average relative difference of these seventeen isotopes was 0.91%. As expected, the test problem with uniform reaction branching produced a much wider spectrum of isotopes than did the analog test problem. Sixty-three isotopes were produced and 19 of these have statistical errors less than 5%. The average relative difference of these isotopes was found to be 2.13%. The variance of some isotopes increased, in comparison to the analog case, because the uniform reaction branching approach biases the solution away from those previously likely isotopes. In some cases, this also resulted in larger deviations from the deterministic solution.

In particular, there were 15 isotopes from each case that had a statistical error less than 5%. The analog problem had two isotopes that were not detected by the uniform reaction branching problem. They were ^{59}Co and ^{60}Co because they occurred at least five reactions from the initial isotope, ^{56}Fe, and the uniform reaction branching widened and implicitly shortened a reaction tree for the same number of Monte Carlo particles as the analog case. Since the analog case allowed more histories to follow the reaction pathways with high reaction rates, more histories were able to reach deep isotopes in the reaction tree. On the other hand, the uniform reaction branching case produced four new isotopes with statistical errors less than 5%. These isotopes(^{3}H, ^{3}He, ^{51}V and ^{53}Mn) were produced in the analog case with extremely high statistical errors, as high as 44% for ^{3}He. Those results were statistically improved in the uniform reaction branching case because the technique increased contributions from isotopes that were produced through reaction paths with low probability. The light ions, ^{3}H and ^{3}He, benefitted most from the technique because they were produced with low probability at many locations throughout the reaction tree.

In order to study the impact of biased reaction branching on a single isotope, the results for ^{53}Mn were studied. In the analog problem, the statistical error (precision) and the difference relative to the deterministic solution (accuracy) were 13.36% and 8.20%, respectively. The substantial variance for this solution suggested that applying a variance reduction technique to improve precision would likely also lead to a better accuracy of the result. With uniform reaction branching, both precision and accuracy improved, to 3.24% and 2.68% respectively. However, the reaction branching biased specifically toward ^{53}Mn did not perform better than the uniform case as precision and accuracy became 4.92% and 7.84%.

The reaction chains of ^{53}Mn from both cases were carefully examined to explain larger errors of the biased reaction branching problem. The test problem with uniform reaction branching produced sixty-seven reaction chains leading to the production of ^{53}Mn while the biased test problem generated only five such chains, all of which were included in the uniform case. Based on a small number of reaction chains of ^{53}Mn in the latter case, lack of accuracy and precision in the ^{53}Mn result was a direct consequence of the technique's inability to

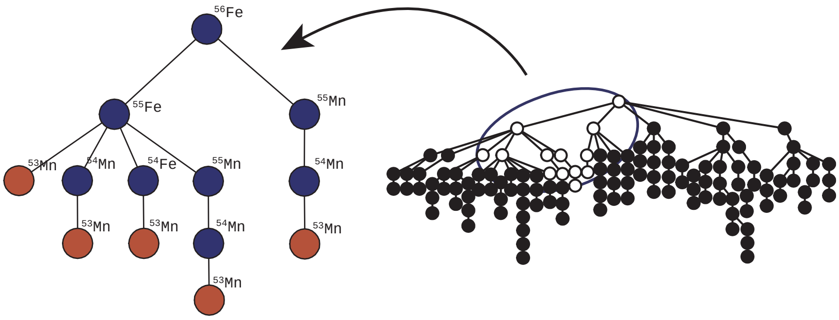

Figure 3.3 Most of the reaction chains leading to productions of ^{53}Mn from a uniform-branching problem, including all five chains from a biased-branching problem (○), are shown. The latter case fails to include most ^{53}Mn's production pathways and thus results in much higher errors.

detect the ^{53}Mn productions through reaction paths containing isotopes with relatively low total effective reaction rate coefficients. Examples of those reaction chains are given below:

$$^{56}\mathrm{Fe} \rightarrow {}^{56}\mathrm{Mn} \rightarrow {}^{56}\mathrm{Fe} \rightarrow {}^{55}\mathrm{Fe} \rightarrow {}^{54}\mathrm{Fe}. \rightarrow {}^{53}\mathrm{Fe} \rightarrow {}^{53}\mathrm{Mn},$$

$$^{56}\mathrm{Fe} \rightarrow {}^{54}\mathrm{Mn} \rightarrow {}^{53}\mathrm{Mn} \rightarrow {}^{52}\mathrm{Mn} \rightarrow {}^{53}\mathrm{Mn} \rightarrow {}^{54}\mathrm{Mn} \rightarrow {}^{53}\mathrm{Mn},$$

$$^{56}\mathrm{Fe} \rightarrow {}^{54}\mathrm{Mn} \rightarrow {}^{53}\mathrm{Mn} \rightarrow {}^{54}\mathrm{Mn} \rightarrow {}^{53}\mathrm{Mn} \rightarrow {}^{54}\mathrm{Mn} \rightarrow {}^{53}\mathrm{Mn},$$

$$^{56}\mathrm{Fe} \rightarrow {}^{54}\mathrm{Mn} \rightarrow {}^{55}\mathrm{Mn} \rightarrow {}^{55}\mathrm{Cr} \rightarrow {}^{55}\mathrm{Mn} \rightarrow {}^{54}\mathrm{Mn} \rightarrow {}^{53}\mathrm{Mn},$$

$$^{56}\mathrm{Fe} \rightarrow {}^{55}\mathrm{Mn} \rightarrow {}^{56}\mathrm{Mn} \rightarrow {}^{56}\mathrm{Fe} \rightarrow {}^{55}\mathrm{Fe} \rightarrow {}^{54}\mathrm{Mn} \rightarrow {}^{53}\mathrm{Mn},$$

$$^{56}\mathrm{Fe} \rightarrow {}^{54}\mathrm{Mn} \rightarrow {}^{53}\mathrm{Mn} \rightarrow {}^{52m}\mathrm{Mn} \rightarrow {}^{52}\mathrm{Mn} \rightarrow {}^{52m}\mathrm{Mn} \rightarrow {}^{52}\mathrm{Mn} \rightarrow {}^{53}\mathrm{Mn}.$$

Biasing only towards the target isotope fails to increase the probability of these relatively rare precursor pathways, whereas uniform reaction branching raises the probability of rare pathways and reduces the probability of likely pathways. Therefore, biasing a reaction tree toward a particular isotope does not always maximize the accuracy and precision of its result as the technique tends to underestimate significant contributions to the isotope's inventory from other reaction pathways. Defining a set of appropriate biasing scores that optimizes the accuracy and precision of the isotope in question is a research challenge and might require prior knowledge of the whole reaction tree and the extensive use of *figure of merit* that will later be discussed.

3.4 Biased Source Sampling

Currently, the source is implemented by randomly sampling an isotopic identity and a birth time from a probability density representing the isotopic compositions of the initial material and from a time-dependent source strength, respectively. The simplest form is the 0-D steady state source which is composed of a single isotope and the birth time is characterized by a delta function. However, it is often not the case in a real world problem, where the initial material can be composed of hundreds different isotopes. With analog source sampling, isotopes with low concentrations give way to relatively small numbers of sampled atom source, leading to statistically poor results for their respective products. The *biased source sampling* technique is introduced to help increase the likelihood of sampling the rare isotopic compositions. As a result, the technique reduces the statistical errors of those products derived from rare initial isotopes. For example, the sampling mechanism can be uniform among isotopic compositions or biased in favor of a specific isotope.

3.4.1 Methodology

The weight of the starting particle will be adjusted according to its real relative concentration and biasing score. The implementation of this technique is strongly analogous to the biased reaction branching technique with source compositions, atomic fractions and the number of initial isotopes replacing reaction products, branching ratios and the number of possible products, respectively. Formulations of biased source sampling hence are omitted here.

3.4.2 Test Problems

The ability of biased source sampling to improve results of product isotopes transmuted from rare initial isotopes was tested by studying the inventory at shutdown following a 10-year steady state irradiation of natural iron(91.75% ^{56}Fe, 5.85% ^{54}Fe, 2.12% ^{57}Fe and 0.28% ^{58}Fe) with a uniform multi-group neutron flux of 5×10^{12} n/cm^{2}s. Three test problems with different sampling schemes were conducted. The first problem was a pure analog test problem. The second one was a test problem with a uniform sampling technique and the third one had its source biased toward ^{58}Fe, which was the least abundant isotope in the source. The test cases were simulated with 10^{10} Monte Carlo particles and FENDL-2/A activation library and FENDL-2/D decay library were used. In addition, the results were compared with deterministic results from ALARA, which solved the activation problems of each initial source isotope individually to the specified truncation tolerance of 10^{-9}.

3.4.3 Simulation Results

The test problem with *uniform source sampling* technique applied was expected to equally distribute initial Monte Carlo particles among isotopic source compositions. Isotopes with relatively high concentrations would be chosen less frequently; therefore, the statistical errors of their respective products would be higher than results from an analog problem. At the same time, the occurrences of the rare source isotopes would be more favorable and would yield results with lower statistical errors than those from an analog problem. As a result, the overall variation in statistical errors of isotopic products would be smaller. The uniform source sampling problem produced 41 products and 27 of those had statistical errors less than 5% while the analog problem yielded 35 products with 26 products having statistical errors less than 5%. Figure 3.4 compared the results from both problems to the deterministic results by showing the relative differences of results with statistical errors less than 5% as a

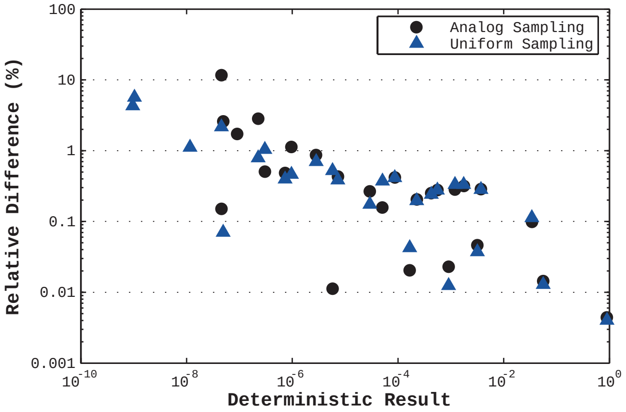

Figure 3.4 Relative Differences between Monte Carlo results with statistical errors less than 5% and deterministic results as a function of the deterministic result.

function of the deterministic results. Slight improvements on both accuracy and precision were achieved as the average relative differences were found to be 0.7582% and 0.9646% and the statistical errors of the averages were 1.32% and 1.79% for uniform source sampling results and analog results, respectively.

It is important to note that *uniform source sampling* is simply equivalent to performing calculations on individual isotopic compositions independently and weight-averaging all of the results, according to their initial source concentrations. The technique is only useful in a problem where there is no target isotope or the overall statistical improvement is desired.

The last test problem was designed to evaluate the capabilities of *biased source sampling.* It was aimed to increase the sampling frequency of the least abundant isotope, ^{58}Fe, and thus reduce statistical errors of its products. ^{59}Fe was a direct product of ^{58}Fe and had a statistical error of 1.27% from an analog problem with 10^{10} particles. The test problem was set up such that ^{58}Fe was likely to be sampled three times as often as the other isotopes combined. As a result, the statistical error of ^{59}Fe was reduced to 0.08% with the same number of simulated particles. However, the statistical error of about 1.20% could be achieved in the biased problem using only 5×10^7 particles. In this case, the computing time was reduced by about two orders of magnitude; however, the improvement of ^{59}Fe's result came at the expense of the other isotopic results' statistical qualities.

3.5 Reaction Path Splitting

As mentioned earlier, a new isotopic identity for a current atom undergoing a reaction is obtained from randomly sampling a probability density function made of a list of possible daughters and a corresponding list of effective reaction rate coefficients. This sampling mechanism results in fewer histories for those daughters with smaller effective reaction rate coefficients. Even though *Biased Reaction Branching* could be used to increase frequencies of such histories, it could essentially create another statistical problem by sampling fewer histories of unbiased isotopes. Moreover, it could also introduce a weight factor substantially larger than one. *Reaction Path Splitting* is implemented to allow a simulation to track down every possible reaction pathway by splitting the atom having a reaction into as many new atoms as the number of pathways and adjusting their weights relatively according to their actual effective reaction rate coefficients. While the technique might still produce large variations in weight factors, it would ensure that all histories of reaction products are followed, regardless of the effective reaction rate coefficients.

3.5.1 Methodology

At a reaction point of a parent isotope, x_i, the atom will be split into x_1, x_2, x_3, ..., x_k, where k is the total number of possible products. A weight, w_j, of each newly created atom must be adjusted, based on the initial weight, w_0 and the branching ratio, P_{ij}, which was previously defined in Equation (3.7).

$$w_j = w_0 \cdot P_{ij} \qquad\qquad j = 1, 2, 3, ..., k \tag{3.10}$$

It can easily be shown that the overall weight is conserved after a splitting process.

$$\begin{aligned}\sum_{j=1}^{k} w_j &= \sum_{j=1}^{k} (w_0 \cdot P_{ij}) \\ &= w_0 \sum_{j=1}^{k} P_{ij} \\ &= w_0\end{aligned}$$

3.5.2 Test Problem

The isotopic inventories following a 10-year steady state irradiation of ^{56}Fe with a uniform multi-group neutron flux of 5×10^{12} n/cm^{2}s were obtained from a test problem in which *Reaction Path Splitting* was applied. FENDL-2/A activation library and FENDL-2/D decay library were used in the simulation.

3.5.3 Simulation Results

The test problem with 15000 simulated particles and a computing time of 524 seconds produced 82 isotopes while the analog problem with a comparable computing time produced 22 isotopes. Table 3.3 quantitatively compares results between the test problem and the analog problem. The test problem detected isotope productions ranging from 9.7780×10^{-54} to 9.8299×10^{-1} with statistical errors of 100% and 0.8227%, respectively. For the analog problem to have a chance to detect this minute production, the problem would require at least 1.0227×10^{53} particles or 4.0908×10^{55} if a statistical error of less than 5% were desired, according to Equation (2.11). Moreover, most isotopes in the test problem were tallied with statistical errors above 10% whereas there were only five such isotopes in the analog case. Based on this metric, the analog case seemed to reach its saturation limit in terms of precision improvement. This suggested that increasing the number of simulated particles in the analog case would not improve the overall precision as much as it would in the test problem. The *reaction path splitting* technique clearly improved the detection limit without spending too much computational effort on the problem while the technique also ensured that every reaction pathway was followed in an event of the atom having a reaction.

To evaluate the validity of the *reaction path splitting* technique, only statistically reliable results of nine isotopes were compared to deterministic results from ALARA. Relative differences and statistical errors were plotted as a function of deterministic results as shown in Figure 3.6. In all cases, the relative differences were less than 5% and, more importantly, lower than statistical errors which indicated that the discrepancies were likely dominated

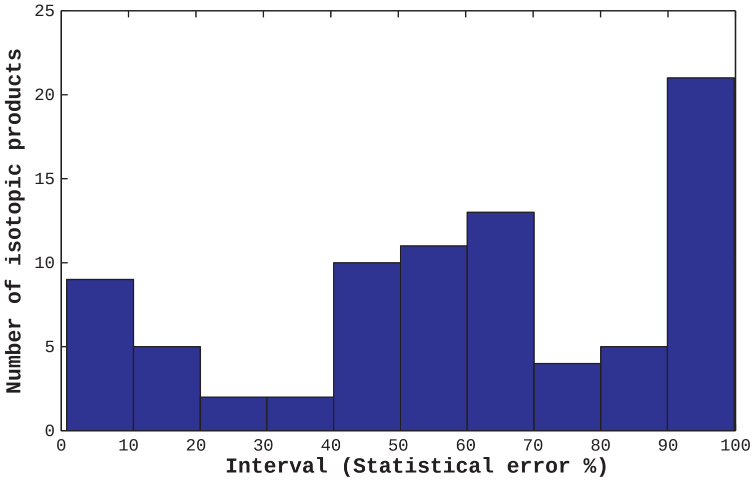

Figure 3.5 A histogram representing numbers of products from a reaction path splitting test problem characterized by statistical errors

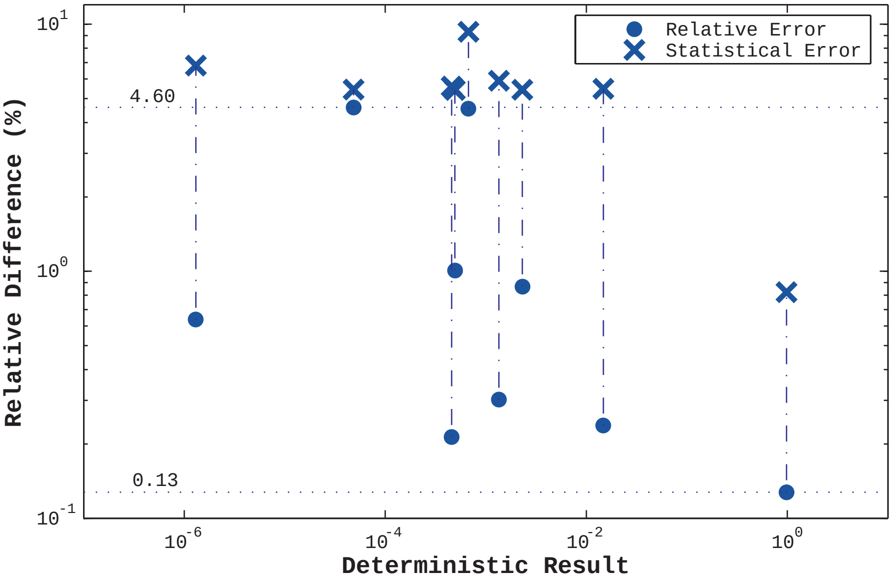

Figure 3.6 Relative Differences between Monte Carlo results with statistical errors less than 10% and deterministic results as a function of the deterministic result. Dash-dot lines connect relative differences to their corresponding statistical errors.

Category	**Analog**	**Reaction Path Splitting**
NPS	250M	15k
Computing Time (s)	546	524
A number of products (n)	22	82
n < 10% stat. error	14	9
10% < n < 20% stat. error	0	5
20% < n < 30% stat. error	2	2
30% < n < 40% stat. error	2	2
40% < n < 50% stat. error	2	10
50% < n < 60% stat. error	0	11
60% < n < 70% stat. error	0	12
70% < n < 80% stat. error	1	5
80% < n < 90% stat. error	0	5
90% < n < 100% stat. error	1	21
Mean statistical error	2.11%	5.58%
Mean relative difference	1.44%	1.40%

Table 3.3 Quantitative comparisons of different characteristic numbers of products between the analog result and the results from a reaction path splitting. The mean relative differences and mean statistical errors are derived from those with statistical error less than 10% in each case.

by statistical variations in the simulation. This relationship suggested that smaller relative differences could be obtained from the simulation with improved statistics.

3.6 Weight Window

The use of variance reduction techniques can increase the number of desired histories but often introduce large fluctuations in the weights of the particles following these histories. The latter effect somewhat negates the purpose of applying variance reduction techniques as these fluctuations usually contribute to larger variances of the results.

Traditionally in Monte Carlo transport, a weight-window technique has been employed to control the weight variations in the non-analog simulation [13]. A weight window, or for short, a window, is defined for each spatial region and energy range and characterized by the upper and lower bound on a particle's weight. If a particle's weight is below the lower bound, Russian roulette is applied and the particle's weight is increased to be within the window or the particle is terminated. On the other hand, if the particle's weight is higher than the upper bound, the particle will be split such that the weights of new particles are within the window. Due to a strong analogy to Monte Carlo transport, Monte Carlo inventory analysis might be able to take full advantage of the well-established concept of window. This chapter introduces the application of window in the current work.

3.6.1 Development Scope

The development is focused on the implementation of the time-dependent window analogous to the space-dependent window in Monte Carlo transport. The time-dependent window in Monte Carlo inventory is strictly defined as a function of control volumes. It is independent of isotopic identities. This type of window is the simplest definition of a weight window which serves as the initial stage of validating the benefits of weight window in Monte Carlo inventory and to provide the concrete stepping stone for future extensions, for example, an automated weight-window generator or a time-isotope dependent weight window.

3.6.2 Methodology

A weight window in any control volume is characteristically defined with a lower-bound(w_l), upper-bound(w_u) and target(w_t) weight. A primary task of weight window is to split or roulette a particle when its weight, w, is higher than the upper-bound weight or less than the lower-bound weight without unbiasedly affecting the simulation. In both cases, the number of newly created particles, n, is given by the combined Russian rouletting & splitting scheme [17]:

$$n = \lfloor \frac{w}{w_t} + \xi \rfloor, \qquad \xi \in Unif[0,1). \tag{3.11}$$

The initial particle is discarded and replaced with n particles, each with the same weight of w_t. It can be shown that the overall weight is conserved after the splitting or rouletting processes by calculating the expected weight of the particles.

$$E(W) = E(w_t n) = w_t \cdot E(n) \tag{3.12}$$

The expected value of n can be calculated with aid from the following expression derived from Equation (3.11).

$$n \;=\; \begin{cases} \lfloor \frac{w}{w_t} \rfloor & \text{if } \xi \leq 1 - (\frac{w}{w_t} - \lfloor \frac{w}{w_t} \rfloor) \\ \lfloor \frac{w}{w_t} \rfloor + 1 & \text{if } \xi > 1 - (\frac{w}{w_t} - \lfloor \frac{w}{w_t} \rfloor) \end{cases} \tag{3.13}$$

Hence,

$$\begin{aligned}
E(n) &= \sum_{i=1}^{k} n_i \cdot P(n = n_i) \\
&= \lfloor\frac{w}{w_t}\rfloor \cdot P(n = \lfloor\frac{w}{w_t}\rfloor) + (\lfloor\frac{w}{w_t}\rfloor + 1) \cdot P(n = (\lfloor\frac{w}{w_t}\rfloor + 1)) \\
&= \lfloor\frac{w}{w_t}\rfloor \cdot (1 - (\frac{w}{w_t} - \lfloor\frac{w}{w_t}\rfloor)) + (\lfloor\frac{w}{w_t}\rfloor + 1) \cdot (\frac{w}{w_t} - \lfloor\frac{w}{w_t}\rfloor) \\
&= \lfloor\frac{w}{w_t}\rfloor - \lfloor\frac{w}{w_t}\rfloor\frac{w}{w_t} + \lfloor\frac{w}{w_t}\rfloor\lfloor\frac{w}{w_t}\rfloor + \lfloor\frac{w}{w_t}\rfloor\frac{w}{w_t} - \lfloor\frac{w}{w_t}\rfloor\lfloor\frac{w}{w_t}\rfloor + \frac{w}{w_t} - \lfloor\frac{w}{w_t}\rfloor \\
&= \frac{w}{w_t} \qquad (3.14) \\
\therefore E(W) &= w_t \cdot \frac{w}{w_t} \\
&= w \qquad (3.15)
\end{aligned}$$

3.6.3 Testing

After the fundamental concept of the window is established, the implementation of the window is tested by applying a number of different weight windows in a simulation expected to have a broad range of particle weights and comparing these results to the deterministic result. The simulation is based on isotopic inventories following a 10-year steady state irradiation of ^{56}Fe with a uniform multi-group neutron flux of 5×10^{12} n/cm^{2}s. The forced reaction technique with a parameter of 1 and the reaction path splitting technique are applied in the simulation. Five weight windows with different lower bounds are used in the simulation to construct five testing problems. The upper-bound and target weight of all windows are 2 and 10^{-2}, respectively, while the lower-bound weights are 10^{-10}, 10^{-20}, 10^{-30}, 10^{-40} and 10^{-50}. All five testing problems run with 10^5 NPS.

Some characteristics of the results are summarized in Table 3.4. As expected, the test problems with wider weight windows produce more products and smaller detection limits than the test problems with narrower windows. The detection limit in each case is slightly lower than its respective lower-bound weight because any simulated particles with weight less than the lower bound is either terminated or promoted by increasing its weight to be within the window. As a result, the smallest possible isotopic result in a single tally bin is equal to a ratio of the lower bound and NPS where only one Monte Carlo particle with the same isotopic identity and the lower bound weight reaches that tally bin in the simulation. Improvements of detection limits and numbers of products come with the expense of computing times and statistical errors. The computing time increases dramatically with increasing the width of the window. This is due to a higher number of Monte Carlo particles being tracked by the simulation. The root-mean-squared relative error also increases with increasing the width of the window, reflecting a larger variance from a higher variation of particles' weights. To verify the validity of the weight window implementation, the results with relative errors less than 10% are compared to the deterministic results from ALARA. They are in good agreements as the average relative differences range from 1.80% to 3.85% and are less than their relative errors in all cases. This relationship suggests that smaller relative differences can be achieved by means of improving statistics, i.e. increasing NPS.

After the implementation of the window is validated, the next challenging task is to select appropriate values of window parameters: lower-bound weight and window width. Defining the latter implies the value of an upper-bound weight. A target weight would be defined within the window. Strong analogy between MC inventory analysis and neutron transport suggests that existing selection process of weight window parameters in neutron transport could be readily applicable to MC inventory. Thus, extensive literature review of this topic has been conduct for possible solutions. Recently, an approach of using a forward deterministic solution to compute weight window for a deep-penetration problem in slab geometry has been studied [18]. Even though this technique greatly increases the efficiency of Monte Carlo simulations, its applicability is likely limited to problems with simple geometry. When the geometry is more complicated, there might not be a theoretical analysis for the optimal width and the selection of the width is empirical.

The default upper bound in MCNP and its descendants is five times the lower bound, although it is observed that different window widths made slight difference to the efficiency of the simulation [19]. In most cases, the weight window is generally quite insensitive to the window width and there is a broad range of window parameters in which the weight

Category	**Lower-bound weight**				
	10^{-10}	10^{-20}	10^{-30}	10^{-40}	10^{-50}
Number of products	23	40	61	84	94
Detection limit (per initial source)	2.99e-14	1.37e-22	3.95e-34	3.43e-44	3.87e-53
Computing time (seconds)	9.05	16.22	89.15	1126.48	14978.90
R.M.S. relative error (percent)	34.47	54.90	59.93	61.00	68.87
Only results with relative errors less than 10% are considered.					
Avg. relative difference (percent)	2.13	1.80	3.16	3.85	2.78
R.M.S. relative error (percent)	3.83	4.11	4.15	4.08	4.02

Table 3.4 Summary of characteristics of the results from the simulations with different definitions of weight window.

window perform equally well [20]. An importance generator, later known as a weight window generator, has been developed to efficiently set the window parameters for energy-dependent problems [20]. Essentially, it is a bookkeeping algorithm which empirically estimates the importance function of a cell for subsequent calculations [14].

In conclusion, an analytic method to determine the optimal parameters for the weight window in general inventory problems may not exist. In addition, the effect of different weight window on computational efficiency is undetermined. For these reasons, along with the goal of providing a more user-friendly environment, a weight window generator and time-isotope dependent window would be the subjects of interest for future development. Borrowing from MCNP, one approach is to model the weight window generator following the forward-adjoint generator [14]. Note that when defining parameters for the window, a precaution must be taken as too narrow window might terminate or split too many particles and too wide window might not improve enough efficiency.

3.7 Delta Tracking

One of the most important issues in many activation problems is accounting for pulsed or intermittent operation of the neutron source. While exact treatment of this pulsing is not always required [21], some cases do require it for accurate determination of the activation products. The current methodology could be used to simulate a pulsed neutron source on a non-flowing material by using the loop and flow capabilities. One control volume would represent the irradiation time (on-time) and another would represent the dwell time (off-time) between pulses. However, there are two potential problems with such an implementation. First, for systems with high pulse frequencies and operation times of many years, this might result in excessive computation as an MC atom passes through the loop many times without any reactions. More importantly, however, is the situation where flowing material, moving through the system with one characteristic frequency, is subjected to a pulsed neutron source of another characteristic frequency. This can result in a complex and potentially long series of control volumes before it repeats. Furthermore, if the physical flowing system is modeled by a complex loop flow, there may be no definable characteristic flow frequency and it would be impossible to define a set of control volumes that would represent all atoms.

The solution is to handle the time-varying nature of the neutron flux in a different manner within the control volumes rather than as a defining aspect of the control volumes. At least two approaches are being considered for this, one that relates to the concept of delta tracking [17] and one that explores the validity of various pulse approximations.

The delta tracking technique is considered to be an interesting approach and is well established in neutron transport. The implementation of delta tracking for MC inventory analysis will follow a close analogy to MC transport.

3.7.1 Methodology

The delta tracking technique is applied in a control volume with a pulsing schedule. In order to demonstrate this technique, the pulsing schedule is limited to include only pulsing time, t_p, and dwelling time, t_d, between two pulses. These two characteristic times must be defined in addition to other quantities necessary for a complete definition of a pulsing control volume. The effective reaction rate coefficient during the pulse, λ_p, can be calculated from a prescribed neutron spectrum in the control volume while the effective reaction rate coefficient during a delay, λ_d, is simply equal to a decay constant.

The underlying methodology of delta tracking is to give a simulated atom a constant effective reaction rate coefficient, λ', which is given by

$$\lambda' = \lambda_T(t) + \lambda_\delta(t), \quad \lambda' \geq \lambda_T(t),\ \lambda_\delta(t) \geq 0 \text{ for all } t > 0, \tag{3.16}$$

where $\lambda_T(t)$ is a true effective reaction rate coefficient and $\lambda_\delta(t)$ is a fictitious effective reaction rate coefficient, representing ”pseudo-reaction” events.

A potential reaction time is randomly sampled based on λ'. This can easily be done using the following expression.

$$t' = -\frac{ln\ \xi}{\lambda'}, \quad \text{where } \xi \in \text{Unif}[0, 1) \tag{3.17}$$

Based on durations of pulsing and dwelling time, an effective reaction rate coefficient at this potential reaction time, $\lambda_T(t')$, can be randomly determined.

$$\lambda_T(t') = \begin{cases} \lambda_p & \text{if } \eta \leq \frac{t_p}{t_p+t_d}, \quad \text{where } \eta \in \text{Unif}[0,1) \\ \lambda_d & \text{Otherwise} \end{cases} \tag{3.18}$$

Whether the simulated atom undergoes a reaction at this point in time entirely depends on a rejection sampling method, which is based on a ratio of $\lambda_\delta(t')$ and λ'. With probability $\frac{\lambda_\delta(t')}{\lambda'}$, this potential reaction time is rejected. Otherwise, the atom undergoes a reaction, the daughter will be randomly sampled from a set of products corresponding to a region which is previously determined from Equation 3.18.

This procedure is repeated until the atom exits the control volume or its history is terminated.

Note that the delta tracking technique should be used in a problem where a pulsing frequency is so high that a duration of each pulse is short compared to the residence time of the control volume. The technique can produce statistically invalid results if it is used in a problem with very long pulses and delays. Equation 3.18 would yield the same expected mean from two problems with drastically different frequencies but same total on-times and off-times.

It can be shown that the delta tracking technique is an unbiased sampling method. The following proof is recast from Monte Carlo Fundamentals by Brown and Sutton [17].

Let $P(u)$ be the total probability of traveling through a time, u, without a real reaction and $P(u|n)$ be the probability of having exactly n pseudo-reactions during this time, u.

Therefore, $P(u) = \sum_{n=0}^{\infty} P(u|n)$.

$$\begin{aligned}
P(u|0) &= 1 - \int_0^u \lambda' e^{-\lambda' t} dt \\
P(u|0) &= e^{-\lambda' u} && (3.19) \\
P(u|1) &= \int_0^u P(t|0)P(u-t|0)\lambda_\delta(t)dt = \int_0^u e^{-\lambda' t} e^{-\lambda'(u-t)} \lambda_\delta(t)dt \\
&= e^{-\lambda' u} \int_0^u \lambda_\delta(t)dt = e^{-\lambda' u}\Theta_\delta(u) \quad \because \Theta_\delta(u) = \int_0^u \lambda_\delta(t)dt && (3.20) \\
P(u|2) &= \int_0^u P(t|1)P(u-t|0)\lambda_\delta(t)dt = \int_0^u \Theta_\delta(t) e^{-\lambda' t} e^{-\lambda'(u-t)} \lambda_\delta(t)dt \\
&= e^{-\lambda' u} \int_0^u \Theta_\delta(t)\lambda_\delta(t)dt = \frac{[\Theta_\delta(u)]^2}{2} e^{-\lambda' u} && (3.21) \\
P(u|n) &= \int_0^u P(t|n-1)\lambda_\delta(t)P(u-t|0)dt = \frac{[\Theta_\delta(u)]^n}{n!} e^{-\lambda' u} \quad \text{for all } n \geq 1 && (3.22) \\
P(u) &= \sum_{n=0}^{\infty} P(u|n) = \sum_{n=0}^{\infty} \frac{[\Theta_\delta(u)]^n}{n!} e^{-\lambda' u} \\
P(u) &= e^{\Theta_\delta(u)} e^{-\lambda' u} = e^{(\Theta_\delta(u) - \lambda' u)} \\
P(u) &= exp\left(\int_0^u \lambda_\delta(t)dt - \int_0^u \lambda' dt\right) = exp\left(-\int_0^u \lambda_T(t)dt\right) && (3.23)
\end{aligned}$$

Equation 3.23 agrees with the interpretation of the total effective reaction rate coefficient in the analog sampling.

3.7.2 Test Problems

The inventories at shutdown following a 10-year pulsing irradiation of ^{56}Fe with a uniform multi-group neutron flux of 5×10^{12} n/cm^{2}s were calculated from two test problems with different schemes to model the same pulsing schedule. The pulsing time and dwelling time between pulses were defined to be three and two minutes, respectively. The first test problem represented an analog approach by defining a loop of two control volumes, one representing a three-minute pulse and the other representing a two-minute delay between pulses. A history of a simulated atom began in the pulsing control volume and continued in a loop until the total simulation time of 10 years was reached. The second test problem was equipped with the delta tracking technique and consisted of only one 10-year control volume. In this case, the simulation was terminated when a simulated atom reached the end of the control volume.

FENDL-2/A activation library and FENDL-2/D decay library were used in the simulations. ALARA was used to produce the benchmark results for both test cases. A truncation tolerance was set to be 10^{-9}.

3.7.3 Simulation Results

The first test problem was simulated with 10^6 particles and the total computing time was 270.05 hours. This large amount of computing time was expected because each simulated atom faced an overwhelming number of decisions to determine the next control volume.

The ALARA results included 37 isotopes whereas results from this test problem only included 12 isotopes. Figure 3.7 showed the relative differences between the two results for 12 of these isotopes as a function of the deterministic results. The line indicates the 2σ statistical error associated with a result of that magnitude in an analog Monte Carlo calculation. The average relative difference of statistically reliable results ($2\sigma < 10\%$) was 2.45%. A good agreement between the Monte Carlo and deterministic results was expected since the analog methodology had been previously validated.

The second test problem was implemented with the delta tracking technique and simulated with 10^7 particles. The total computing time was 67.07 seconds. Results from this test problem included fifteen isotopes and their relative errors with respect to the ALARA results were shown in Figure 3.8. The relative differences were ranged from 0.0038% to 2059.83%. For ten out of fifteen isotopes, the 2σ statistical errors were less than 10% and the average relative difference among them was 3.32%. All but one isotope had their relative errors less than 2σ statistical errors. In this case, the lone exception, which had a relative difference of

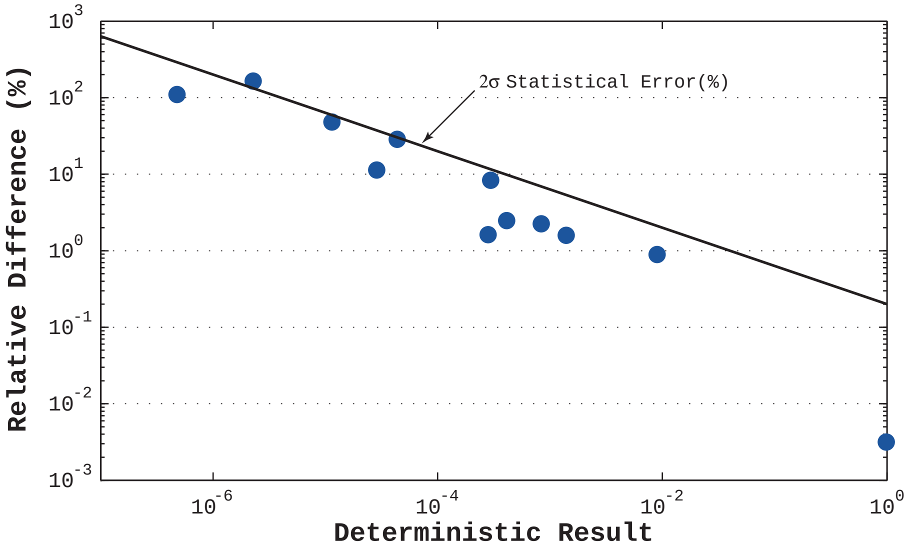

Figure 3.7 Relative differences (%) between deterministic results and Monte Carlo results from the test problem with the exact pulsing schedule were plotted as a function of deterministic results. NPS = 10^6.

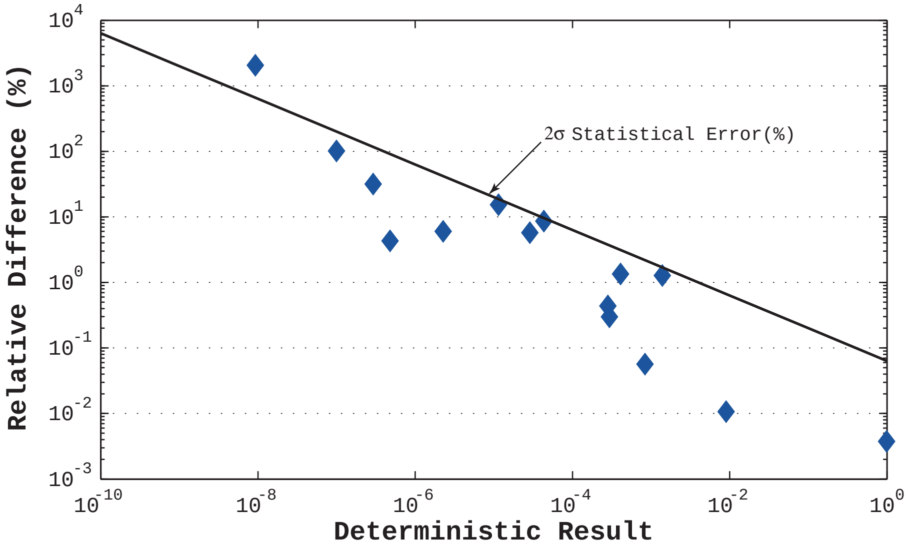

Figure 3.8 Relative differences (%) between deterministic results and Monte Carlo results from the test problem with the delta tracking technique were plotted as a function of deterministic results. NPS = 10^7.

2059.83%, occurred in a region where a statistical error was too high that this result would be disregarded.

Having statistical errors higher than relative differences suggested that the differences were likely dominated by the statistical variations in the results and smaller differences could result from improved statistics of the simulation. More importantly, this behavior verified that the delta tracking technique had been successfully implemented.

Computing times of both test problems were compared to evaluate their efficiency to model the pulsing schedule. The first test problem required 270.05 hours while the second test problem with the delta tracking technique only needed 67.07 seconds to perform the same physical task. In addition to a significant reduction in a computing time, the second problem was able to simulated ten times more particles than the first problem. Clearly, employing the delta tracking was a better alternative to using a loop of two control volumes representing a pulse and a delay as evident by a substantial difference of computing times by several orders of magnitude.

3.8 Summary

In addition to simply increasing the number of simulated particles, variance reduction techniques are alternative methods to improve the precision of the results of isotopic inventory problems. To this point, six variance reduction techniques: *forced reaction*, *biased source sampling*, *biased reaction branching*, *reaction path splitting*, *weight window* and *delta tracking* have been studied and successfully implemented. With variance reduction techniques applied , precision, accuracy and efficiency of the problem have been tremendously improved. However, using only one technique at a time might not produce the most efficient modeling scheme in most situations. The combination of several techniques and appropriate parameter inputs are recommended. As an example, *forced reaction* and *reaction path splitting* would be used together to both deepen and broaden a reaction tree. Nonetheless, finding suitable parameters for each technique that yields optimal performance is quite a challenging task. Furthermore, use of variance reduction techniques can be less efficient than the analog simulation because the statistical improvement might not be high enough to surplus the increase in computing time per each Monte Carlo history. A figure of merit was then introduced as a tool to evaluate the efficiencies of different modeling schemes on the same physical problem, leading to the optimal variance reduction parameters.

Chapter 4

Figures of Merit

Monte Carlo isotopic inventory analysis is directly analogous in many ways to Monte Carlo neutral particle radiation transport; instead of neutral particles traveling through 3-dimensional space and having interactions with the underlying materials that change their energy, inventory analysis simulates atoms moving through (1-D) time and having interactions with the underlying neutron flux that change their isotopic identity. After a description of the fundamental Monte Carlo methodology, including some basic variance reduction methods, and of the motivation and goals for the development of a figure of merit, this chapter will explore a number of possible figures of merit and discuss their applicability to different types of simulations.

4.1 Introduction and Importance of Figure of Merit

Even though the variance reduction techniques have tremendously reduced the statistical error and increased the spectrum of isotopes generated in the Monte Carlo simulation, they also increase the computer time spent calculating each history and thus are not guaranteed to optimize the computing resource for such calculations. That is, in some cases it may be more efficient to simply simulate more histories than use a variance reduction technique. A figure of merit (FOM) is introduced to monitor the efficiency of the Monte Carlo code as different variance reduction techniques are attempted on the same problem [11]. FOMs representing relative efficiencies from biased and unbiased runs of the same physical problem can be calculated and compared quantitatively, assisting a user in determining the optimal variance reduction parameters. This chapter will first consider the desired properties of a figure of merit and then introduce a number of possibilities for the figure of merit, discussing situations where each may be a useful measure.

4.2 Principles and Constraints of Figure of Merit

Since the underlying distribution that governs the random walk process is rarely known *a priori*, determining the most computationally efficient modeling scheme requires testing a variety of schemes and comparing their performance. In order to be useful, however, a quantitative metric is necessary to permit this comparison. This is the role of a figure of merit (FOM), and as such, defines the characteristics of an ideal figure of merit. In practice, a FOM will be used to determine which set of variance reduction parameters are most efficient for a given problem by comparing the FOMs that result from short problems, each with different variance reduction parameters. The set of parameters with the best FOM would be used to run a simulation with many more histories to achieve the final answer with sufficient precision. Therefore, a FOM should be a quantitative measure that is somehow proportional to the overall efficiency of the problem. This allows a user to compare two alternative modeling schemes. In addition, an ideal FOM is independent of the number of Monte Carlo histories so that a simulation with few histories can be used as an indication of the efficiency of a simulation with many histories. Finally, an ideal FOM should have a clear mathematical relationship to the statistical quantities used to measure the performance and one-to-one functional relationship with the computational cost. This allows a user to estimate the number of histories required to achieve the desired level of precision/performance. If the statistical performance metric, P_t, is measured over a short test time, T_t, and the performance goal is P_g, then an ideal FOM would allow a determination of the time to reach the goal, T_g, as:

$$\begin{aligned} FOM = f(T_t)\, g(P_t) = f(T_g)\, g(P_g) = Constant \\ T_g = f^{-1}\left[\frac{FOM}{g(P_g)}\right] = f^{-1}\left[\frac{f(T_t)\, g(P_t)}{g(P_g)}\right] \end{aligned} \tag{4.1}$$

In summary, an ideal figure of merit has the following characteristics:

- quantitative measure of statistical performance,
- independent of number of Monte Carlo histories, and
- a one-to-one function of the computational cost.

While previous work on determining the efficiency of simulations provides a rigorous decision-theoretic framework evaluating and possibly determining the efficiency of simulations [22], this work takes an approach based more directly on the desired physical outcomes of the simulation. Future work can be carried out to reconcile the efficiency measures developed here with the mathematical development in [22].

The following sections will consider a variety of potential FOMs, both for these characteristics and for other ways that they provide information about the problems performance.

Test Problem

The performance of each FOM was tested by calculating the proposed FOM at shutdown following a 10-year steady state irradiation of ^{56}Fe with a uniform multi-group neutron flux of 5×10^{12} n/cm^2 s. In all cases the FENDL-2/A activation library and FENDL-2/D decay library were used. The results for the analog case were compared to non-analog cases with forced reaction parameters of 1, 2, 3, 5, and 8. The forced reaction parameter indicates the number of times an isotope will be forced to undergo a reaction within the 10-year irradiation period. The FOM was calculated for each case as a function of time, in increments of 1000 seconds of computer time.

4.3 Development of Figures of Merit

Based on the above characteristics, developing a Figure of Merit requires first choosing a statistical performance metric and then examining its relationship to the computational cost to arrive at a formulation that is independent of the number of histories. A variety of statistical performance metrics are available and they form the basis for distinguishing among the four FOM formulations proposed in this section. The behavior of the specific statistical performance metric will be considered first and then its usefulness in formulating a FOM will be addressed.

4.3.1 Statistical Error of Single Result ($1 / R^2T$)

The strong analogy between this methodology and Monte Carlo neutral particle transport results in an obvious suggestion for a FOM based on the statistical error of the result. In this case, the statistical performance metric is the square of the relative statistical error, R, which is known to vary inversely with the number of Monte Carlo particles and hence inversely with the computational cost, T. Thus, a FOM based on this metric is

$$FOM = \frac{1}{R^2T} \tag{4.2}$$

Implicitly, this metric/FOM is based on the relative error of a single tally result, or single tally bin. Consequently, optimizing this FOM amounts to optimizing the results for only that tally bin and only improves the whole problem to the extent that the tally bin in question represents the rest of the problem. In the current Monte Carlo inventory implementation, the tally bins are based on time (analogous to space in Monte Carlo transport) and/or isotopic identity (analogous to energy in Monte Carlo transport). Using this FOM, therefore, requires the choice of a specific time and isotopic identity.

It is important at this stage to point out a distinct difference between the inventory analysis and the neutral particle transport methods. The energy domain of neutral particle transport is a continuous dimension where two different energies have a clear physically meaningful relationship to each other. This often allows a single energy bin (or the total over all energy bins) to be representative of the results over the entire energy domain. The isotopic identity domain is discrete and two isotopic identities may not have any clear relationship to each other. Hence a single isotopic identity bin is unlikely to be representative of many other isotopic identities, and rarely representative of the whole problem. This FOM is therefore only valuable in optimizing the modeling scheme for a particular isotope, i. For this study, the inventories at the end of a 10-year irradiation period were used to calculate while the FOMs, comparing results for a variety of specific represented isotopes, still remained in question.

Since R^2 is inversely proportional to T and T is directly proportional to the number of histories, FOM should be constant with respect to the number of histories (allowing for statistical fluctuations at very small numbers of histories). Three isotopes from the test problem, ^{56}Fe, ^{54}Cr and ^{59}Co, with different relative expected end-of-problem inventories of 9.82×10^{-1}, 3.10×10^{-5} and 4.29×10^{-7}, were chosen to be isotopes in question. The behaviors of the three resulting FOM values are shown in Figure 4.1(a-c), demonstrating the effects of increasing the forced reaction parameter. The FOM for all three isotopes are constant as expected. For ^{56}Fe, this FOM suggests that the analog scheme is much more efficient than forced reactions technique. This agrees with the physical nature of the problem; because ^{56}Fe is the initial isotope, forcing a reaction will only reduce the variance of the products in the reaction chain, but will make each history have a higher computational cost. On the other hand, both ^{54}Cr and ^{59}Co are produced predominantly from the third reaction from ^{56}Fe and the forced reaction technique with parameter of 3 improves the likelihood of producing these isotopes with the minimum increase in the computational cost of each history. This FOM confirms that this is the optimal choice for these isotopes.

Finally, this FOM can be used to estimate a computing time to achieve a target error for the isotope in question:

$$T_g = \frac{1}{R_g^2 \cdot FOM} = \frac{R_t^2 T_t}{R_g^2}, \tag{4.3}$$

as described in Equation (4.1). This FOM has all of the characteristics of an ideal FOM defined above, but the performance metric itself is only useful in special circumstances. Since the important isotopes are not always known *a priori* and one isotope's results are rarely indicative of another's, other potential performance metrics and FOMs will be explored.

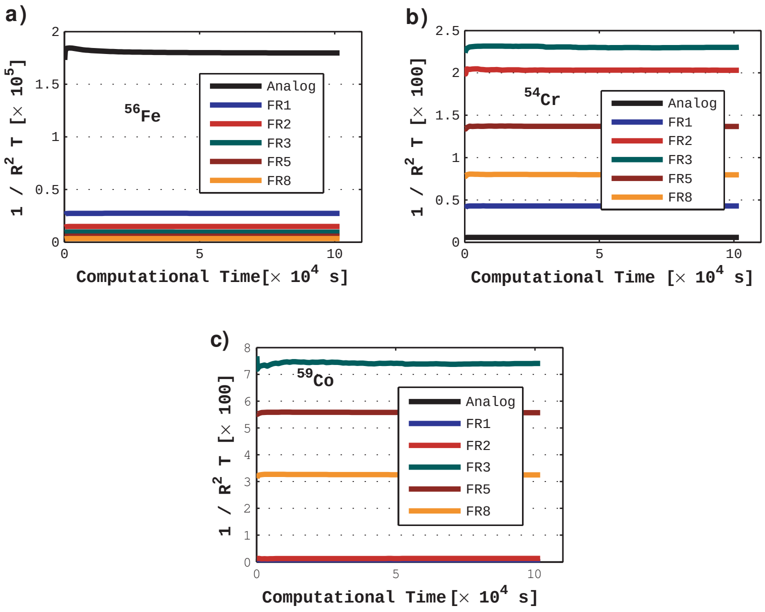

Figure 4.1 Traditional figure of merit based on relative error, shown for three different isotopes as a function of time and for different forced reaction(FR) parameters: a)^{56}Fe b)^{54}Cr c)^{59}Co.

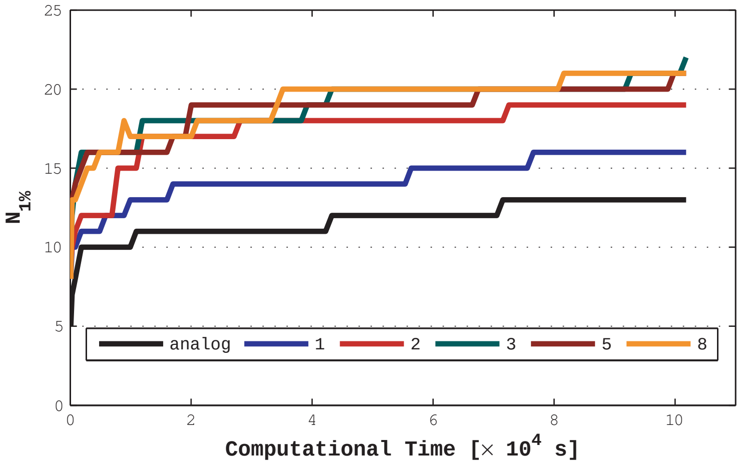

Figure 4.2 Number of qualified isotopes with relative error less than 1%. The performances of the test problem with different FR parameters are compared using the number of qualified isotope metric.

4.3.2 Number of Qualified Isotopes (N_k)

Another performance metric for the Monte Carlo inventory method is the number of isotopes produced by a given set of modeling parameters. If the statistical error for a particular isotope is too high; however, it should be disregarded. The number of qualified isotopes, N_k, is defined as the number of isotopes that have relative errors less than k percent. This quantity is the simplest measurement of the performance for a given modeling technique.

Figure 4.2 shows the results for this performance metric for a k of 1% and for a variety of modeling schemes represented by the forced reaction parameter. For very short run times, all cases produce approximately the same number of qualified isotopes. As the computing time progresses, Figure 4.2 clearly shows that forced reaction problems with higher parameter(3, 5 and 8) perform similarly, but better than problems with lower forced reaction parameters. Increasing the number of Monte Carlo particles and thus computing time would decrease relative errors of all isotopes. Consequently, more isotopes would be counted as qualified isotopes. This performance measure is expected to have this step behavior until the maximum number of isotopes is qualified, with the more efficient variance reduction schemes approaching this maximum more quickly. (In theory, the maximum number of qualified isotopes is equal to the full scope of the data library since any isotope has a finite probability of being produced, even if minute. In a different study using a forced reaction parameter of 8 and a computing time of 3×10^6 s, 94 isotopes were included for this ^{56}Fe problem, of which 30 had relative errors below 1%.) While this measurement does provide quantitative information about the performance of the modeling scheme, its functional relationship to the number of simulated histories is unclear making it difficult to form a FOM that meets the other criteria: independent of number of histories and a one-to-one functional relationship with computational cost. This measure could be retained for comparing the efficiency of two schemes, but does not provide all the necessary information expected of a figure of merit.

4.3.3 Detection Limit ($1\,/\,D_kT$)

Often, an isotope with a relatively small inventory may have a disproportionate importance to the analysis in question due to some property of the isotope (e.g. its contribution to an engineering response such as the overall activity, the radiotoxicity or the waste disposal rating). The ability of a simulation to detect such a small existence of a particular isotope should also be taken into consideration when creating a FOM for an inventory problem. Moreover, since the specific isotope in question might not be known, it is important to use a metric that provides information about the overall precision of the simulation. The detection limit can serve that purpose.

Detection Limit in Monte Carlo Isotopic Inventory

A k-percent detection limit (D_k) is defined as the lowest relative production (yield) of all isotopes with relative error less than k percent. Based on the definitions of the relative error and yield given by equations (2.10) and (2.11), the k-percent detection limit for an analog problem is therefore

$$D_k = \frac{100^2}{N \cdot k^2} \tag{4.4}$$

For a given a value of k the detection limit for analog Monte Carlo simulations is inversely proportional to N. However, this continuous $1/N$ behavior implicitly assumes that the isotopic yields are continuous, that is, an uncountably infinite number of isotopes exist. This is certainly not the case for the Monte Carlo inventory method where the isotopic yields are distributed discretely.

For any results from a Monte Carlo isotopic inventory simulation, there can be only a finite number of isotopic products. The results will form a set of yields, $\{Y_j\}$, which can be sorted in descending order. At any point, the detection limit, D_k, will be defined by one of those isotopes, i, that has the smallest yield of all the isotopes with relative error less than k percent. The isotope, $i+1$, has a smaller yield and a relative error larger than k percent. As N is increased, the relative error of both isotopes i and $i+1$ will decrease ($R^2 \propto 1/N$), but the detection limit will remain unchanged until the relative error of isotope $i+1$ drops below k percent, at which point D_k will drop suddenly to the value Y_{i+1}. The overall shape of the detection limit in a discrete problem should therefore be a series of steps where the leading edge follows the $1/N$ ($\propto 1/T$) dependence.

Analyzing the detection limit in a real problem

Figure 4.3 shows the 1% detection limits for an analog case and three different forced reaction parameters for the test problem. As expected, the detection limits for the analog case exhibits a $1/T$ dependence. In addition to the step behavior caused by the discrete nature of the isotopic yields, the detection limits for the non-analog cases are all lower than that of the analog case and appear to depend similarly on $1/T$. Power law curves were fit to the leading edge of each of these results to examine the relationship with T. The parameters of each fit are shown in the figure, where the multiplicative constant represents the relative improvement of the variance reduction method and the exponents are reasonably close to -1. Once again, the discrete nature of the detection limit combined with the discrete time sampling of this test problem can contribute to an apparent departure from the $1/T$ behavior.

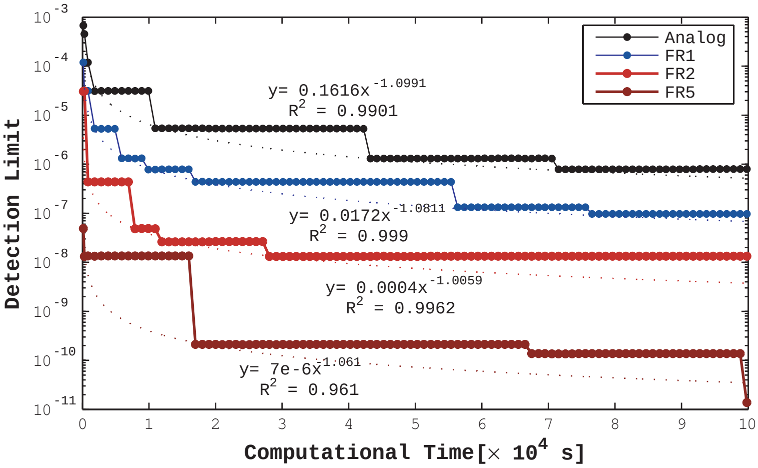

Figure 4.3 Detection limit as a function of computing time for an analog problem and three different forced reaction (FR) parameters. For each case, the points at the leading edge have been used to generate a power law fit whose parameters are also shown.

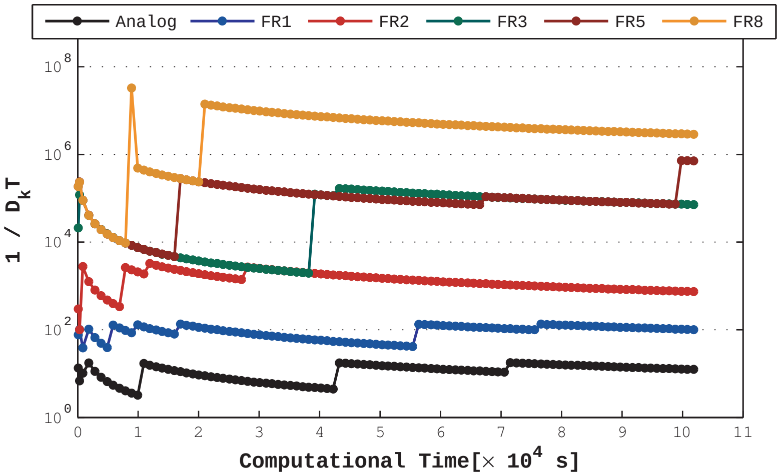

Figure 4.4 The detection limit based figure of merit is shown for the analog case and 5 different forced reaction (FR) variance reduction parameters.

The detection limit, D_k, can be used to evaluate the overall performance of the modeling scheme since a lower value D_k indicates a greater precision in the answer. In Figure 4.3, orders of magnitude improvement are seen in the precision of the problem by invoking forced reaction variance reduction. Because of the $1/T$ dependence of the detection limit, the most appropriate choice for a FOM is

$$FOM = \frac{1}{D_k T} \tag{4.5}$$

This FOM for the various cases of the test problem are shown in Figure 4.4. As expected, the overall shape of detection-limit-based FOM still exhibits the step behavior from $1/D_k$. However, the $1/T$ factor helps to lessen a strong step-function behavior and causes the FOM to oscillate about a constant value.

4.3.4 Error Corrected Detection Limit ($1/D_k R^2 T$)

The fluctuations in the detection limit based FOM are due to the $1/T$ factor while the detection limit, D_k, is constant. Similarly, the relative error, R_i, of the isotope, i, that is defining the detection limit is declining continuously with time while the detection limit is constant at that isotope's yield, Y_i. It should therefore be possible to mitigate the oscillatory

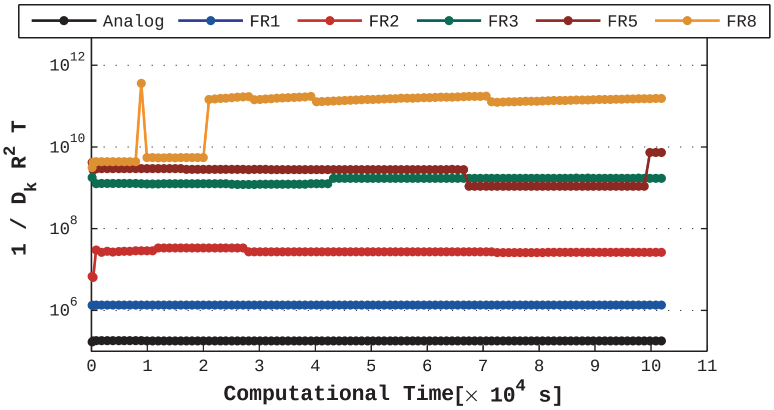

Figure 4.5 Figure of merit using error corrected detection limit provides a measure of the overall efficiency of the problem with a nearly constant value for a given modeling scheme.

behavior of the detection-limit-based FOM by using the relative error as a correction. In particular, it can be shown that a figure of merit, $1/D_kR^2T$, is constant for the analog case.

$$FOM = \frac{1}{D_kR^2T} \tag{4.6}$$

In regions where D_k is constant, this FOM is constant since R^2 behaves as $1/T$. Consider how D_k and R^2 vary across a jump in the detection limit:

$$\frac{D_k^-}{D_k^+} \equiv \frac{Y_i}{Y_{i+1}} = \frac{N_{i+1}}{N_i} = \frac{T_{i+1}}{T_i}$$
$$\frac{R_-^2}{R_+^2} \equiv \frac{R_i^2}{k^2} = k^2\,\frac{T_i}{T_{i+1}}\,\frac{1}{k^2} = \frac{T_i}{T_{i+1}},$$

$$\therefore D_k^-\,R_-^2 = D_k^+\,R_+^2 \tag{4.7}$$

where D_k^- and D_k^+ are the detection limit on the left and right of the jump, respectively, and R_-^2 and R_+^2 are the squares of the relative errors on the left and right of the jump, respectively. Thus, for analog problems this FOM is constant across a jump in the detection limit as well as during the periods where the detection limit does not change.

Figure 4.5 shows results for an FOM with this formulation. The results agree with the analytic calculation that FOM is constant for analog case and nearly constant for the variance reduction cases. Even though, this FOM is likely to experience some fluctuations due to the discrete behavior of the detection limit, it can be used in a problem without a target isotope to compare the overall efficiency of different schemes. Most importantly, it is effective at providing an estimate of the necessary computing time for a given modeling technique to achieve a certain overall precision, as indicated by the detection limit.

4.4 Summary

A number of statistical measures can be employed to assess the performance of different Monte Carlo modeling schemes for a given isotopic inventory problem. From these, two valuable figures of merit have been derived that meet the criteria described above: a figure or merit should provide quantitative information about statistical performance, independent of the number of simulated histories, providing guidance on the relationship between computational cost and performance. The FOM based on the relative error of a single tally result $(1/R^2T)$ is recommended for the problem with a known target isotope. In these situations, the modeling scheme can be optimized for that single result and the necessary computing time to achieve a target precision can be calculated. However, since many problems do not have readily identified target isotopes, or may have multiple important isotopes, a FOM based on the detection limit, corrected by the relative error, $(1/D_kR^2T)$ is useful for assessing the overall efficiency of the problem. With this FOM, the modeling scheme can be optimized against the detection limit and then the necessary computing time to achieve a target detection limit can be calculated.

Chapter 5

Efficiency Assessment

This chapter uses the figures of merit defined in the previous chapter to evaluate the possible computational efficiency improvements for a typical problem. A combination of variance reduction techniques will be used, each with varying parameters, to determine a best choice for different cases from a standard test problem. Study problem 1 is concerned with a scenario in which a statistical quality of one specific isotopic product is of interest. Study problem 2 is intended to study efficiency from using a reaction path splitting technique as a means to improve the global efficiency of the Monte Carlo simulation. Both problems illustrate how FOM responds to changing variance reduction parameters.

5.1 Problem Definitions

5.1.1 Standard test problem

A standard test problem is defined as the analog simulation in which isotopic inventories following 10-year steady-state irradiation of ^{56}Fe under a uniform neutron flux of 5×10^{12} n/cm^{2}s are calculated. It is used in the study problems where each problem employs a different set of variance reduction techniques. The FENDL-2/A activation library and FENDL-2/D decay library are used.

5.1.2 Study problem 1

Following the irradiation in the standard test problem, several isotopic products are selected such that their statistical errors are in distinctive ranges. Each chosen isotope is assumed to be an isotope of interest in separate study cases. Each study case is composed of many short test problems with different sets of variance reduction parameters. FOMs from short test problems are used to determine a set of variance reduction parameters that yields the most efficient scheme for producing that particular isotope. The *forced reaction* and *biased reaction branching* techniques are used in all cases. The biased reaction branching scheme is configured to increase the probability of the isotope of interest when it appears as a product, but otherwise to invoke *uniform reaction branching* to ensure that each reaction branch is followed with equal probability. The number of simulated particles in each short test problem is 10^6.

5.1.3 Study problem 2

In this study problem, a forced reaction and reaction path splitting technique are applied in the analog problem, aiming to obtain a deep and wide reaction tree. Six separate runs are constructed from using different forced reaction parameters: 1, 2, 4, 6, 7 and 8. For each run, an FOM, the error-corrected detection limit ($1/D_k R^2 T$), is calculated to quantitatively evaluate the global efficiency. The number of simulated particles in each run is 10^5.

5.2 Simulation Results

5.2.1 Study problem 1

Based on an analog problem with 10^{10} simulated particles, four isotopes, ^{51}Cr, ^{49}Ti, ^{53}Mn and ^{60}Ni, with statistical errors of 100%, 37.80%, 13.74% and 8.80%, respectively, were chosen in the study. The reaction tree obtained from ALARA was used to make preliminary choices for variance reduction parameter sets to be tested. In addition, the test sets were defined based on an assumption that the overall statistical quality of a particular isotope depends heavily on the qualities of the reaction branches that dominate the production of that isotope. Thus, improving statistical qualities of those branches was likely to subsequently better the statistical quality of the result.

Case	**Forced Parameter**	**Biasing Score**	**Relative Error (%)**	**FOM[s^{-1}]** $1/R^2T$	**FOM[s^{-1}]** $1/D_1R^2T$
0	analog	analog	100.00	4.98×10^{-5}	4.98×10^{5}
1	3	5	8.95	2.4026	1.21×10^{10}
2	4	5	11.16	1.1158	1.21×10^{10}
3	5	5	32.42	0.1252	1.17×10^{10}
4	3	10	9.93	2.2060	1.50×10^{10}
5	**4**	**10**	**5.28**	**5.9746**	$\mathbf{1.15 \times 10^{10}}$
6	5	10	5.04	5.1763	1.18×10^{10}
7	3	100	15.79	0.9112	1.51×10^{10}
8	4	100	13.35	0.9355	1.63×10^{10}
9	5	100	11.21	1.0478	1.12×10^{10}

Table 5.1 The values of figure of merit ($1/R^2T$) were calculated from nine test runs and the analog problem (10^{10} particles for case 0) when ^{51}Cr was a target isotope. The values of one-percent error corrected detection limit ($1/D_1R^2T$) were included to compare the general efficiencies of all test cases. One million simulated particles were used for each test problem.

Target Isotope	**Dominant Reaction Chains**
^{49}Ti	$^{56}\mathrm{Fe} \rightarrow {}^{52}\mathrm{Cr} \rightarrow {}^{49}\mathrm{Ti}$ $^{56}\mathrm{Fe} \rightarrow {}^{53}\mathrm{Cr} \rightarrow {}^{52}\mathrm{Cr} \rightarrow {}^{49}\mathrm{Ti}$ $^{56}\mathrm{Fe} \rightarrow {}^{53}\mathrm{Cr} \rightarrow {}^{50}\mathrm{Ti} \rightarrow {}^{49}\mathrm{Ti}$
^{53}Mn	$^{56}\mathrm{Fe} \rightarrow {}^{55}\mathrm{Fe} \rightarrow {}^{55}\mathrm{Mn} \rightarrow {}^{54}\mathrm{Mn} \rightarrow {}^{53}\mathrm{Mn}$ $^{56}\mathrm{Fe} \rightarrow {}^{55}\mathrm{Fe} \rightarrow {}^{53}\mathrm{Mn}$ $^{56}\mathrm{Fe} \rightarrow {}^{55}\mathrm{Fe} \rightarrow {}^{54}\mathrm{Fe} \rightarrow {}^{53}\mathrm{Mn}$
^{60}Ni	$^{56}\mathrm{Fe} \rightarrow {}^{57}\mathrm{Fe} \rightarrow {}^{58}\mathrm{Fe} \rightarrow {}^{59}\mathrm{Fe} \rightarrow {}^{59}\mathrm{Co}$ $\rightarrow {}^{60}\mathrm{Co} \rightarrow {}^{60}\mathrm{Ni}$ $^{56}\mathrm{Fe} \rightarrow {}^{57}\mathrm{Fe} \rightarrow {}^{58}\mathrm{Fe} \rightarrow {}^{59}\mathrm{Fe} \rightarrow {}^{59}\mathrm{Co}$ $\rightarrow {}^{60m}\mathrm{Co} \rightarrow {}^{60}\mathrm{Co} \rightarrow {}^{60}\mathrm{Ni}$

Table 5.2 Reaction channels leading to the most productions of ^{49}Ti, ^{53}Mn and ^{60}Ni were described and used for estimating the optimal values of variance reduction parameters.

The first study case was concerned with ^{51}Cr as the isotope of interest. ^{51}Cr was produced predominantly from the following reaction chain:

$$^{56}\mathrm{Fe} \rightarrow {}^{53}\mathrm{Cr} \rightarrow {}^{52}\mathrm{V} \rightarrow {}^{52}\mathrm{Cr} \rightarrow {}^{51}\mathrm{Cr}.$$

The observed occurrence in the reaction tree of ^{51}Cr suggested a value of four for a *forced parameter*. Combinations of initial guessed values of *forced parameter*, 3, 4 and 5, and *biasing scores* of 5, 10 and 100 were used to construct a test set for finding the best modeling scheme for ^{51}Cr.

According to Table 5.1, the test case when *forced parameter* and *biasing score* are 4 and 10, respectively, produced the highest value of FOM. It implied that this combination of variance reduction parameters is the most efficient scheme for detecting ^{51}Cr. Based on a previous analog problem with 10^{10} Monte Carlo particles, ^{51}Cr was produced with a relative error of 100%, and a computational time of 5.58 hours. With the optimal scheme, the relative error of ^{51}Cr was improved to 5.28% while the computing time was reduced to 60 seconds. Based on Equation (4.3), the test case would need about 67 seconds of computing time to produce ^{51}Cr with a relative error less than 5%. The relative error from the analog case was statistically unreliable and could not be used to predict the computing time necessary to achieve a certain precision. The deterministic result of 8.420×10^{-11} was chosen as a reference and used with Equation (4.4) to estimate a required number of particles to obtain a result with relative error less than 5%. As a result, the analog problem would need about 4.80×10^{12} particles translating to about 9.64×10^{6} seconds (112 days) of computing time.

It is interesting to consider an overall efficiency of the problem, which was designed to improve only one particular result. The values of one-percent error corrected detection limit ($1/D_1R^2T$) were used to assess an overall efficiency of each test case. Comparing the relative magnitudes of these values implies that each test case performed at a similar level of overall efficiency. As expected, the optimal scheme for calculating a result for one particular isotope was not the most efficient scheme when an overall efficiency of the problem was of interest.

As stated, *biased reaction branching* was not applied at a reaction where ^{51}Cr was not present as a product. This has a negative impact on the performance compared to a case that biases towards the pathways that eventually produce the target isotope. Further increase in efficiency may be achieved with a more elaborately defined sets of variance reduction parameters for every reaction.

Table 5.2 shows the reaction pathways with the most production of ^{49}Ti, ^{53}Mn and ^{60}Ni. It is important to point out that *uniform reaction branching* was not used in the study case with ^{60}Ni because both of the product channels in the chains resulting in ^{60}Ni were extremely active and thus probable. The use of *uniform reaction branching* would, in fact, decrease frequency of ^{60}Ni-terminated histories and consequently worsen the precision of ^{60}Ni's detection.

The most efficient sets of *forced parameter* and *biasing score* for calculating the inventories of ^{49}Ti, ^{53}Mn and ^{60}Ni were summarized in Table 5.3. With a simple application of variance reduction techniques, as large as four orders of magnitude improvement in efficiency was obtained in the study case of ^{49}Ti. According to Table 5.4, the results of ^{49}Ti and ^{60}Ni showed significant improvements in both statistical errors and computing time, with the statistical errors errors under two percent and computing time of 54 and 136 seconds, respectively. Although the statistical errors of ^{53}Mn was only improved slightly, the computing time for this studied isotope was greatly reduced from 5.58 hours to 54 seconds.

The simulation results confirmed the initial guess that the optimal values of *forced parameter* were in the proximity of the position of the target isotope in the dominant reaction channels. For example, for ^{49}Ti, the target isotope appeared 3th and 4th within the reaction channels, and the optimal forced parameter for ^{49}Ti is 3. On the other hand, the most efficient choices of *biasing score* were determined on a trial-and-error basis. It was also worth noting that the effect of *biased reaction branching* tended to be insignificant in a case when a target isotope was the most active product. ^{60}Ni was produced predominantly from a β^- decay of ^{60}Co. This reaction channel was far more active than others of ^{60}Co. A high value of *biasing score* for this reaction channel would decrease the importance of each history due

Product	**Force Parameter**	**Biasing Score**
^{49}Ti	3	300
^{53}Mn	3	100
^{60}Ni	7	5

Table 5.3 The most efficient configurations of variance reduction parameters for detecting three isotopes in the study cases are shown.

to weight adjustment and thus would not provide an efficient model. As a result, the optimal value of *biasing score* for ^{60}Ni turned out to be as low as 5.

This strategy of performing a number of small scale simulations to assess an optimum set of variance reduction parameters that are then used for a larger scale production calculation is common in Monte Carlo radiation transport. It is important to recognize that since the goal is to achieve an answer with sufficient statistical quality in a fixed total amount of wall-clock, this strategy amounts to a trade-off between user time to optimize the variance reduction parameters and computer time to solve a problem with a given statistical quality. As such, as a user gains more experience, they will be able to achieve the bulk of the improvement in computational efficiency with a minimal investment. In particular, a user should take care not to spend too much time optimizing variance reduction parameters such that the total time required to achieve the desired statistical quality is longer than simply running the analog problem. The comparisons reported here are simple comparisons between the computer time and do not reflect the total time required for the user to accomplish the task.

5.2.2 Study Problem 2

Before discussing the results of the study problem, it is useful to consider the efficiency of the analog simulation by calculating an FOM or the error-corrected detection limit. In

Product	**Analog Problem**			**Study Case**		
	Relative Error	**Comp. Time (s)**	**F.O.M**	**Relative Error**	**Comp. Time (s)**	**F.O.M**
^{51}Cr	100%	20088	0.00005	5.28%	60	5.97
^{49}Ti	30.15%	20088	0.00055	1.87%	54	52.76
^{53}Mn	13.13%	20088	0.00290	11.08%	54	1.51
^{60}Ni	8.64%	20088	0.00670	0.73%	136	139.37

Table 5.4 Comparisons of relative error, computing time and FOM between an analog problem and study cases with optimal sets of variance reduction parameters are shown. Improvements in all areas from the analog problem are observed in all cases.

Category	**Study Case**					
	F.P. 1	**F.P. 2**	**F.P. 4**	**F.P. 6**	**F.P. 7**	**F.P. 8**
Computing time (s)	192	274	3584	32902	97616	268823
Number of products	71	76	117	126	129	135
D_k, $k = 10\%$	4.36e-13	1.92e-14	1.85e-21	1.93e-21	3.82e-28	4.19e-28
$1/D_kR^2T$, $k = 10\%$	2.66e16	2.11e17	2.49e23	2.73e24	3.38e29	1.51e29
D_k, $k = 5\%$	5.86e-9	4.09e-10	5.50e-17	1.93e-21	3.82e-28	4.19e-28
$1/D_kR^2T$, $k = 5\%$	9.44e12	6.15e13	4.53e20	2.73e24	3.38e29	1.51e29

Table 5.5 Comparison of some characteristics of the results from the six study cases with different force parameter.

this case, the FOM can be derived from Equation (4.4) and Equation (4.6) and given by

$$\begin{aligned}\text{FOM}_{\text{analog}} &= \frac{1}{D_k R^2 T} \\ &= \frac{N}{100^2 k^2}\frac{100^2 k^2}{T} \\ &= \frac{N}{T} \qquad (5.1)\end{aligned}$$

where N is the number of histories and T is the total computing time. Since N is linearly proportional to T, this quantity should always be constant. Based on the analog simulation with 5×10^6 histories, the FOM is found to be 8.17e11. This FOM will later be used as a basis to justify the efficiency gained for each study case. Note that for each study case two values of FOMs are calculated: the error-corrected detection limit at 10% and 5%. A magnitude comparison between these two FOMs provides a crude indication of the efficiency limit for the current variance reduction techniques. That is, if the two values are exact, the current simulation is unable to detect the next lowest product with a statistical error less than 10%. Modifying parameters of the variance reduction techniques in use is not likely to significantly decrease the detection limit, i.e. increase the efficiency.

Table 5.5 summarizes some characteristics of the results, which are important to the efficiency assessment of the simulations. As expected, the numbers of products increase with increasing force parameter. With higher force parameter, the simulation is able to follow the particles deeper in a reaction tree and, at the same time, split the particles to capture more possible reaction pathways. However, such an improvement is computationally expensive as the computing time grows from 192 seconds to 74 hours when force parameter is increased from 1 to 8, respectively. All FOMs from the study cases indicate that each study case performs with a higher efficiency than the analog simulation. In addition, they suggest that the study case with force parameter of 7 is the most efficient scheme. In fact, it seems that a combination of forced reaction and reaction path splitting technique reaches its efficiency limit when a force parameter is equal to 6 and both values of FOM are identical. More evidently, the decreases in both FOMs after a force parameter of 7 indicate that the simulation does not reduce the statistical errors as much as it increases the computing time. Other variance reduction techniques are recommended for a further improvement in efficiency. In this situation, a weight window technique is expected to be an appropriate addition as it helps eliminate histories with insignificant weights.

5.3 Summary

A reaction tree from a deterministic calculation was an important input for defining an initial set of variance reduction parameters to optimize the efficiency of production toward one particular isotope. It was shown that an optimal value of forced parameters depended on the position of that isotope in the reaction chain with the most relative production. Another factor that influenced the efficiency was biasing scores, which were more difficult to predict. The magnitude of biasing score of each reaction branch was likely to depend on its relative contribution toward that isotope's result. Improving the efficiency by all means would likely require *a priori* knowledge of a reaction tree, which sometimes can be computationally expensive.

A combination of forced reaction and reaction path splitting technique greatly broadens and deepens a reaction tree, resulting in decreasing a detection limit and increasing a number of isotopic products. The efficiency of this strategy is monitored by using FOM defined as the error-corrected detection limit. Based on its defnition, this type of FOM can be used to provide an estimate of the efficiency limit of the current variance reduction techniques.

Chapter 6

AVA: Adaptive Variance-reduction Adjustment

During the initial stage of MCise development, there are six different types of variance reduction techniques. All of them have distinct advantages and require specific parameters to operate. Optimizing these parameters by hand to create an efficient Monte Carlo simulation for calculating a result of interest is a challenging task. For example, a simple simulation might involve as many as thirty isotopes and each isotope is assumed to have ten possible reaction products. The biased reaction technique, if used, needs three hundreds independent parameters for each of the control volumes to make up a complete set of biasing scores. Such a task is difficult to impossible to do within a reasonable amount of time. In fact, experts in Monte Carlo transport, Booth and Hendricks, voice their opinion on selecting parameters for variance reduction techniques and state, "The selection is more art than science, and typically, the user makes a few short trial runs and uses the information these trials provide to better guess the parameters; that is, the user learns to adjust parameters on the basis of previous experience."[14].

Fortunately, it is possible to develop an algorithm for the computer to recognize important reaction pathways. The algorithm, which is described in more detail in the next section, is called the Adaptive Variance-reduction Adjustment, or AVA for short. The algorithm is an iterative process that adjusts variance reduction parameters for subsequent calculations based on the information from a current short trial run. The algorithm is terminated when a specific number of iterations or a desired efficiency are reached and a set of variance

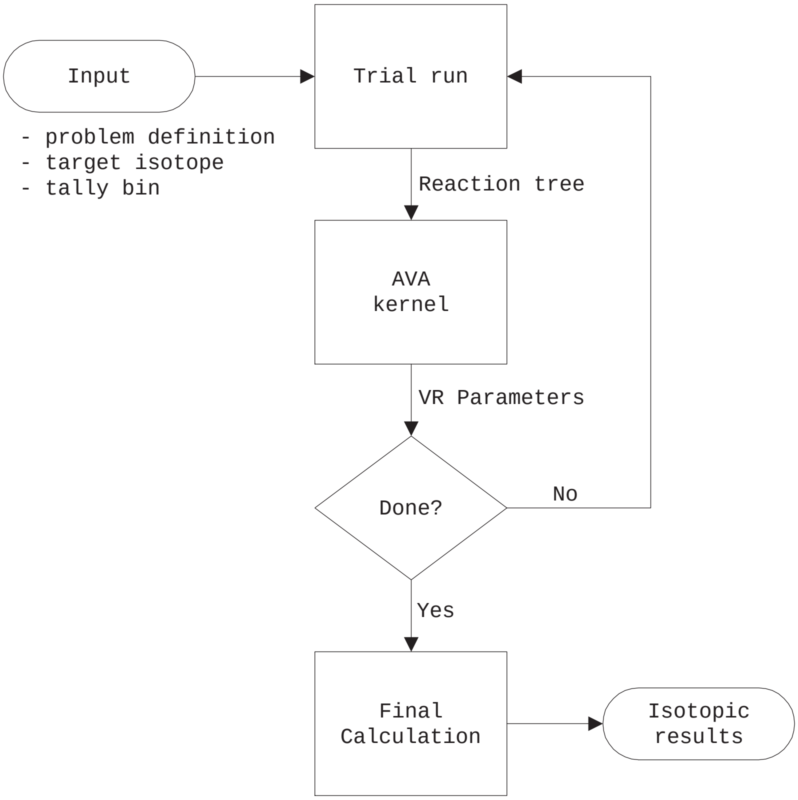

Figure 6.1 Data flowchart of AVA algorithm.

reduction parameters from the final iteration is used in an actual calculation with a much higher number of simulated particles. The data flowchart of AVA is shown in Figure 6.1.

6.1 Algorithm

During the initial development stage of AVA, it was determined that an AVA scheme should be intuitively simple and yet applicable to generic MCise simulations. More importantly, the scheme should be devised based on existing MCise capabilities. One possible scheme was to exploit information from a reaction tree, which was automatically generated during the simulation, to estimate importances of any isotopes to the production of a target result. These importances were used as primary inputs to define variance reduction parameters.

AVA iteratively modifies complete sets of parameters for three different variance reduction techniques to optimize the detection of a target isotope in a tally bin. The target isotope and tally bin must be identified in advance for each specific problem. The techniques included in AVA are forced reaction, biased reaction branching and biased source sampling. In each AVA iteration, a short trial problem is simulated to obtain a reaction tree, generating tally result in the bin of interest. Only valid reaction chains are extracted from the reaction tree. The valid reaction chains are defined as linear reaction chains leading to the generation of the target isotope in the specified tally bin. A sample schematic of valid reaction chains is shown in Figure 6.2. Each valid reaction chain contains three types of nodes– a source node, intermediate node and target node– and a relative contribution. The relative contribution of any given valid reaction chain is defined as a fraction of the score of the target isotope produced from that particular chain. Generally, a node carries an isotopic identity and contains the hierarchical information about its parent and daughter nodes. A reaction chain has only one source node and one target node, but may have multiple intermediate nodes in the chain. Isotopic identities and physical locations of the nodes, along with relative contributions from the reaction chains, are primarily used to initialize parameters for the three variance reduction techniques as described below.

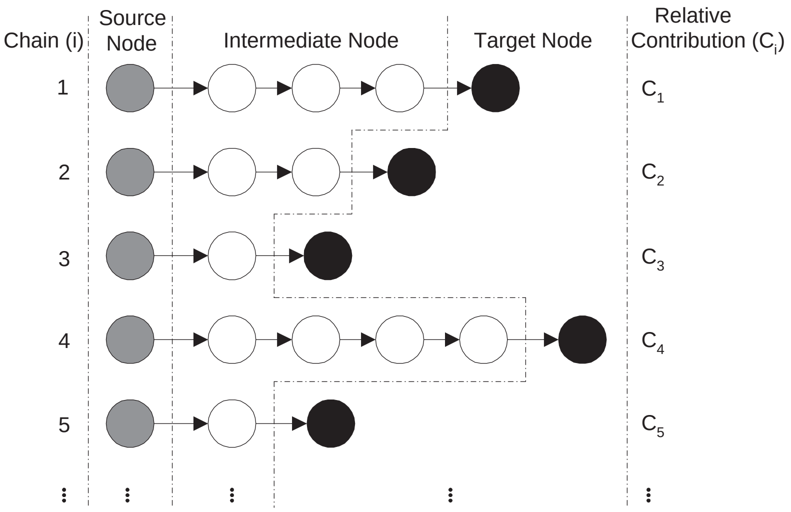

Figure 6.2 A schematic illustration of reaction chains with relative contributions (C_i) to the target isotope is shown. A gray, white and black circle represent a source, intermediate and target node, respectively.

6.1.1 Forced Reaction

Since the sole purpose of a forced reaction technique is to force a simulated atom to undergo a specific number of reactions, the numbers of reactions and relative contributions from reaction chains are primarily inputs used to define a parameter for this technique.

A force reaction parameter is defined as the weight-averaged number of reactions among the valid reaction chains. Its mathematical expression is given below:

$$Force\ Parameter = \sum_{i=1}^{k} (n_i + 1) C_i, \tag{6.1}$$

n_i = a number of intermediate nodes in the i^{th} chain,

C_i = a relative contribution to the target result from the i^{th} chain,

k = a total number of valid chains.

This initialization is designed to give considerations to all valid reaction chains, yet emphasize the ones with highest relative contributions. It implies that the simulation does not force the simulated atoms to have many more reactions than the length of the reaction chain that dominates the production of the target result. Note that the algorithm's performance matches the experience of previous chapters under these conditions.

6.1.2 Biased Reaction Branching

Typically, at any reaction point a reacting atom will be randomly assigned a new isotopic identity from a discrete probability density function (PDF) based on a list of possible products. The PDF is calculated from the individual pathway cross-sections weighted by the current neutron flux and/or decay rates. However, during an MCise simulation, this PDF can be artificially modified by using a biased reaction branching technique. This technique alters the PDF in favor of specified product isotopes and appropriately adjusts the weight of a resultant product to ensure a fair simulation.

AVA uses information from the extracted reaction chains to define degrees of preference of all product isotopes. The degrees of preference are subsequently used during the simulation by a biased branching technique when it is modifying a discrete PDF for sampling a reaction product. A probability of sampling each possible product at any reaction point is set to be equal to its normalized degree of preference. For example, it is assumed that only isotopes, a, b and c, have degrees of preference of D_a, D_b and D_c, respectively. A parent isotope, x, is having a reaction and its possible daughter products are isotopes, a, b and f. In this case, the sampling probabilities of a, b and c are given by $\frac{D_a}{D_a+D_b}$, $\frac{D_b}{D_a+D_b}$ and 0 and correspond to B_{xa}, B_{xb} and B_{xf} from the definition of B_{ij} in Equation 3.8. Nonetheless, the analog sampling is used if all of possible daughter isotopes has degree of preference equal to zero.

The degree of preference is designed based on an assumption that increasing simulated populations of isotopes in the chains leading to the target isotope results in a more efficient simulation for detecting the target isotope. Therefore, the degree of preference of a product isotope is derived from the occurrences of the product isotope in the chains and the chains' relative contributions to the target result. A degree of preference of an isotope j is defined as a relative frequency of nodes representing an isotope j in a chain weighted-averaged by the chain's relative contribution. Mathematically, the degree of preference of any product isotope j is given by:

$$D_j = \sum_{i=1}^{k} \frac{\delta_{ij}}{m_i} C_i, \tag{6.2}$$

C_i = a relative contribution from the i^{th} valid chain,

k = a total number of valid chains,

δ_{ij} = a number of nodes that represent the isotope j in the i^{th} valid chain,

m_i = a total number of nodes in the i^{th} chain.

A fraction number of nodes is used, instead of a number of nodes representing a particular isotope, to prevent AVA from assigning too high preferences for product isotopes in the long valid chains. In addition, it preserves relative importances among the valid chains, based on their relative contributions, C_i.

6.1.3 Biased Source Sampling

Currently, an isotopic identity of a source atom in an analog MCise simulation is randomly sampled from a discrete PDF characterizing the isotopic compositions of the initial material. The biased source sampling technique is implemented to help increasing the likelihood of sampling the initial isotopes of interest. During an AVA process, this technique uses information from AVA to adjust an underlying discrete PDF of the initial source composition, aiming to improve statistics of the target result.

AVA provides degrees of preference of all source isotopes for the biased source sampling technique, using a similar approach to the biased reaction branching technique. In this case, only source nodes and relative contributions from the reaction chains are considered. A degree of preference of a source isotope j is defined as the sum of relative contributions from all valid reaction chains that have a source isotope as a source node. Mathematically, a degree of preference of a source isotope j is expressed by the following:

$$D_j = \sum_{i=1}^{k} \beta_{ij} C_i, \tag{6.3}$$

C_i = a relative contribution from the i^{th} valid chain,

k = a total number of valid chains,

$$\beta_{ij} = \begin{cases} 1, & \text{if the isotope } j \text{ is a source isotope for the } i^{th} \text{ valid chain,} \\ 0, & \text{otherwise.} \end{cases}$$

The degree of preference is designed such that a source isotope occurring more frequently and heading the valid reaction chain with a higher relative contribution is given a higher importance. This implementation ensures that reaction chains, which dominate the target result, are more likely to be followed more often than those reaction chains with smaller relative contributions.

6.2 Sample Problems

Two sample problems were designed to test the performance of AVA in two areas. The first problem focused on the ability of AVA to adjust biasing scores for biased source sampling. The inventory of ^{53}Mn at shutdown following a 10-year steady-state of a mixture with a uniform multi-group neutron flux of 5×10^{12}n/cm^{2}s was calculated from a problem using AVA. The mixture was made up of equal atom fractions of chromium[1], manganese[2], iron[3], cobalt[4] and nickel[5]. The test problem was defined to have ten iterations and each iteration ran for 10^3 NPS. Prior to the AVA process, uniform reaction branching, uniform source sampling and forced reaction with a force parameter of one were initially applied to generate inputs necessary to define parameters for the first iteration. Biased reaction branching was turned off during the AVA iterations. The final set of parameters from AVA would be applied in the problem with 10^5 NPS. The result would then be compared with a deterministic relative production of 4.505×10^{-5} from ALARA.

The second problem had the same description as the first one except that the activated mixture was replaced with ^{56}Fe to simplify the source definition of the problem. This problem focused on the ability of AVA to adjust biasing scores for biased reaction branching. A deterministic relative production from ALARA for this case was 6.1×10^{-9}.

6.3 Results and Discussions

The value of NPS used in the preliminary run was set to be ten times higher than the one used during AVA iterations. It initialized the set of parameters which would be updated in subsequent AVA iterations. The larger amount of NPS is expected to provide good initial estimates of the parameters, which in turn should give a final result with smaller statistical error.

---

[1] Atom percent abundances: ^{50}Cr - 4.35%, ^{52}Cr - 83.79%, ^{53}Cr - 9.50% and ^{54}Cr - 2.36%

[2] Atom percent abundance: ^{55}Mn - 100%

[3] Atom percent abundances: ^{56}Fe - 91.75%, ^{54}Fe - 5.85%, ^{57}Fe - 2.12% and ^{58}Fe - 0.28%

[4] Atom percent abundance: ^{59}Co - 100%

[5] Atom percent abundances: ^{58}Ni - 68.08%, ^{60}Ni - 26.22%, ^{61}Ni - 1.14%, ^{62}Ni - 3.63% and ^{64}Ni - 0.93%

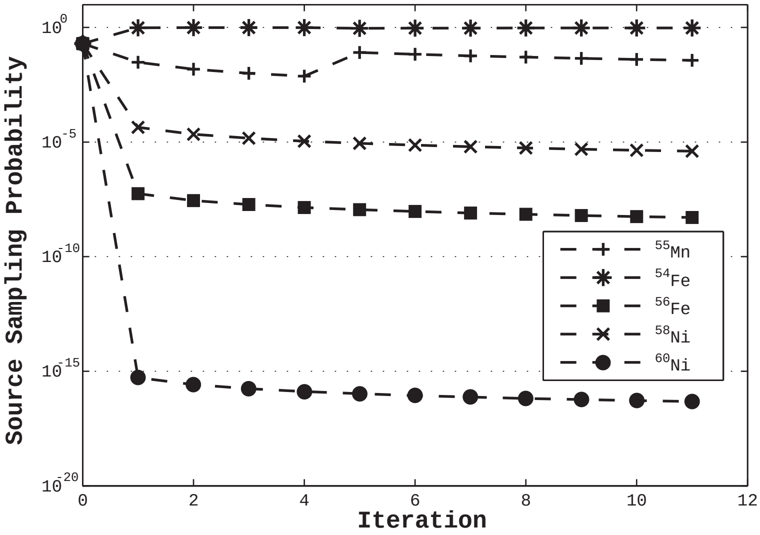

Figure 6.3 Probabilities of source sampling from the first sample problem were shown as a function of iterations. There were five source isotopes present after the preliminary run. Each iteration was run for 10^4 NPS.

A preliminary run from the first test problem produced twenty five reaction chains leading to the production of ^{53}Mn. Out of fifteen possible source isotopes, ^{54}Fe, ^{55}Mn, ^{58}Ni, ^{56}Fe and ^{60}Ni, in an increasing order of relative contributions, were found at the top of those reaction chains. The probabilities for source sampling were initialized and iteratively increased according to Equation (6.3). The evolutions of those probabilities are illustrated in Figure 6.3.

Probabilities for sampling ^{54}Fe heavily dominated other probabilities at all iterations. They contributed to the fact that ^{53}Mn occurred predominantly from two reactions: $^{54}\text{Fe} \xrightarrow{(n,np)} {}^{53}\text{Mn}$ and $^{54}\text{Fe} \xrightarrow{(n,d)} {}^{53}\text{Mn}$. Increasing frequencies of source isotopes leading to ^{53}Mn was the only means to statistically improve its result since biased reaction branching was unavailable. The other source isotope that was significant to the production of ^{53}Mn was ^{55}Mn by a reaction, $^{55}\text{Mn} \xrightarrow{(n,2n)} {}^{54}\text{Mn} \xrightarrow{(n,2n)} {}^{53}\text{Mn}$. At the end of the AVA process, the probabilities for source sampling ^{54}Fe and ^{55}Mn were approximately 96.30% and 3.70% while the probabilities for other sources were extremely small that could be negligible. The final value of the force

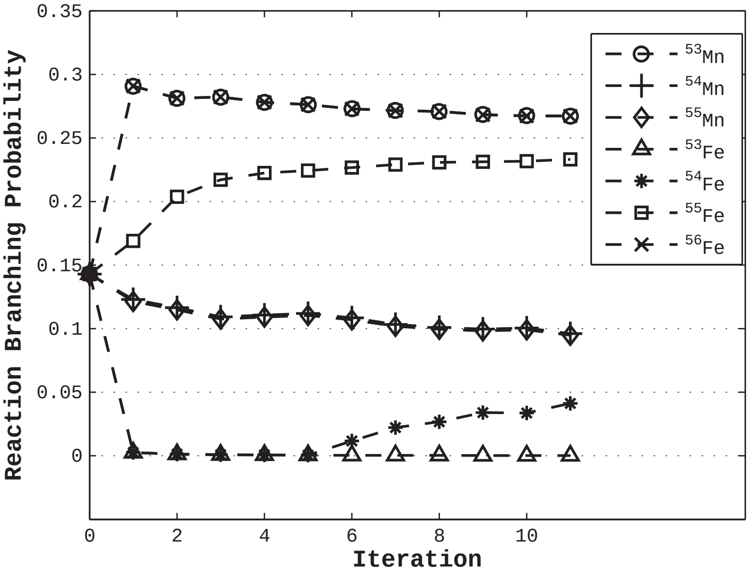

Figure 6.4 Probabilities of reaction branching from the second sample problem were shown.

parameter was 1.00675 which agreed with a physical observation that a majority of ^{53}Mn was from a two-node reaction chain starting with ^{54}Fe.

The inventory of ^{53}Mn from the final calculation was 4.512×10^{-5} with a statistical error of 1.09%. The result was in great agreement with the deterministic result as the relative difference was 0.16%. The simulation required a total computing time of 5.97 seconds, including the AVA process, to achieve these levels of accuracy and precision. To evaluate the efficiency of AVA, an analog problem with 10^7 NPS was run and timed with a computing time of 35.71 seconds. The analog problem would require at least 1.87×10^8 NPS if it were to reproduce the result of ^{53}Mn with the same accuracy and precision. This amount of NPS translated into a computing time of about 668 seconds. The difference of those computing times showed that AVA performed with a reasonable efficiency.

The next test problem involved adjusting biasing scores for biased reaction branching. Once again, a preliminary run preceding the AVA was required. Initially, five valid reaction chains containing nineteen nodes were obtained. Each node was considered to initialize a probability for sampling a reaction product in favor of its corresponding isotope, according to Equation (6.2). The initial force parameter was initialized to be 2.514. After all, seven different isotopes were given initial probabilities which would be thr basis for subsequent AVA iterations. Those seven isotopes included a source isotope, ^{56}Fe, a target isotope, ^{53}Mn, and five intermediate isotopes, ^{54}Mn, ^{55}Mn, ^{53}Fe, ^{54}Fe, and ^{55}Fe. The first AVA iteration produced nineteen valid reaction chains; however, there were only two different parent isotopes, ^{55}Fe and ^{54}Mn, in those chains before the target. Almost all occurrences of ^{55}Fe came from the reaction chain, $^{56}\mathrm{Fe} \xrightarrow{(n,2n)} {}^{55}\mathrm{Fe} \xrightarrow{(n,t)} {}^{53}\mathrm{Mn}$. On the other hand, ^{54}Mn appeared in many reaction chains due to an active loop reaction, $^{54}\mathrm{Mn} \underset{(n,\gamma)}{\overset{(n,2n)}{\rightleftharpoons}} {}^{53}\mathrm{Mn}$. The sizes of those reaction chains ranged from three to seven nodes. The probability progressions of all seven isotopes at all iterations were shown in Figure 6.4.

Expectedly, biasing probabilities for ^{56}Fe and ^{53}Mn were higher than others since they appeared in every valid reaction chain as a source and target node, respectively. Overall, marginal changes of probabilities were observed after the first iteration and the probabilities seemed to converge after a few iterations. In the final calculation, a relative production of ^{53}Mn was 6.42×10^{-9} with a statistical error of 5.31%. A relative error with respect to a deterministic result was 5.01%. Having the statistical error higher than the relative error implied that the accuracy could be improved by increasing NPS during the simulation. The total computing time was 8.47 seconds which was by far less than the projected computing time of 47.66 hours for the analog problem[6] aiming to achieve the same level of success.

So far, the values of the variance reduction parameters have been iteratively defined, based on two properties of a reaction chain: a composition and a contribution to the target isotope. The final set of parameters is then used for the final calculation. This implementation raises one important question. Does this final set produce the most efficient scheme for calculating the inventory of the target isotope? Since a figure of merit (FOM) is a metric indicating the efficiency of the simulation, the simplest solution is to compare FOMs for all iterations. If the FOM from the final iteration step is the highest, the final set will yield the most efficient scheme.

To evaluate the efficiency of the AVA process, the second sample problem is rerun with 400 iterations. FOMs, based on the statistical errors of ^{53}Mn, are calculated for all iterations and are shown in Figure 6.5. Some large deviations in FOMs are observed; however, they are expected because of strong statistical variations in MC problems with a small NPS, 1000, in this case. Since the production of a target isotope is very small ($\sim 10^{-9}$), a few more or fewer counts in a tally can lead to statistical fallacies as seen through some occasional irregular behaviors of FOM. Most FOMs fluctuate along the trend line as the variance reduction parameters are being adjusted. The overall trend of the plot suggests that the efficiency of the simulation continuously improves at early iterations and seems to reach the performance limit about after 100 iterations.

In addition to increasing the efficiency of the simulation, a result from the final calculation shows that accuracy and precision are improved from a previous problem with a fewer number of iterations. The relative production of ^{53}Mn is 6.132×10^{-9} with a statistical error of 2.43%.

---

[6] An analog problem with 10^7 NPS requires 26.166 seconds of computing time.

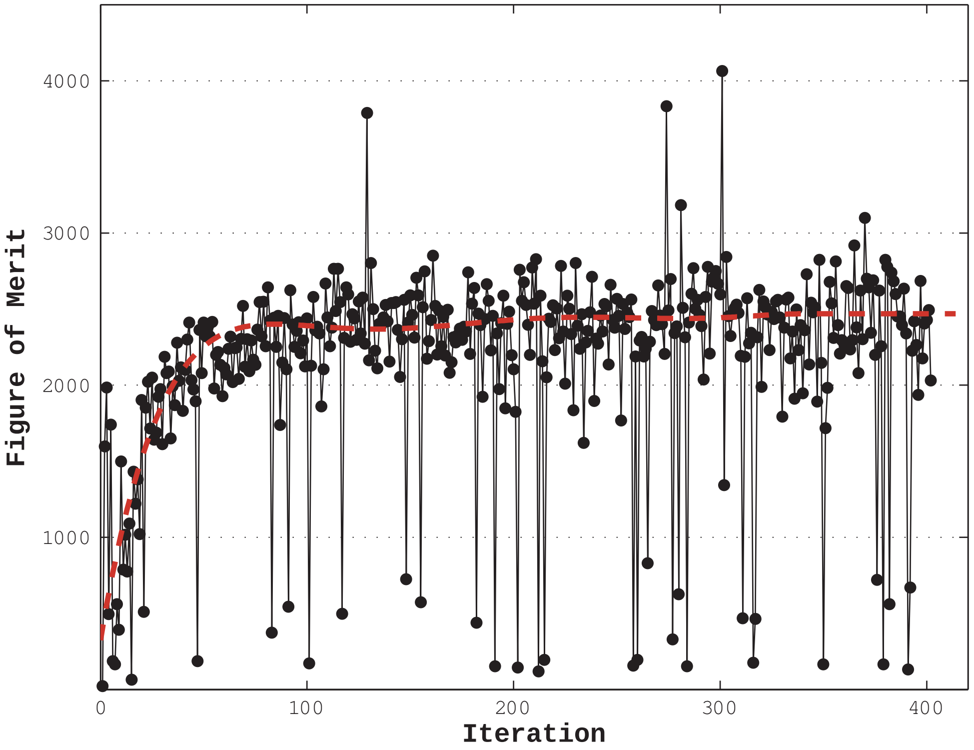

Figure 6.5 Figures of merit from the second sample problem with 400 iterations are shown. Note that FOMs are based on the statistical errors of ^{53}Mn and a dash red line indicates the overall trend of FOMs.

When compared to the deterministic result, a relative error is found to be 0.525%. The total computing time is 29.18 seconds.

6.4 Summary

To employ variance reduction techniques to the highest capabilities, their parameters must be properly defined. Traditionally, the parameters have been computed manually. First, the initial set of parameters is derived from intuition and experience. A short problem is run and its result is considered to determine whether or not it is satisfactory. If not, those parameters are re-adjusted. AVA is developed to eliminate the guesswork in developing the initial set of parameters and a series of trials for manually adjusting those parameters. Based on two sample problems, AVA is successfully implemented to define an efficient set of parameters for forced reaction, biased reaction branching and biased source sampling techniques. Precision and accuracy of AVA problems are greatly improved from an analog problem as evident from dramatic decreases in both computing time and relative error.

Chapter 7

Applications

In this chapter, isotopic inventories of three systems with flowing materials are examined to demonstrate capabilities of MCise in modeling the activation process without having to deploy approximation strategies on an irradiation schedule. The first system is a hypothetical problem taken from *Introduction to Nuclear Engineering 2nd Edition* by John R. Lamarsh (Problem 10.35)[23]. In this problem, an activity at equilibrium is determined analytically, and is compared to a numerical result from MCise. This problem serves as a good benchmark for MCise because an analytical solution can be derived. The second system involves the study of transmutation and burnup of liquid fuel in *In-Zinerator*[24]. This system poses a unique challenge in that the model must incorporate the on-line fission product separation and time-dependent continuous feed of fresh fuel hoping to keep a thermal power constant. Lastly, the activation assessment of a LiPb liquid breeder in the ARIES compact stellarator power plant or *ARIES-CS*[25] is investigated. A challenge in modeling this system is due to the fact that the breeder passes through two different radial blankets and hence experiences two different spectrums. Two outflows then mix in the external vessel where tritium is extracted and re-enter the blankets.

7.1 Coolant Activation

The problem description below is excerpted from *Introduction to Nuclear Engineering 2nd Edition* by John R. Lamarsh (Problem 10.35):

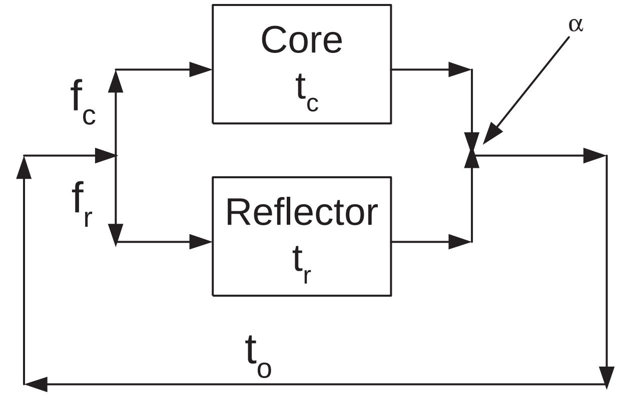

Figure 7.1 The coolant circuit is composed of core, reflector and outer circuit.

In many water cooled reactors the water acts as moderator and reflector as well as coolant. The coolant circuit is then as shown in [Figure 7.1], where the fraction f_c of the coolant entering the reactor passes through the core, the remaining fraction f_r going to the reflector. The average activation rates per unit volume in the core and reflector are $(\Sigma_{act}\phi_{av})_c$ and $(\Sigma_{act}\phi_{av})_r$, respectively, and the water spends the times t_c, t_r and t_o in the core, reflector and outer circuit. Show that the specific activity leaving the reactor is given by

$$\alpha = \frac{f_c(\Sigma_{act}\phi_{av})_c(1-e^{-\lambda t_c}) + f_r(\Sigma_{act}\phi_{av})_r(1-e^{-\lambda t_r})}{1 - f_c e^{-\lambda(t_c+t_o)} - f_r e^{-\lambda(t_r+t_o)}}. \tag{7.1}$$

7.1.1 Problem Modifications

Several modifications are made to the problem so that the comparison between analytical and MCise results are well presented. These modifications are described as follows.

Neutron Flux

The neutron fluxes in the core and the reflector in this study are obtained from the real values in the University of Wisconsin's Nuclear Reactor. [1] The flux is normalized to simulate an energy production of 1000 MWth, as shown in Figure 7.2. Although these values are not

---

[1] Benjamin Schmitt, a UWNR operator, provides the sample neutron fluxes.

perfect representatives of the operational fluxes in the actual power plants, they are readily available and are sufficient for our purposes.

Coolant

In general, there are a few important reactions by which coolants are activated [23]: ^{16}O(n,p)^{16}N, ^{17}O(n,p)^{17}N, ^{18}O(n,γ)^{19}O, ^{23}Na(n,γ)^{24}Na and ^{40}Ar(n,γ)^{41}Ar. The first three reactions are the primary sources of radioactivity in the water cooled reactor while the last two reactions are significant contributors in the reactors with sodium and air coolant, respectively. In the context of this exercise, a sodium activation has a distinct advantage over oxygen activation because its activation can occur with neutrons at all energies. Therefore, sodium coolant is assumed to be used and a reaction, ^{23}Na(n,γ)^{24}Na, is considered.

Output Response

The amount of ^{24}Na relative to an initial amount of ^{23}Na is the current output response from MCise tally. The final solution in (7.1) must be manipulated to give the answer comparable to the output from MCise. Terms, $(\Sigma_{act}\phi_{av})_c$ and $(\Sigma_{act}\phi_{av})_r$, must be replaced with the effective reaction rate coefficients for a reaction, $^{23}\mathrm{Na} \xrightarrow{(n,\gamma)} {}^{24}\mathrm{Na}$, in the core and reflector, respectively. They can be calculated by collapsing the (n, γ) cross section with the neutron fluxes for the core and reflector. With simple manipulations on Equation (7.1), the relative amount of ^{24}Na is given by

$$\frac{N_{Na-24}}{N_{Na-23}} = \frac{f_c \frac{(\sigma_\gamma \phi_{av})_c}{\lambda}(1 - e^{-\lambda t_c}) + f_r \frac{(\sigma_\gamma \phi_{av})_r}{\lambda}(1 - e^{-\lambda t_r})}{1 - f_c e^{-\lambda(t_c + t_o)} - f_r e^{-\lambda(t_r + t_o)}}. \tag{7.2}$$

7.1.2 MCise Simulation

To construct the model in MCise, the initial values for the variables are assigned in Table 7.1. Note that a parametric study can be performed by varying each variable in question individually while keeping other variables fixed. Three control volumes are defined to represent components through which simulated atoms must progress. The core and reflector

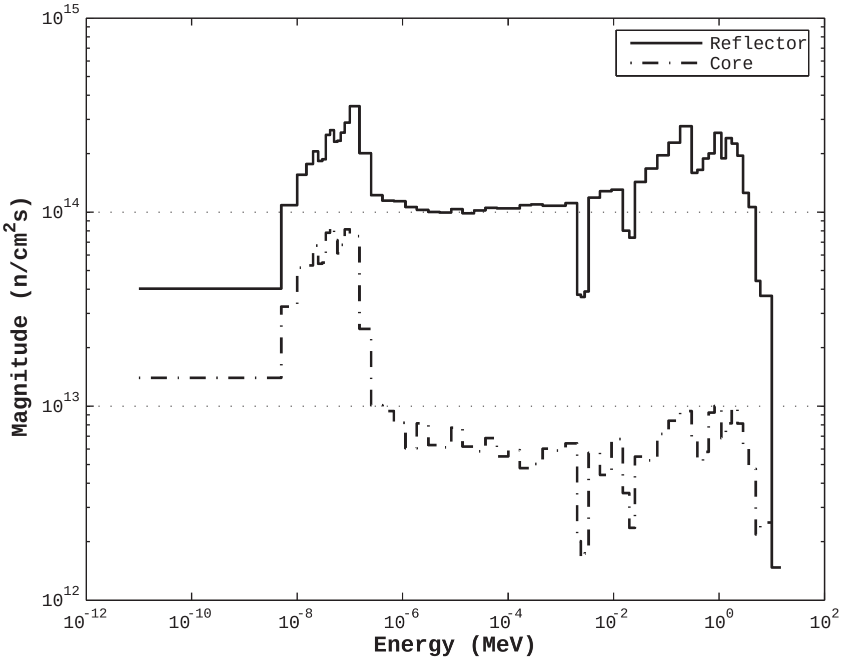

Figure 7.2 Sample neutron fluxes are taken from UWNR and normalized to an operating condition of 1000 MW.

Variable	Value
t_c	2600 s
t_r	3600 s
t_o	1000 s
f_c	50%
f_r	50%

Table 7.1 Residence times in the core, reactor and outer circuit, and relative volumetric flow rates in the core and reactor are assumed.

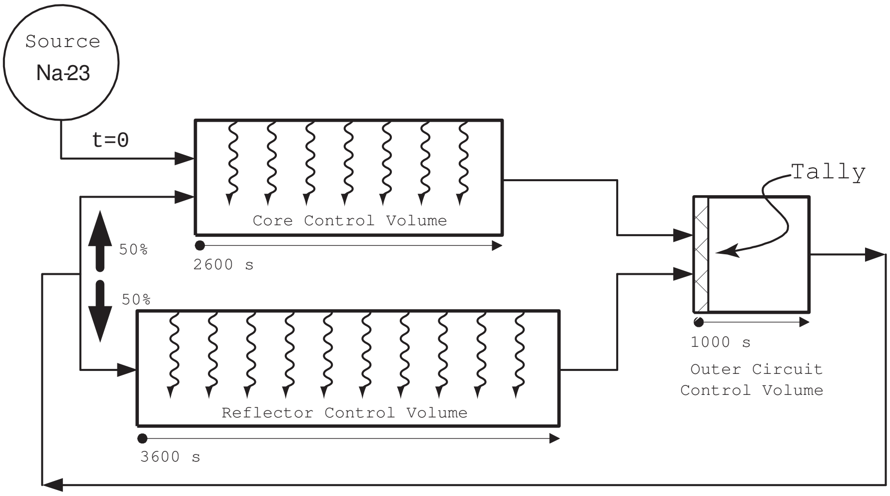

Figure 7.3 An MCise model for a coolant activation problem is consisted of three control volumes, one source and one tally.

control volumes contain prescribed neutron fluxes while the outer circuit control volume does not have a neutron flux. All simulated atoms created from a ^{23}Na point source enter the core control volume at $t = 0$. Upon exiting the core control volume, they enter the outer circuit control volume where they are tallied based on their arrival times and isotopic identities. After that, the atoms are forced to enter the core or reflector control volume with predefined probabilities. An illustration of the model is shown in Figure 7.3. The atoms continue their histories in the cycle until a desired total simulation time is reached. The atoms are expected to spend 4100 seconds on average for one cycle because they have equal chances of entering the core and the reflector. This amount of time is therefore defined as one average cycle. Aiming to have a buildup of ^{24}Na attained a saturation, the total simulation time is set to 240 hours. The simulation uses 4×10^8 NPS.

7.1.3 Numerical Result

Figure 7.4 illustrates the buildup of ^{24}Na as a function of operation time. As expected, the production level of ^{24}Na initially increases exponentially before starting to level off to equilibrium after approximately 100 average cycles. The MCise model predicts a relative production of ^{24}Na at the equilibrium to be 5.7929×10^{-5} with a statistical error of 0.186%.

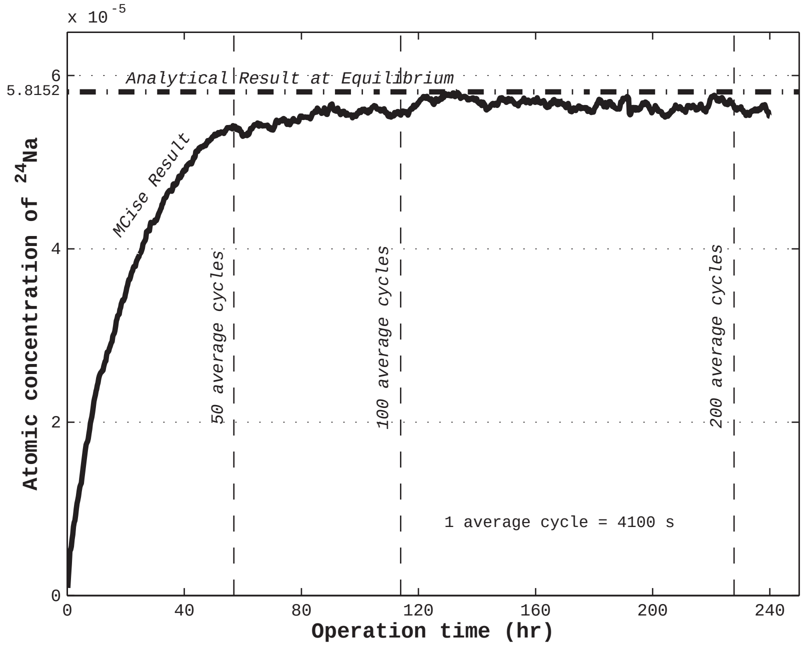

Figure 7.4 A atomic concentration of ^{24}Na from MCise is plotted as a function of operation time. A dash-dot line indicates a relative production at equilibrium from a deterministic calculation.

This numerical result is in remarkable agreement with the result of 5.812×10^{-5} calculated using the deterministic model. However, a high-frequency fluctuation at the equilibrium observed in the MCise result with this small statistical error is not typical. After a careful review of the problem description, the reasoning behind this unusual characteristic can be explained as follows.

As the coolant leaves the outer circuit control volume, it faces a decision whether to enter the reflector or the core control volume. In MCise model, the probabilities of entering either control volumes is assumed to be the same. Each particle history can be viewed as a unique physical realization of a stochastic irradiation history. The statistical nature of the problem requires large numbers of physical realizations to see convergence, adding significant complication to the calculation. In this particular case, a number of required physical realizations can be calculated and given by 2^k, where k is a number of cycles. As the system reaches equilibrium, the number of possible physical realizations grows to about 2^{100}, which is in the order of 10^{30}. This situation in the inventory analysis is analogous to that of particle transport in stochastic mixtures[26].

To attain the ensemble average of the solution is a simple but extremely computationally expensive procedure– a Monte Carlo simulation and tally of the quantities of interest is recorded for each particular physical realization before averaging. Given infinite computing resources, this procedure yields the exact solution. Nevertheless, it is clearly impractical for routine use. Therefore, many efficient algorithms have been developed to produce reasonable approximations to the exact solution. An algorithm proposed by Zimmerman[27] and its later extensions by Donovan and Danon[28] are based on the use of a chord-length sampling technique to avoid the need to create a set of physical realizations in order to obtain the solution. This problem is a potential research direction for inventory analysis which requires further extensive investigation and is beyond the scope of this thesis.

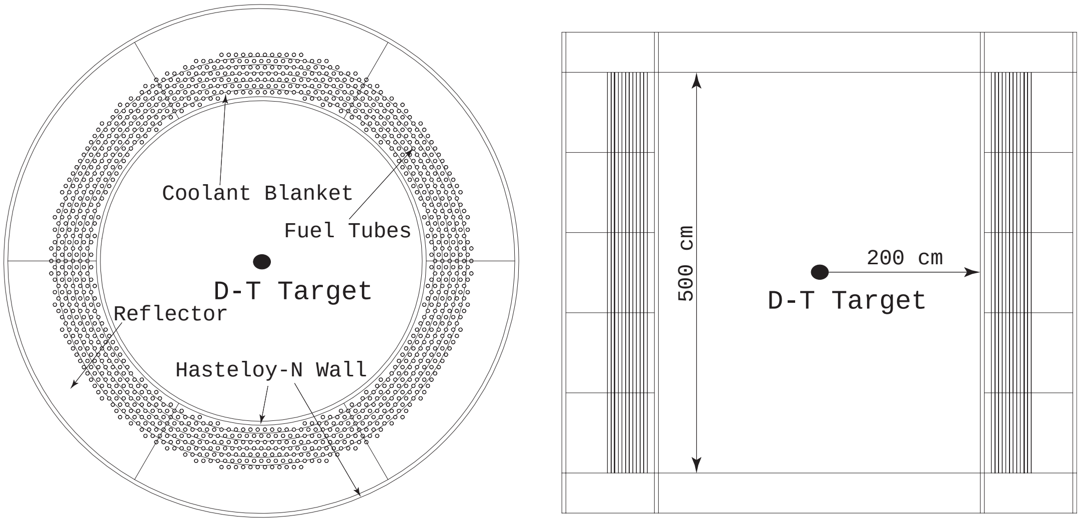

Figure 7.5 Axial and radial cross section of the MCNP model of the In-Zinerator.

7.2 In-Zinerator

The Z-pinch transmuter uses a D-T fusion target, which produces a point source of 14.1-MeV neutrons, to drive sub-critical cylindrical channels containing actinides in a fluid form. The 200-MJ fusion target is ignited every ten seconds to provide a 20-MW fusion source for the blanket. The In-Zinerator, with its MCNP model shown in Figure 7.5, is designed to keep the channels sub-critical and to maintain a desired power level of 3000 MWth. The fusion target is located in the center of the chamber and is 2 meters from the first wall. The first wall is a 5-cm thick cylindrical sheet of Hasteloy-N. The coolant blanket is 57-cm thick. The actinides are contained in a fluid fuel form within 1150 tubes in the blanket. Each tube is made of Hasteloy-N and has an inner and outer radius of 2.2 cm and 2.4 cm, respectively. Surrounding the coolant blanket are a 50-cm and 5-cm thick layer of lead and Hasteloy-N, respectively. The former serves as a reflector to increase neutron multiplications.

The liquid fuel is an eutectic at 675 °C formed by LiF and AnF_3 (actinides fluoride) with a molar ratio of 2 to 1. Actinides in the problem are made of transuranic isotopes(TRU) from spent LWR fuel. One advantage of liquid fuel is that, a portion of fluid can be taken out of the reactor and processed to remove fission products. The processed fuel is then replenished

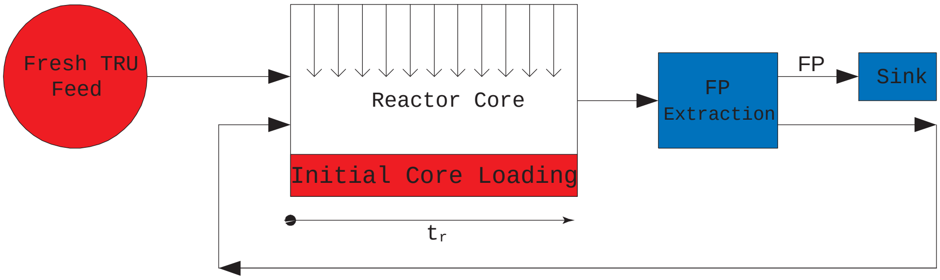

Figure 7.6 Schematic of In-Zinerator MCise model, showing sources in red and sinks in blue.

with some fresh TRU necessary to maintain constant inventories and returns to the reactor. While most, if not all, traditional tools are not suitable for performing activation and burnup calculation on this type of fuel cycle, MCise is implemented with capabilities to handle online material addition into and extraction out of the system.

The goal of this study problem is to use MCise to calculate detailed isotopic distributions at all operation times.

7.2.1 MCise Simulation

A schematic of the MCise model of the In-Zinerator is illustrated in Figure 7.6. The two control volumes in this schematic are the reactor core and fission product extraction environments. The reactor core is characterized by the average neutron flux that the eutectic fuel experiences while the second control volume has a neutron flux of zero. For the purpose of this analysis, a residence time of 100 days in the reactor was chosen corresponding to the processing of 1% of the total inventory per day in the fission product extraction step. The residence time of the FP extraction represents a processing period of the fuel and was chosen to be zero during the initial stages of this study.

All of the flow leaving the reactor core goes to the FP extraction process, but the flow leaving the FP extraction process is divided into two streams based on the atomic species. All fission products flow to the sink and all actinides (and Li and F) are returned to the reactor core. This model was chosen to represent an ideal separations process and the flow distribution of each species can be adjusted to represent the real separations efficiencies.

There are two atom sources in the In-Zinerator model. Isotopic distributions of both sources are summarized in Table 7.2.

The first one is the source representing the isotopic mix of the initial core loading and is assigned to the reactor core control volume. Mathematically, its time-dependent source strength is defined as

$$r_1(t_{sim}) = R_1 \delta(t_{sim}), \tag{7.3}$$

where R_1 is the total number of atoms at the initial core loading. Since the atoms sampled from this source would start their history uniformly inside the reactor core, a PDF describing their remaining residence time is given by:

$$p_1(t_{rem}) = 1/t_r. \tag{7.4}$$

The other source accounts for the addition of fresh fuel (TRU) to replace the consumed fuel. For this model, it was assumed that actinides could only be added as rapidly as fission products were being removed, to maintain a constant inventory in the reactor. More precisely, since each actinide fission results in two fission products, the rate of addition of actinides should be half the rate of removal of fission products. The fission product removal rate is determined by the inventory of fission products in the system. Under the assumption of a constant power level in the reactor, this can be calculated analytically:

$$\dot{F} = \kappa P - \frac{\varepsilon \dot{C}}{I} F, \tag{7.5}$$

$$F(0) = 0, \tag{7.6}$$

Isotope	**Initial Core Loading** (atomic fraction)	**Feed Stream** (atomic fraction)
Li-6	1.2501e-2	-
Li-7	2.3753e-1	-
F-19	6.2507e-1	-
Np-236	9.0012e-9	7.3147e-8
Np-237	9.0761e-3	7.3435e-2
Np-238	-	3.1085e-11
Np-239	-	1.7966e-8
Pu-236	-	1.4384e-12
Pu-238	3.3129e-3	2.6630e-2
Pu-239	5.6632e-2	4.5452e-1
Pu-240	3.2879e-2	2.6288e-1
Pu-241	1.1576e-3	9.2095e-3
Pu-242	7.2382e-3	5.7352e-2
Pu-243	1.4127e-6	1.3491e-16
Pu-244	-	1.1055e-5
Am-241	1.1576e-2	9.2075e-2
Am-242	2.0627e-5	1.9542e-9
Am-242m	-	1.6305e-4
Am-243	2.6003e-3	2.0530e-2
Am-244	-	1.5457E-20
Cm-242	4.9754e-8	3.9434e-7
Cm-243	3.5004e-6	2.7573e-5
Cm-244	2.6878e-4	2.1100e-3
Cm-245	1.1051e-4	8.6423e-4
Cm-246	2.4878e-5	1.9336e-4
Cm-247	4.8005e-7	3.7225e-6
Cm-248	5.5381e-8	4.2804e-7
Bk-249	1.2501e-10	-
Cf-249	1.2501e-10	-
Cf-250	1.2501e-10	-

Table 7.2 Isotopic compositions of sources used in the MCise simulation are shown.

where

$$\begin{aligned} F &= \text{a total inventory of fission products [atoms]} \\ P &= \text{a desired power level [energy/time]} \\ \kappa &= \text{a number of fission products produced for an average fission energy released} \\ &\approx \frac{2}{180MeV}\text{atoms/energy} \\ \varepsilon &= \text{an efficiency of a fission product separation process [dimensionless]} \\ \dot{C} &= \text{a processing capacity rate [atoms/time]} \\ I &= \text{a total initial inventory [atoms],} \end{aligned}$$

therefore,

$$F(t) = \frac{\kappa PI}{\varepsilon \dot{C}} \left(1 - e^{-\varepsilon \dot{C} t/I}\right). \tag{7.7}$$

The feed rate of fresh TRU needed is also equivalent to the time-dependent source strength of the second source in the MCise simulation and given by:

$$r_2(t_{sim}) = \frac{1}{2}\frac{\varepsilon \dot{C}}{I} F(t_{sim}) = \frac{\kappa P}{2} \left(1 - e^{-\frac{\varepsilon \dot{C} t_{sim}}{I}}\right), \quad 0 < t_{sim} < T_{sim}. \tag{7.8}$$

Since the feed stream always enters at the beginning of the reactor control volume, a PDF describing the remaining residence time of the feed is defined with a delta function,

$$p_2(t_{rem}) = \delta(t_{rem} - t_r). \tag{7.9}$$

The CINDER90 nuclear data library is used in this study. It uses a 63 group energy structure and includes both transmutation reactions and fission reactions with fission product yields. The fission product yields are not explicitly dependent on the neutron flux spectrum, but are defined for a number of representative spectrum types: thermal, fast and high-energy. For some isotopes, spontaneous fission product yields are also given. CINDER does not provide fission yields for all possible fission reactions. In such cases, when a fission reaction occurs, the product isotopes will be assigned a placeholder isotopic identity, *unknown fission product*. This isotope is stable and neutronically transparent and will accumulate. An accumulation of this isotope could result in underestimating decay heat and specific activity of the system.

Parameter	Value	Description
P	3.7233×10^3 $\mathrm{MW_{th}}$	A F6 tally in MCNP is used to detect energy absorption in the reactor structure. The fusion source strength is taken to be $7.1 \times 10^{18} s^{-1}$.
I	2.8293×10^{29}	A total number of atoms from the initial core loading
ε	100%	Assumed
$\dot{C}$	$I/100$ day^{-1}	Assumed
t_r	100 days	$I/\dot{C}$

Table 7.3 Values for six parameters necessary for the MCise simulation are assumed and shown.

7.2.2 Analysis Methodology

As in any fissile system, a calculation of the long term isotopics requires a tight coupling between the neutron transport calculation and the changing isotopics. In this system, justified in part by the constant replenishment of TRU fuel, the system was modeled with a constant neutron flux, both magnitude and energy spectrum, and assumed to have a constant power level. Even though the assumptions are not realistic, they provide a good starting point for the analysis.

In addition to these assumptions, several key parameters must be assumed to initiate an MCise simulation. Those parameters are summarized in Table 7.3. The neutron flux at the initial core loading can be obtained from MCNP and is shown in Figure 7.7 using the same 63 energy groups defined by the CINDER data library.

Based on these assumptions and parameters, an MCise simulation is performed with a constant neutron flux in the reactor core for 20,000 days of operation, with isotopic inventory results recorded every 20 days.

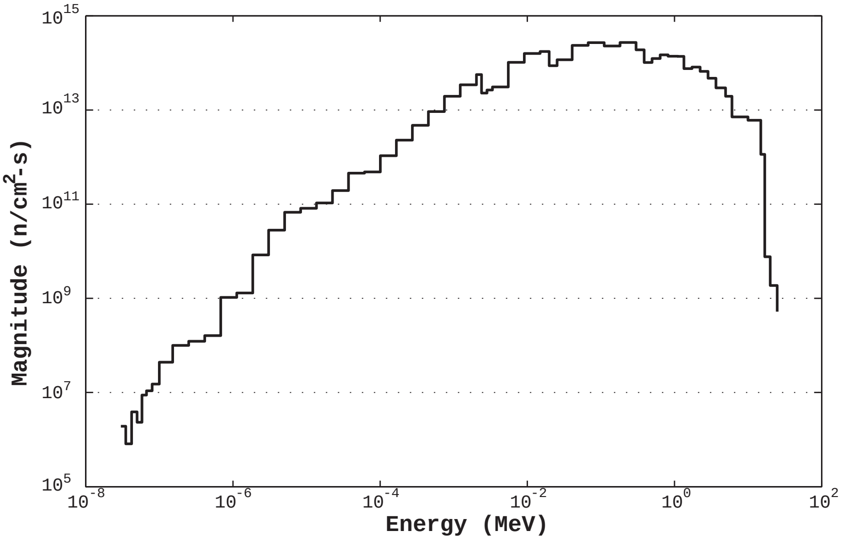

Figure 7.7 The initial flux is obtained from MCNP. The number of energy groups and energy structures are in correspondence to a CINDER data format.

7.2.3 Results and Discussion

Results for the 11 isotopes with the highest concentrations and fission products are shown in Figure 7.8. Fission products build up very rapidly at the beginning of the system's life. Many actinides approach equilibrium levels after about 10 years of operation. Other actinides gradually reach the equilibrium at times closer to 30 years.

The tritium breeding ratio (TBR), energy multiplication and k_{eff} are calculated as a function of time and are shown in Figures 7.9 to 7.11, respectively. Energy multiplication is calculated by dividing the total thermal power, measured in MeV per source neutron (total neutron and photon heating in entire problem geometry) by 12.8 MeV per source neutron (the average neutron energy as it leaves the target region). Error bars in the figures represent 1σ statistical errors. These are calculated using MCNP with material compositions based on the results of MCise.

Original results based on a replenishment of only TRU do not take into account the substantial depletion of ^{6}Li during the operation. This depletion is partly responsible for a decrease in tritium breeding ratio and increase in energy multiplication. Results are also shown with a constant ^{6}Li inventory, based on the same MCise isotopic inventory results but with the ^{6}Li inventory maintained in the MCNP input file. As expected, the tritium breeding ratio increases and equilibrium is reached within about 1 year based on the energy multiplication and multiplication factor.

The rapid drop in energy multiplication at early times affects the fission product accumulation. At early times, the fission product inventory increases towards an equilibrium value that is a function of the power level. Since the power level drops on the same time scale that the fission product inventory is accumulating, the fission product inventory reaches a level that is higher than the long term equilibrium level and must drop to reach that level.

These results demonstrate that a reactivity control mechanism will be necessary to ensure a constant energy multiplication over the life of the system. If such a mechanism were to preserve the neutron energy spectrum and magnitude, then the modeling assumptions made here would continue to be valid. However, preliminary results show that this may not

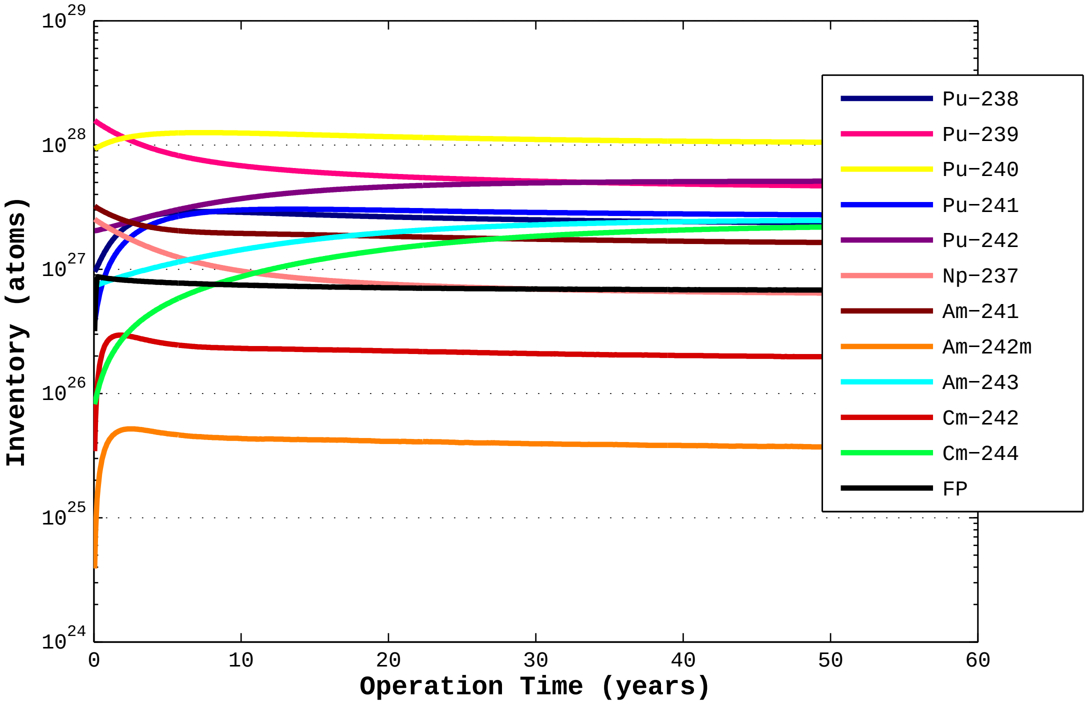

Figure 7.8 Inventories of eleven isotopes with highest concentrations and fission products as a function of operation times are shown.

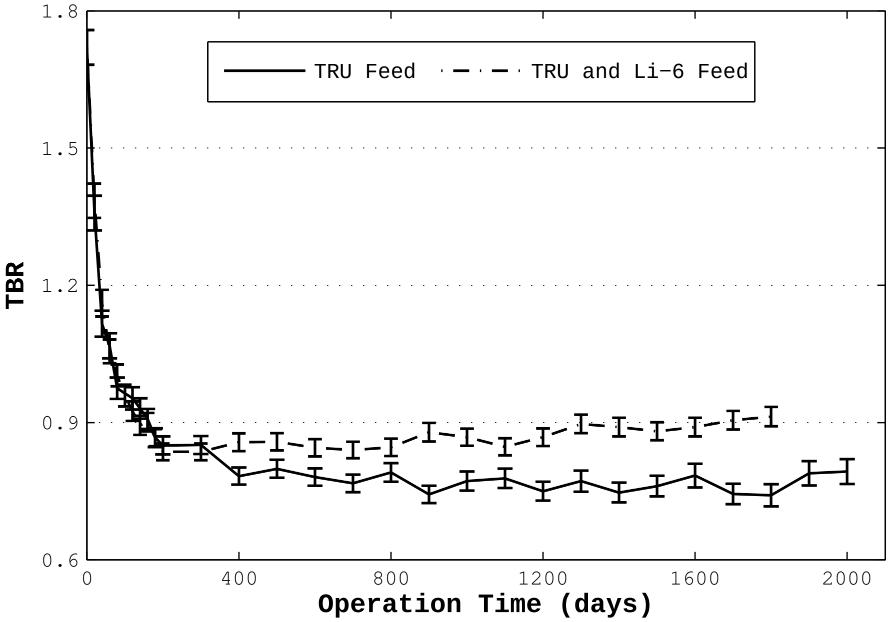

Figure 7.9 Tritium breeding ratio (TBR) for whole system, with and without replenishment of ^{6}Li.

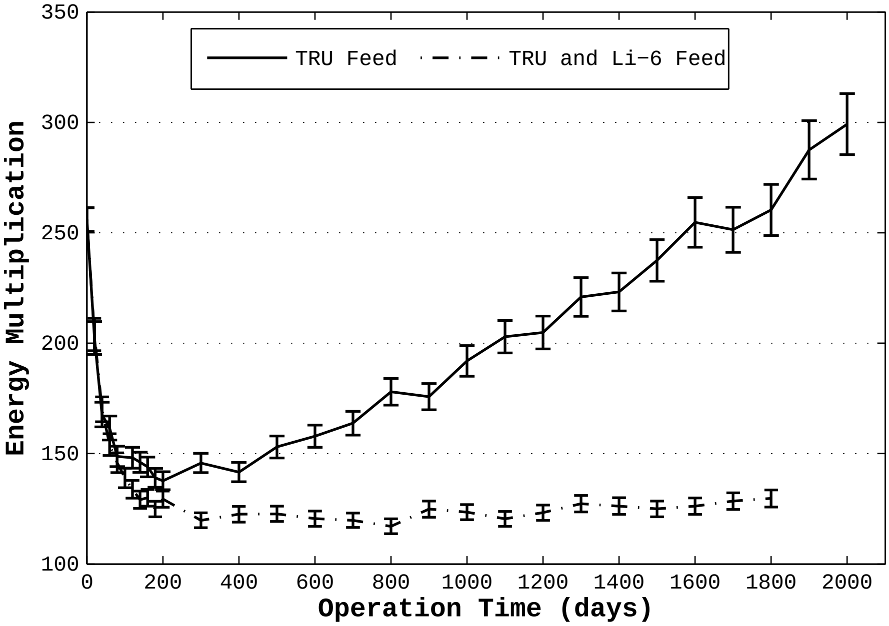

Figure 7.10 Energy multiplication for whole system with and without replenishment of ^{6}Li.

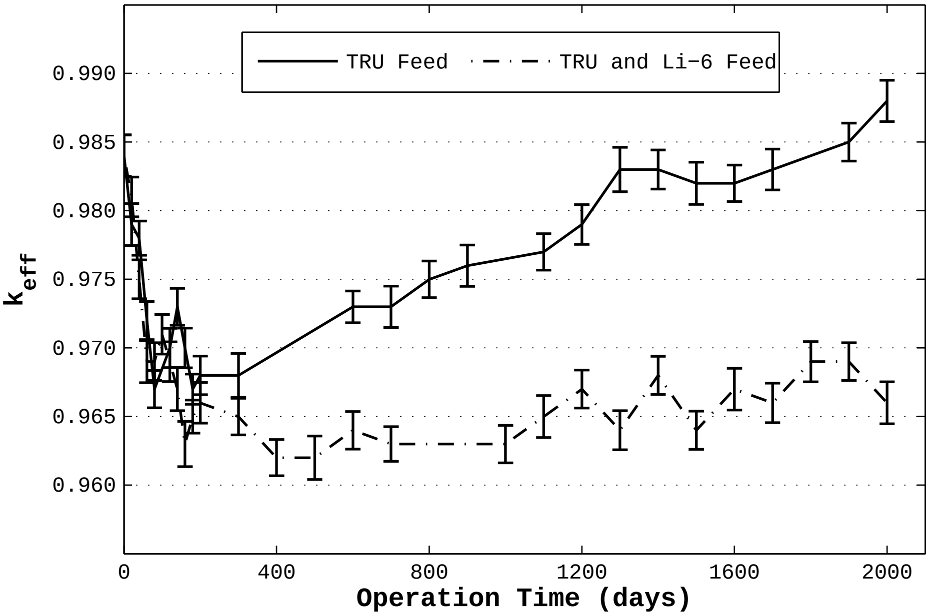

Figure 7.11 Total system multiplication factor with and without replenishment of ^{6}Li.

be the case, requiring a tighter coupling between the neutronics, isotopics, and reactivity configuration of the system.

An iterative calculation between MCNP and MCise must be employed to accurately determine burnup and activation of the materials. The following iterative scheme is proposed for the future work.

1. At time, t_i, use MCNP to **iteratively** find the reactivity control state, S_i, that achieves a desired energy multiplication for the current isotopic inventory state, I_i,
2. Use the neutron flux from step 1 with MCise to determine isotopic distributions for the next time step, I_{i+1}.

7.3 ARIES-CS

This problem is developed to assess the activation level of LiPb liquid breeder in ARIES-CS. In this system, the breeder consistently flows into and out of two radial breeding zones for on-line tritium removal. As the breeder returns to the breeding zones, it may not enter the same zone it previously exits. In addition, the ARIES-CS neutronics is radially dependent; therefore, the breeding zones have different spectra. This flowing nature makes it impossible for a deterministic activation code to design an exact pulsing schedule for a realistic irradiation history. On the other hand, MCise is able to follow histories of individual atoms as they go through a network of different irradiation volumes. Therefore, MCise can realistically model this type of system by taking advantages of its underlying methodology, which does not require a definition of an irradiation schedule.

7.3.1 MCise Simulation

This study problem is based on an ongoing development of ARIES-CS, whose radial builds and compositions are fully described in [29]. Only aspects of ARIES-CS relevant to the MCise simulation are discussed here.

Element	Weight Fraction(%)
Pb	99.29
Li	0.70
Zn	1e-3
Fe	1e-3
Bi	4.3e-3
Cd	5e-4
Ag	5e-4
Sn	5e-4
Ni	2e-4

Table 7.4 Isotopic compositions of the LiPb liquid breeder. Li is 90-percent enrichment with ^{6}Li. The theoretical density is 8.80 g/cm^3.

In the most recent ARIES-CS design, the LiPb liquid breeder flows through in-blanket and ex-vessel where it spends 1 and 1.5 minutes, respectively. The in-blanket contains two tritium-breeding zones. Each breeding zone is divided into thirteen radial regions. The DANTSYS transport code[30] is used to calculate neutron spectrums in those regions. Therefore, twenty six control volumes are defined to represent all regions in the two breeding zones. All of the flows leaving the breeding zones go to a control volume that represents the ex-vessel and the tritium extraction process. Two streams, one containing only tritium and the other carrying all other atoms, leave the ex-vessel. The tritium stream flows to the sink while the other stream returns to the breeding zones. This cycle is repeated until the total operation time reaches one year.

The total decay heat at the end of one-year operation is a target of this study. Simulated atoms are originated at the initial time from a source with isotopic compositions shown in Table 7.4. Detailed number densities of the isotopes are recorded using the atom population tally, which covers the last second of the simulation. The atom population tally is aimed to detect the existence of very short-lived isotopes that are the major contributors to the total decay heat at shutdown. These results are then used as an input for a calculation of the total decay heat at shutdown.

A schematic of MCise model is shown in Figure 7.12.

7.3.2 Numerical Results

A total computing time of the simulation with 7×10^6 NPS is 618.93 hours. A major contribution to this long computing time is due to the large number of decisions on the next control volume each simulated atom must face in a single history. At shutdown, the simulation produces 205 isotopes with a histogram of relative statistical errors shown in Figure 7.13.

The decay heat contributed from any isotope, H_i, is calculated by multiplying its resultant number density, N_i, with a corresponding decay constant and average decay energy, $(\lambda E)_i$,

$$H_i = N_i(\lambda E)_i. \tag{7.10}$$

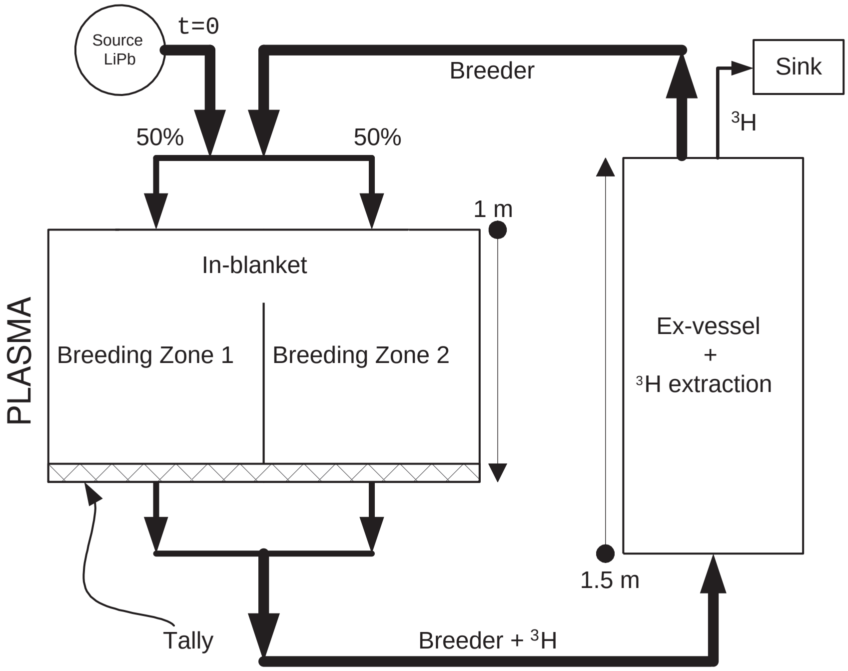

Figure 7.12 An MCise schematic showing the two breeding zones and the tritium extraction process. This cycle repeats for one year.

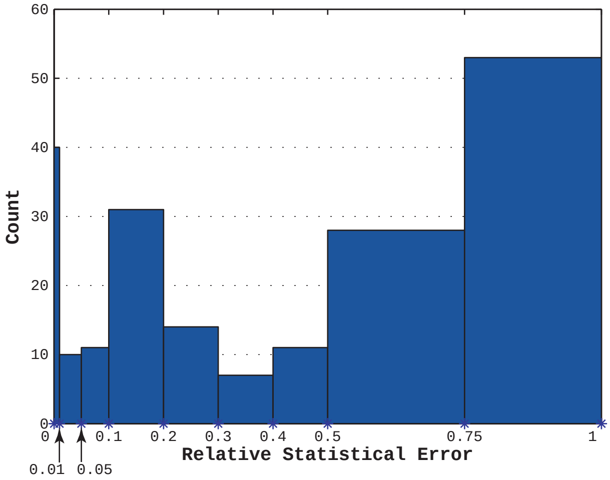

Figure 7.13 A histogram of relative statistical errors from the tally at the end of one-year operation.

The total decay heat, H, is simply the sum of decay heat from all isotopes, which can be represented in a vector form as,

$$H = \vec{N} \cdot \overrightarrow{(\lambda E)}. \tag{7.11}$$

Substituting in the values for all variables on the right-handed side of Equation 7.11, the total decay heat is found to be 1.6623×10^5 W/m^3. The relative statistical error associated with the total decay heat must also be evaluated. This composite statistical error is determined using the error propagation formula to properly combine all related statistical errors. There is an associated standard deviation, σ_i, for each resultant number density, N_i, whereas a decay constant and average decay energy have no associated uncertainty. In this case, the relative statistical error of the total decay heat is given by

$$\begin{aligned} R_H &= \frac{\sqrt{(\sigma_1\lambda_1E_1)^2 + (\sigma_2\lambda_2E_2)^2 + (\sigma_3\lambda_3E_3)^2 + \ldots}}{H} \\ R_H &= \frac{\sqrt{\overrightarrow{(\sigma\lambda E)} \cdot \overrightarrow{(\sigma\lambda E)}}}{H} \end{aligned} \tag{7.12}$$

According to Equation 7.12, the statistical error of the total decay heat is found to be 49.47%. This value is extremely high, making the resultant total decay heat unacceptable. With an already lengthy computation, increasing the number of simulated particles in the current simulation is not a viable option for improving the statistics. Additional use of variance reduction techniques will be explored in the following section as a possible approach to this problem.

7.3.3 Statistical Improvement Using ALARA-based AVA

As described in Section 6.1, AVA uses the results from the forward calculation to generate variance reduction parameters that optimize statistics of a target number density. This present AVA strategy is not appropriately designed for the problem at hand because in this case the forward calculation requires too much computing time and the physical response of interest is not a number density. Hence, AVA must be modified to address these two issues before it can be used efficiently.

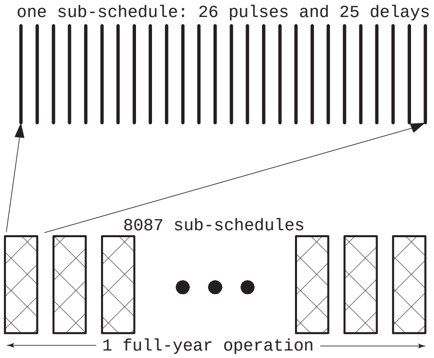

Figure 7.14 The periodic irradiation schedule used in ALARA to estimate the forward solution for AVA.

ALARA is used to calculate the forward deterministic solution for AVA. The use of ALARA greatly decrease the computational time by eliminating the time-consuming iterative Monte Carlo calculations. While ALARA is unable to model the pulsing schedule with materials being randomly exposed to different fluxes over time, it is capable of handling a pre-defined irradiation schedule. As shown in Figure 7.14, the irradiation schedule for ALARA contains one type of sub-schedule which is repeated for 8087 times. This sub-schedule is composed of twenty six 1-min pulses randomly selected from all radial zones and twenty five 1.5-min dwelling times between pulses. This is physically similar to the problem of interest, and so ALARA's result and reaction tree for such problem are considered to be decent substitutes for the initial Monte Carlo results.

A response metric for AVA is changed to the total decay heat. In this case, the first six isotopes that contribute most to the total decay heat are considered target isotopes. They are Pb-207m, Pb-203, Zn-65, Zn-69, Mn-54 and Ag-110m. Improving statistical results of these six isotopes are likely to increase the precision of the total decay heat to a certain degree. Therefore, these six isotopes are set to be target isotopes when AVA is predicting the optimal set of variance reduction parameters. In addition, the forced reaction technique is applied in the last control volume of the simulation.

With the implementation of the ALARA-based AVA, a relative statistical error of the total decay heat at shutdown is 1.32%, and the computing time is reduced to 328.26 hours.

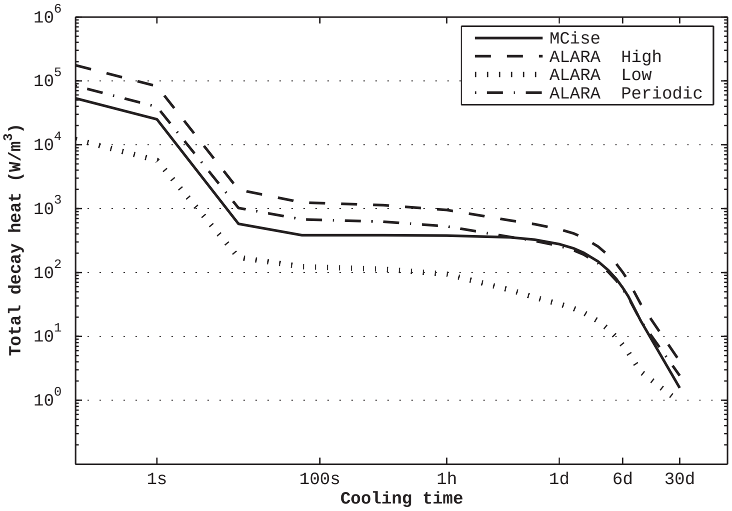

Figure 7.15 Total decay heat at various cooling times from MCise and ALARA

Significant improvement in efficiency is observed when comparing figures of merit from the two simulations. Quantitatively, the overall efficiency is increased by a factor of 2600. The total decay heat is found to be 5.803×10^4 W/m^3.

The total decay heat after shutdown is another response that is important to safety assessment, especially in the loss of coolant accident analysis. The total decay heat at each cooling time can easily be derived from its respective isotopic number densities, using the procedure mentioned earlier. A pure decay simulation, which has its initial source defined as the isotopic distribution at shutdown, is set up to calculate isotopic number densities at various cooling times. This simulation is run sufficiently long that the numerical solutions approach the analytical solutions and the statistical errors of resultant decay heat are inherited from the initial isotopic distribution.

While ALARA cannot produce an exact deterministic solution to be used as a benchmark for MCise, it can nonetheless provide expected bounds of the total decay heat. Two ALARA problems are defined with two different pulsing schedules to generate these reference decay heat values. The pulsing schedules are designed to calculate the highest and lowest possible decay heat. To obtain the highest possible decay heat, the LiPb breeder is always exposed to the highest neutron fluence in a region closest to the plasma. On the other hand, the LiPb breeder which is assumed to always return to a region furthest away from the plasma is expected to yield the lowest decay heat over times. In addition, the average decay heat of twenty periodic pulsing schedules, each representing a different physical realization of Figure 7.14, is included. This effort is made in order to better capture the random flowing nature of the LiPb breeder in the breeding zones. The total decay heat after shutdown up to 30 days are shown in Figure 7.15.

Qualitatively, decay heat from MCise is consistent with the expectation since it is within the reference bounds from ALARA. This realistic ARIES-CS problem demonstrates that MCise can be used to accurately perform activation analysis of materials in complex nuclear systems. Unavoidable calculational burden associated with some applications can make MCise impractical for production calculations. Nevertheless, it can serve as a reliable benchmark for evaluating approximation made by other deterministic tools.

Chapter 8

Future Research and Summary

8.1 Weight Window Development

Based on a successful implementation of a time dependent weight window, an extension of this type of window, a time-isotope dependent weight window, can be developed. This weight window allows MCise to control weight variations of all simulated atoms, specifically according to their time domain and isotopic identities. In terms of data structure and handling of the time-isotope dependent weight window, an additional index must be added to associate the existing time dependent weight window with an isotopic identity. This implementation should be a straightforward extension.

Another interesting research area is the development of a weight window generator for isotopic inventory analysis. The generator is designed to automatically define the weight window parameters for each time and isotope domain to optimize the simulation's efficiency. Ultimately, defining proper weight window parameters is a matter of correctly estimating particle importances of all time-isotope regions in the problem. The importance is then used to define a lower bound for its respective region by the following,

$$w_l = \frac{A}{Importance} \ , \tag{8.1}$$

where A is a constant chosen appropriately for a reference region.

The importance function can be determined using either Monte Carlo or deterministic method [31]. At this stage of the MCise development, implementing a Monte Carlo approach seems to be more logical for the next work phase as it involves many particle-tracking

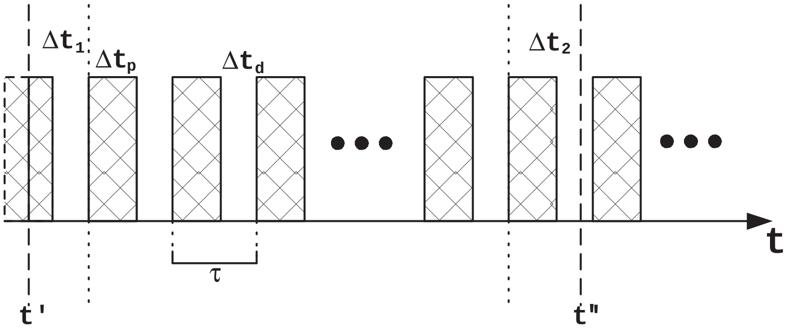

Figure 8.1 Implementation of the analog delta tracking.

features, some of which have already been implemented. The Monte Carlo method uses statistical results of the forward particle simulation to estimate the importance function for subsequent calculations. The importance of each time-isotope region can be estimated as [14]

$$\text{Importance} = \frac{\text{total score due to particles entering the region}}{\text{total weight entering the region}}. \tag{8.2}$$

Importances throughout the problem are then updated every certain number of histories. It is hoped that the optimum importance function can be achieved from a reasonable number of iterations.

8.2 Analog Delta Tracking

Currently, the delta tracking technique characterizes an irradiation state of a simulated particle by using a rejection technique based on relative durations of pulse and delay. This is statistically valid only for a high-frequency pulsing problem. The analog delta tracking can be implemented to eliminate the need to justify whether or not a given problem is high-frequency.

This technique determines an irradiation state of a simulated particle by properly keeping track of two characteristic times during the simulation: a pulsing schedule and a simulation time. This process is graphically shown in Figure 8.1. In a given pulsing problem, it is supposed that a pulse duration and a dwelling time between pulses are Δt_p and Δt_d, respectively. Based on a current simulation time, t', and a known time difference to the next pulse,

Δt_1, it is always possible to indicate a position in a pulsing period of another simulation time, t''. The modulo operation between $(t'' - (t' + \Delta t_1))$ and τ is used to calculate Δt_2, which ultimately determines the location of t''. If Δt_2 is less than Δt_p, t'' will be in the pulsing region. It will fall in one of the dwelling times, otherwise.

8.3 Automated ALARA-based AVA

A coupled Monte Carlo-deterministic method or a hybrid method, which has been pursued in the area of neutron transport [32, 33], has motivated a similar approach to promote efficiency in inventory analysis problem. This approach is to apply an iterative algorithm starting with the approximation of the overall reaction tree obtained from a deterministic calculation. The importance of each reaction pathway is evaluated based on the contribution it may eventually lead to the response metric.

The concept of a hybrid method is experimented when ARIES-CS is being analyzed (Section 7.3.3). In this sample problem, AVA driven by the initial input from ALARA is proved to be a promising technique. However, setting up the hybrid simulation is done manually and requires a great deal of intrinsic code modifications. These issues must be resolved before the ALARA-based AVA can be available for a production calculation in a more practical manner. One solution is to develop interfaces within AVA to handle the output response from ALARA. AVA then processes the imported information into its usable fashion. After that, other AVA routines are proceeded as usual.

The automated ALARA-based AVA is hoped to provide an automated and efficient way of defining a set of parameters for several variance reduction techniques.

8.4 Research Summary

MCise is a unique activation code that employs a Monte Carlo technique to simulate transmutation or decay processes of materials in complex systems with a variety of flowing conditions. The basic concept of this Monte Carlo method enables the code to provide additional modeling capabilities, for example, a chemical process, an atom sink and a continuous source. The analog methodology has been successfully implemented and its solutions of various activation problems have been validated against comparable solutions produced by a well validated deterministic activation code, ALARA.

In order to improve precision and accuracy of the analog methodology, several variance reduction techniques have been developed. Each technique has its own unique implementation and advantages that determine a type of simulation in which it can be best applied. Every implemented technique is proved to provide a distinctive improvement on the corresponding analog model. Using any variance reduction technique typically increases a computing time per history and therefore creates a concern over the efficiency. The efficiency of any Monte Carlo simulation is quantitatively measured by a figure of merit. Two types of figure of merit offer rigorous approaches to monitor the efficiency of the simulations: $(1/R^2T)$ for a simulation with a target isotope and $(1/D_kR^2T)$ for any generic simulation. Both figures of merit are successfully tested with different types of simulations. Their performances are as expected.

Adaptive Variance-reduction Adjustment (AVA) is a simple iterative scheme proposed to automatically adjust parameters for some variance reduction techniques with a goal to improve a statistical result of a target isotope. The sample problems demonstrate that AVA achieves the same accuracy and precision as the analog simulation, with a considerably shorter computing time.

Finally, the proposed methodology is proved to be applicable to performing a transient isotopic inventory analysis in nuclear systems with mixing and splitting of material flows as several engineering samples are examined. As many of the future fuel cycle designs tend to involve complex processes including chemical reactions, mixing of flow paths, and sources and sinks of material, MCise is hoped to become a reliable activation code and a benchmark for a deterministic approximation in this research area.

BIBLIOGRAPHY

[1] P. P. H. Wilson. *ALARA: Analytic and Laplacian Adaptive Radioactivity Analysis.* PhD thesis, University of Wisconsin–Madison, 1999.

[2] R. F. Burstall. *FISPIN – A Computer Code for Nuclide Inventory Calculations*, October 1979. ND–R–328(R).

[3] R. A. Forrest and J-Ch. Sublet. *FISPACT3 – Users Manual*, April 1993. AEA/FUS 227.

[4] J. Jung. *RACC: Theory and Use of the Radioactivity code RACC.* Argonne National Laboratory, May 1979. ANL/FPP/TM–122.

[5] M. J. Bell. *ORIGEN – The ORNL Isotope Generation and Depletion Code.* Oak Ridge National Laboratory, May 1973. ORNL–4628.

[6] D. L. Henderson and O. Yasar. *DKR-ICF: A Radioactivity and Dose Rate Calculation Code Package (Volume 1).* Fusion Technology Institute, University of Wisconsin, April 1987. UWFDM–714.

[7] T. R. England and et al. *CINDER–7: An Interim Report for Users.* Los Alamos National Laboratory, April 1975.

[8] H. Bateman. Proc. cambridge phil. soc., 1910.

[9] N. Metropolis and S. Ulam. The Monte Carlo method. *Journal of the American Statistical Association*, 44:335–341, 1949.

[10] M. H. Kalos and P. A. Whitlock. M*onte* C*arlo Methods.* J.Wiley and Sons, 1986.

[11] J.M. Hammersley and D.C. Handscomb. M*onte* C*arlo Methods.* Fletcher & Son Ltd., 1964.

[12] J. F. E. Briesmeister. *MCNP – A General* M*onte* C*arlo N-Particle Transport Code, Version 4C.* Los Alamos National Laboratory, 2000.

[13] Iván Lux and László Koblinger. M*onte* C*arlo Particle Transport Methods: Neutron and Photon Calculations.* CRC Press, 1991.

[14] Thomas E. Booth and John S. Hendricks. Importance estimation in forward Monte Carlo calculations. *Nuclear Technology/Fusion*, 5:90–100, January 1984.

[15] K. A. Van Riper and et al. Generation of a Monte Carlo variance reduction map from a deterministic transport calculation. Technical report, Los Alamos National Laboratory, 1995.

[16] J. Spanier and E. M. Gelbard. M*onte* C*arlo Principles and Neutron Transport Problems*. Addison–Wesley Pub. Co., 1969.

[17] F.B. Brown and T.M. Sutton. M*onte* C*arlo Fundamentals*. Knolls Atomic Power Laboratory, 1996.

[18] Marc A. Cooper. *An Automated Variance Reduction Method for Global* M*onte* C*arlo Neutral Particle Transport Problems*. PhD thesis, University of Michigan, 1999.

[19] John S. Hendricks. Private communication, 2006.

[20] Thomas E. Booth. Private communication, 2006.

[21] J. F. Latkowski, J. Sanz, and J. L. Vujic. Impact of pulsed irradiation upon neutron activation calculations for inertial and magnetic fusion energy power plants. *Fusion Technology*, 30(3):1470–1474, December 1996.

[22] P. W. Glynn and W. Whitt. The asymptotic efficiency of simulation estimators. *Operations Research*, 40(3), May–June 1992.

[23] John R. Lamarsh. *Introduction to Nuclear Engineering*. Addison Wesley, 2nd edition, February 1983.

[24] B. B. Cipiti. Fusion transmutation of waste and the role of the in-zinerator in the nuclear fuel cycle. Technical Report SAND2006-3522, Nuclear and Risk Technologies, Sandia National Laboratories, P.O. Box 5800 Albuquerque, NM 87185-0748, June 2006.

[25] L. El-Guebaly, P. Wilson, and D. Paige. Initial activation assessment for aries compact stellarator power plant. *Fusion Science & Technology*, 47(3):440–444, April 2005.

[26] G. C. Pomraning. *Linear Kinetic Theory and Particle Transport in Stochastic Mixtures*. World Scientific Publishing Co. Pte. Ltd., 1991.

[27] G. B. Zimmerman. Recent developments in Monte Carlo techniques. Technical Report UCRL-JC-105616, Lawrence Livermore National Laboratory, 1990.

[28] T. J. Donovan and Y. Danon. Application of Monte Carlo chord-length sampling algorithms to transport through a two-dimensional binary stochastic mixture. *Nuclear Science and Engineering*, 143:226–239, 2003.

[29] L. El-Guebaly. Fusion Technology Institute, Department of Engineering Physics, University of Wisconsin-Madison. http://fti.neep.wisc.edu/aries-cs/builds/build.html.

[30] R. E. Alcouffe, F. W. Brinkley, D. R. Marr, R. D. O'Dell, and W. F. Walters. *DANTSYS: A Diffusion Accelerated Neutral Particle Transport Code System.* Los Alamos National Laboratory, 1995. LA-12969-M.

[31] M. W. Mickael. A fast, automated, semideterministic weight windows generator for MCNP. *Nuclear Science and Engineering*, 119:34–43, January 1995.

[32] Alireza Haghighat and John C. Wagner. Monte Carlo variance reduction with deterministic importance functions. *Progress in Nuclear Energy*, 42(1):25–53, 2003.

[33] Edward W. Larsen. Hybrid Monte Carlo-deterministic methods for nuclear reactor-related criticality calculatons. Technical Report DE-FG07-00ID13920, Department of Energy, 2003.